

NO-A192 056

EARLY SMOKE PLUME AND CLOUD FORMATION BY LARGE AREA
FIRES(U) PACIFIC-SIERRA RESEARCH CORP LOS ANGELES CA
K E HEIKES ET AL. 29 MAY 87 PSR-1728 DNA-TR-87-176

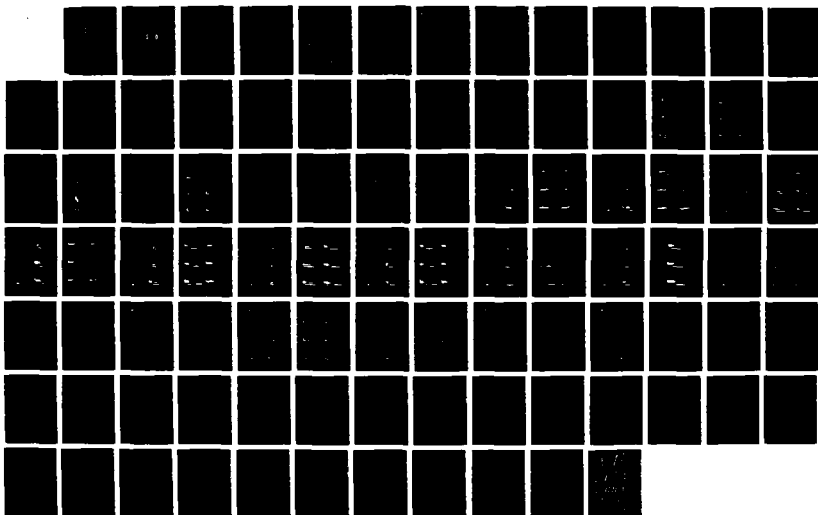
1/1

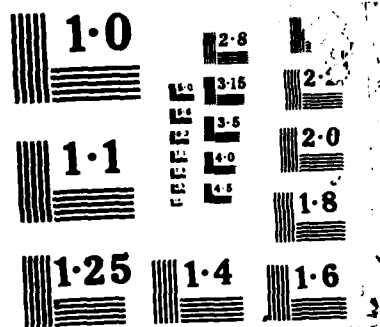
UNCLASSIFIED

DNA001-05-C-0009

F/G 4/1

ML





4

AD-A192 056

DNA-TR-87-176

DTIC FILE COPY

**EARLY SMOKE PLUME AND CLOUD FORMATION
BY LARGE AREA FIRES**

**K. E. Heikes
L. M. Ransohoff
R. D. Small
Pacific-Sierra Research Corporation
12340 Santa Monica Boulevard
Los Angeles, CA 90025-2587**

29 May 1987

**DTIC
ELECTE
MAR 10 1988
S D**

Technical Report

CONTRACT No. DNA 001-85-C-0089

**Approved for public release;
distribution is unlimited.**

**THIS WORK WAS SPONSORED BY THE DEFENSE NUCLEAR AGENCY
UNDER RDT&E RMC CODE B3110864662 RD RB 00009 25904D.**

**Prepared for
Director
DEFENSE NUCLEAR AGENCY
Washington, DC 20305-1000**

88 3 09 108

Destroy this report when it is no longer needed. Do not return to sender.

PLEASE NOTIFY THE DEFENSE NUCLEAR AGENCY
ATTN: TITL, WASHINGTON, DC 20305 1000, IF YOUR
ADDRESS IS INCORRECT, IF YOU WISH IT DELETED
FROM THE DISTRIBUTION LIST, OR IF THE ADDRESSEE
IS NO LONGER EMPLOYED BY YOUR ORGANIZATION.



DISTRIBUTION LIST UPDATE

This mailer is provided to enable DNA to maintain current distribution lists for reports. We would appreciate your providing the requested information.

- ☐ Add the individual listed to your distribution list.
- ☐ Delete the cited organization/individual.
- ☐ Change of address.

NAME: _____

ORGANIZATION: _____

OLD ADDRESS

CURRENT ADDRESS

TELEPHONE NUMBER: () _____

SUBJECT AREA(s) OF INTEREST:

DNA OR OTHER GOVERNMENT CONTRACT NUMBER: _____

CERTIFICATION OF NEED-TO-KNOW BY GOVERNMENT SPONSOR (if other than DNA):

SPONSORING ORGANIZATION: _____

CONTRACTING OFFICER OR REPRESENTATIVE: _____

SIGNATURE: _____

CUT HERE AND RETURN



Director
Defense Nuclear Agency
ATTN: [REDACTED] TITL
Washington, DC 20305-1000

Director
Defense Nuclear Agency
ATTN: [REDACTED] TITL
Washington, DC 20305-1000

UNCLASSIFIED
SECURITY CLASSIFICATION OF THIS PAGE

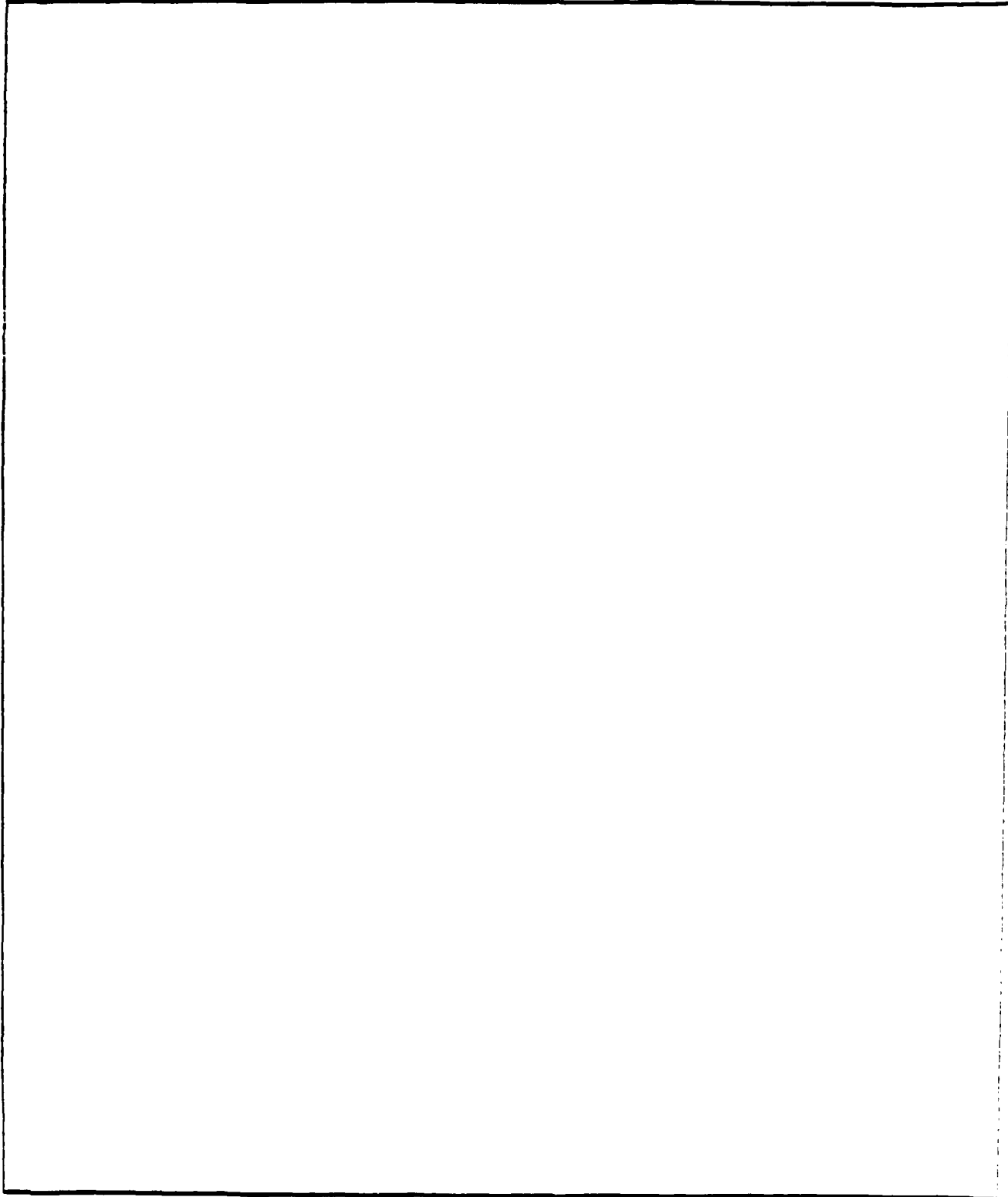
AD-A 192 056

REPORT DOCUMENTATION PAGE

1a. REPORT SECURITY CLASSIFICATION UNCLASSIFIED		1b. RESTRICTIVE MARKINGS	
2a. SECURITY CLASSIFICATION AUTHORITY N/A since Unclassified		3. DISTRIBUTION/AVAILABILITY OF REPORT Approved for public release: distribution is unlimited.	
2b. DECLASSIFICATION/DOWNGRADING SCHEDULE N/A since Unclassified			
4. PERFORMING ORGANIZATION REPORT NUMBER(S) PSR Report 1728		5. MONITORING ORGANIZATION REPORT NUMBER(S) DNA-TR-87-176	
6a. NAME OF PERFORMING ORGANIZATION Pacific-Sierra Research Corporation	6b. OFFICE SYMBOL (if applicable)	7a. NAME OF MONITORING ORGANIZATION Director Defense Nuclear Agency	
6c. ADDRESS (City, State, and ZIP Code) 12340 Santa Monica Boulevard Los Angeles, CA 90025-2587		7b. ADDRESS (City, State, and ZIP Code) Washington, DC 20305-1000	
8a. NAME OF FUNDING/SPONSORING ORGANIZATION	8b. OFFICE SYMBOL (if applicable) RDTR/Flohr	9. PROCUREMENT INSTRUMENT IDENTIFICATION NUMBER DNA 001-85-C-0089	
8c. ADDRESS (City, State, and ZIP Code)		10. SOURCE OF FUNDING NUMBERS	
		PROGRAM ELEMENT NO. 62715H	PROJECT NO. RD
		TASK NO. RB	WORK UNIT ACCESSION NO. DH008791
11. TITLE (Include Security Classification) EARLY SMOKE PLUME AND CLOUD FORMATION BY LARGE AREA FIRES			
12. PERSONAL AUTHOR(S) Heikes, K. E.; Ransohoff, L. M.; Small, R. D.			
13a. TYPE OF REPORT Technical	13b. TIME COVERED FROM 841115 to 870529	14. DATE OF REPORT (Year, Month, Day) 870529	15. PAGE COUNT 92
16. SUPPLEMENTARY NOTATION This work was sponsored by the Defense Nuclear Agency under RDT&E RMC Code B3110864662 RD RB 00009 25904D.			
17. COSATI CODES		18. SUBJECT TERMS (Continue on reverse if necessary and identify by block number)	
FIELD	GROUP	SUB-GROUP	
18	03	Cloud Formation, Precipitation Scavenging, Urban Fires	
05	05	Fire Heating, Smoke Injection	
		Nuclear Winter, Smoke Plume	
19. ABSTRACT (Continue on reverse if necessary and identify by block number)			
<p>It is likely that a nuclear burst over an urban area would cause a large number of fires burning simultaneously over hundreds of square kilometers. The atmospheric heating produced by these fires would result in low-level convergence over a broad region and a highly buoyant upward mass flux over the fire, lofting large quantities of smoke and moisture to high altitudes.</p> <p>This report presents the results of highly resolved numerical calculations describing the early-time cloud and smoke plume formation by large city fires. The simulations show that atmospheric moisture contributes significantly to plume evolution through latent heat release. The model indicates that early scavenging of smoke particles by precipitation is likely to reduce the amount of smoke injected into the upper atmosphere. A principal result is that plume rise is controlled primarily by fire intensity and atmospheric stratification rather than fire size.</p>			
20. DISTRIBUTION/AVAILABILITY OF ABSTRACT <input type="checkbox"/> UNCLASSIFIED/UNLIMITED <input checked="" type="checkbox"/> SAME AS RPT. <input type="checkbox"/> DTIC USERS		21. ABSTRACT SECURITY CLASSIFICATION UNCLASSIFIED	
22a. NAME OF RESPONSIBLE INDIVIDUAL Sandra E. Young		22b. TELEPHONE (Include Area Code) (202) 325-7042	22c. OFFICE SYMBOL DNA/CSTI

UNCLASSIFIED

SECURITY CLASSIFICATION OF THIS PAGE



UNCLASSIFIED

SECURITY CLASSIFICATION OF THIS PAGE

SUMMARY

Fires burning simultaneously over hundreds of square kilometers could be one result of a nuclear weapon explosion. The strong buoyancy field of such large area fires induces high-velocity fire winds that turn upward in the burning region and vertically transport a large quantity of water vapor. In this report, we numerically model the rise of moisture-laden, free-convection columns and examine the development of clouds as a function of relative humidity, fire size, and burning or heat release rate. The rise is controlled principally by the fire heat release and the atmospheric stratification. In most of our simulations, enough moisture is lofted to form large cumulus clouds early in the plume development.



Accession For	
NTIS CRA&I	<input checked="" type="checkbox"/>
DTIC TAB	<input type="checkbox"/>
Unannounced	<input type="checkbox"/>
Justification	
By	
Distribution/	
Availability Codes	
Dist	Avail and/or Special
A-1	

PREFACE

This work was sponsored by the Defense Nuclear Agency under contract DNA 001-85-C-0089. The work was monitored by Dr. Michael J. Frankel and Mr. Mark Flohr.

CONVERSION TABLE

Conversion factors for U.S. Customary to metric (SI) units of measurement

MULTIPLY \longrightarrow BY \longrightarrow TO GET
TO GET \longleftarrow BY \longleftarrow DIVIDE

angstrom	1.000 000 X E -10	meters (m)
atmosphere (normal)	1.013 25 X E +2	kilo pascal (kPa)
bar	1.000 000 X E +2	kilo pascal (kPa)
barn	1.000 000 X E -28	meter ² (m ²)
British thermal unit (thermochemical)	1.054 350 X E +3	joule (J)
calorie (thermochemical)	4.184 000	joule (J)
cal (thermochemical)/cm ²	4.184 000 X E -2	mega joule/m ² (MJ/m ²)
curie	3.700 000 X E +1	*giga becquerel (GBq)
degree (angle)	1.745 329 X E -2	radian (rad)
degree Fahrenheit	$t_F = (t_C + 459.67)/1.8$	degree kelvin (K)
electron volt	1.602 19 X E -19	joule (J)
erg	1.000 000 X E -7	joule (J)
erg/second	1.000 000 X E -7	watt (W)
foot	3.048 000 X E -1	meter (m)
foot-pound-force	1.355 818	joule (J)
gallon (U.S. liquid)	3.785 412 X E -3	meter ³ (m ³)
inch	2.540 000 X E -2	meter (m)
jerk	1.000 000 X E +9	joule (J)
joule/kilogram (J/kg) (radiation dose absorbed)	1.000 000	Gray (Gy)
kilotons	4.183	terajoules
kip (1000 lbf)	4.448 222 X E +3	newton (N)
kip/inch ² (ksi)	6.894 757 X E +3	kilo pascal (kPa)
ktop	1.000 000 X E +2	newton-second/m ² (N-s/m ²)
micron	1.000 000 X E -6	meter (m)
mil	2.540 000 X E -5	meter (m)
mile (international)	1.609 344 X E +3	meter (m)
ounce	2.834 952 X E -2	kilogram (kg)
pound-force (lbs avoirdupois)	4.448 222	newton (N)
pound-force inch	1.129 848 X E -1	newton-meter (N-m)
pound-force/inch	1.751 268 X E +2	newton/meter (N/m)
pound-force/foot ²	4.788 026 X E -2	kilo pascal (kPa)
pound-force/inch ² (psi)	6.894 757	kilo pascal (kPa)
pound-mass (lbm avoirdupois)	4.535 924 X E -1	kilogram (kg)
pound-mass-foot ² (moment of inertia)	4.214 011 X E -2	kilogram-meter ² (kg-m ²)
pound-mass/foot ³	1.601 846 X E +1	kilogram/meter ³ (kg/m ³)
rad (radiation dose absorbed)	1.000 000 X E -2	*Gray (Gy)
roentgen	2.579 760 X E -4	coulomb/kilogram (C/kg)
shake	1.000 000 X E -8	second (s)
slug	1.459 390 X E +1	kilogram (kg)
torr (mm Hg, 0°C)	1.333 22 X E -1	kilo pascal (kPa)

*The becquerel (Bq) is the SI unit of radioactivity; 1 Bq = 1 event/s.

**The Gray (Gy) is the SI unit of absorbed radiation.

TABLE OF CONTENTS

Section	Page
SUMMARY	iii
PREFACE	iv
CONVERSION TABLE	v
LIST OF ILLUSTRATIONS	vii
 1 INTRODUCTION	 1
2 MODEL DESCRIPTION	4
Numerical model	4
Governing equations	5
Initial and boundary conditions	6
Heat and smoke source terms	7
Water phase transitions	8
3 RESULTS	10
Input parameters	10
Baseline water cloud	11
Baseline smoke cloud	14
Comparison between dry and moist atmosphere	15
Effect of fire area and heating rate	17
Fire winds	17
Effect of grid resolution	20
Individual cases	22
4 DISCUSSION	62
5 LIST OF REFERENCES	64
 Appendices	
A SMOKE PRODUCTION	67
B WATER PROCESSES	69
C WATER CONTENT DUE TO COMBUSTION	73

LIST OF ILLUSTRATIONS

Figure		Page
1	Moisture cloud simulation for 0.5-kW/m ³ heating rate and 7-km radius fire	12
2	Smoke cloud simulation for 0.5-kW/m ³ heating rate and 7-km radius fire	13
3	Comparison of moist and dry smoke clouds for 0.5-kW/m ³ heating rate and 7-km radius fire at 60 min	16
4	Comparison of smoke clouds obtained at 60 min for constant heating and variable radius and for constant radius and variable heating	18
5	Radial velocity at 8-km radius for three heating rates for 7-km radius fire at 10 min intervals	19
6	Smoke clouds at 45 min for fire 7 km in radius with 0.50 kW/m ³ volume heating rate	21
7	Moisture cloud, streamlines, and neutral buoyancy isotherms for case 1--high heating rate (1.00 kW/m ³), large radius (10 km)	23
8	Moisture cloud, streamlines, and neutral buoyancy isotherms for case 2--medium heating rate (0.50 kW/m ³), large radius (10 km)	25
9	Moisture cloud, streamlines, and neutral buoyancy isotherms for case 3--low heating rate (0.25 kW/m ³), large radius (10 km)	27
10	Moisture cloud, streamlines, and neutral buoyancy isotherms for case 4--high heating rate (1.00 kW/m ³), medium radius (7 km)	29
11	Moisture cloud, streamlines, and neutral buoyancy isotherms for case 5--medium heating rate (0.50 kW/m ³), medium radius (7 km)	31
12	Moisture cloud, streamlines, and neutral buoyancy isotherms for case 6--low heating rate (0.25 kW/m ³), medium radius (7 km)	33
13	Moisture cloud, streamlines, and neutral buoyancy isotherms for case 7--medium heating rate (0.50 kW/m ³), small radius (5 km)	35

14	Streamlines and neutral buoyancy isotherms for case 8-- dry atmosphere	37
15	Moisture cloud, streamlines, and neutral buoyancy iso- therms for case 9--low-resolution grid	39
16	Smoke cloud and velocity vectors for case 1--high heating rate (1.00 kW/m ³), large radius (10 km)	41
17	Smoke cloud and velocity vectors for case 2--medium heating rate (0.50 kW/m ³), large radius (10 km)	43
18	Smoke cloud and velocity vectors for case 3--low heating rate (0.25 kW/m ³), large radius (10 km)	45
19	Smoke cloud and velocity vectors for case 4--high heating rate (1.00 kW/m ³), medium radius (7 km)	47
20	Smoke cloud and velocity vectors for case 5--medium heating rate (0.50 kW/m ³), medium radius (7 km)	49
21	Smoke cloud and velocity vectors for case 6--low heating rate (0.25 kW/m ³), medium radius (7 km)	51
22	Smoke cloud and velocity vectors for case 7--medium heating rate (0.50 kW/m ³), small radius (5 km)	53
23	Smoke cloud and velocity vectors for case 8--dry atmosphere	55
24	Smoke cloud and velocity vectors for case 9--low-resolution grid	57

SECTION 1

INTRODUCTION

A nuclear burst over an urban area is likely to cause a large number of fires. The initial distribution of ignitions is related to the thermal radiation output of the bomb and the disruptive effects (secondary ignitions) of the blast wave. The precise distribution of fire starts depends on the city structure, weapon yield, and height of burst. It is reasonable to assume a frequency of ignitions decreasing with distance from the burst. For a 1-MT weapon, ignitions are likely as far as 10 km from the burst; for smaller yields, the range decreases.

Initially, many thousands of fire starts would be distributed across an urban area. Not all buildings would be involved simultaneously, but it is likely that all would eventually burn. That was suggested by the area fires that occurred at Hamburg, Dresden, Hiroshima, etc. [Bond, 1946]. During the course of an area fire, which may last several hours, some structures would be actively burning, some would be in preliminary stages of involvement, and others would have already completely burned out. The spread responsible for the continual burning (or heat release) of the city is limited to the area of fire starts. That is, a large area is not burned by a front sweeping across a city, but rather, by an evolving complex of fires.

Energy would be released over a large area rather than in a narrow fire line, generating a broad-based convective flow or plume. This flow would be supported by high-velocity fire winds induced by the fire complex [Larson and Small, 1982; Small, Larson, and Brode, 1984; Small and Larson, 1984/85]. The interactions are straightforward. Buoyancy created by heat release generates pressure gradients, which in turn induce fire winds. Those turn upward to form the convective flow. Radiative cooling rapidly reduces (over $\sim 10^3$ m) the temperature above the heat release region. The net effect is a high-momentum convective flow with only a moderate temperature excess

(several degrees) or density deficit from the ambient. For axisymmetric flows, the differential is largest near the centerline.

The initial momentum and temperature excess of the plume depend directly on the fire size and heat release. These determine, in part, the plume rise and deposition of smoke in the atmosphere. Entrainment of ambient air during the rise plays a minor role in diffusing the plume momentum and buoyancy, since the mixing takes place at the plume edge, far from the largest concentrations of buoyancy. Consequently, atmospheric structure (lapse rate, inversion height, and upper-level winds) is the primary factor in determining the ultimate plume rise. Fires from a nuclear burst can create plume motions that extend to the tropopause [Hassig and Rosenblatt, 1983; Small, Remetch, and Brode, 1984, 1985; Penner, Haselman, and Edwards, 1986; Bacon, Sarma, and Proctor, 1986; Cotton, 1985; and Tripoli and Kang, 1987].

The high-velocity fire winds induced by a large area [$0(100) \text{ km}^2$] city fire would entrain, at low altitude, significant amounts of water vapor. Except for extremely dry atmospheres, the entrained moisture is roughly an order of magnitude greater than the water produced by combustion. In the plume, large cloud structures evolve from condensation of the entrained moisture. The release of latent heat drives the plume higher; evaporation decreases the buoyancy. Cloud formation by the fire-generated convective motion occurs rapidly. Such cloud development is common in naturally occurring wildland fires, and rain often results. Large area city fires would produce even larger and more intense clouds.

Condensation and cloud formation not only influence the plume motion, but also enable the scavenging of smoke by water droplets, and to some extent, ice. Early cloud formation may account for some scavenging of smoke with particularly high soot content, produced soon after the fires start. Precipitation may limit the amount of smoke lofted to high altitude. Black rain was noted at Hiroshima [Committee for the Compilation of Materials on Damage Caused by the Atomic Bombs in Hiroshima and Nagasaki, 1981], implying that fire-generated precipitation removed at least some of the smoke.

The rate and extent of cloud formation depends on the low-level entrainment of humid, ambient air and its distribution in the plume. Both the fire winds and plume structure depend directly on the buoyancy field or details of the fire. Numerical simulation of cloud formation thus requires a grid fine enough to properly resolve the fire-generated flow, as well as the larger scale atmospheric response. In this report, we consider two-dimensional (axisymmetric) approximations for fire-generated flows in a stratified, moist atmosphere. We have determined in detail the amount of water lofted, plume motion, cloud development, and smoke transport for several fire sizes and burning rates.

SECTION 2

MODEL DESCRIPTION

NUMERICAL MODEL.

Our numerical simulation employs a Lagrangian-Eulerian algorithm to model atmospheric convection driven by a large area fire, and is applicable to compressible, two-dimensional fluid flows over a wide range of flow speeds [Hirt, Amsden, and Cook, 1974]. Compressibility is important near the fire because of the high temperatures. The Lagrangian-Eulerian technique is a compromise between fully explicit, compressible calculations and partially implicit calculations associated with the anelastic approximation [Ogura and Phillips, 1962] for deep convection. The Lagrangian phase advects the mesh vertices with the fluid, assuming no flux across cell boundaries. In the Eulerian phase, the vertices are restored to their original positions and fluxes into the cells are accounted for. Upwind, or donor cell, differencing is used in the Eulerian phase; centered differences in the Lagrangian phase. The technique allows high resolution solutions using variable zoning of the compressible flow near the fire and within the plume and, at the same time, it permits time steps much larger than possible with purely explicit schemes.

The algorithms used in this study include many enhancements to the original Lagrangian-Eulerian scheme used by Hirt, Amsden, and Cook [1974]. Pressure is calculated implicitly at the end of each time step. Temperature T is determined from the energy equation, which includes a radiation term proportional to T^4 and, therefore, the temperature is also found implicitly. We have also modified the original program to include latent heating or cooling due to water vapor phase transitions, thermal diffusion, volumetric heating in the fire region, and the advection of water and smoke.

Variable zoning is used. Fine resolution is achieved near the lower boundary, the centerline, and the fire region. A fixed number of grid points (19 radial, including the axis; 4 vertical, including the ground) is usually used within the fire volume independent of fire

radius. The spacing increases by a factor of approximately 1.1 for cells outside the fire region. The axial grid spacing within the fire volume is 33 m, increasing to about 1 km at the tropopause. The computational domain extends vertically to 30 km and radially to 70 km.

GOVERNING EQUATIONS.

The simulations are based on the compressible, nonhydrostatic Navier-Stokes equations with velocity components (u,v), in the radial and axial directions (r,y):

$$\begin{aligned} \frac{\partial u}{\partial t} + u \frac{\partial u}{\partial r} + v \frac{\partial u}{\partial y} &= - \frac{1}{\rho} \frac{\partial p}{\partial r} + K_M \left(\frac{\partial}{\partial r} \frac{1}{r} \frac{\partial ru}{\partial r} + \frac{\partial^2 u}{\partial y^2} \right) , \\ \frac{\partial v}{\partial t} + u \frac{\partial v}{\partial r} + v \frac{\partial v}{\partial y} &= - \frac{1}{\rho} \frac{\partial p}{\partial y} - g + K_M \left(\frac{1}{r} \frac{\partial}{\partial r} r \frac{\partial v}{\partial r} + \frac{\partial^2 v}{\partial y^2} \right) , \end{aligned} \quad (1)$$

where t is time, p is pressure, K_M is eddy viscosity, and g is gravitational acceleration. The ideal gas equation of state is used. Although velocities are subsonic, $O(1)$ changes in temperature and density occur as a result of the large heat release within the fire volume. The full continuity equation is thus required:

$$\frac{\partial \rho}{\partial t} + \frac{1}{r} \frac{\partial}{\partial r} (r \rho u) + \frac{\partial}{\partial y} (\rho v) = 0 . \quad (2)$$

The energy equation is

$$\begin{aligned} \frac{\partial c_v T}{\partial t} + u \frac{\partial c_v T}{\partial r} + v \frac{\partial c_v T}{\partial y} &= - RT \left(\frac{1}{r} \frac{\partial ru}{\partial r} + \frac{\partial v}{\partial y} \right) + K_T \left(\frac{1}{r} \frac{\partial}{\partial r} r \frac{\partial T}{\partial r} + \frac{\partial^2 T}{\partial y^2} \right) \\ &+ \dot{q}_f + \dot{q}_r + \dot{q}_w , \end{aligned} \quad (3)$$

where \dot{q}_f , \dot{q}_r , and \dot{q}_w are heat sink/source terms for heating by the

fire, radiative cooling, and latent heating due to changes in water phase, respectively. The gas constant R and specific heat volume c_v are mass-weighted properties:

$$\begin{aligned}\rho &= \rho_d + \rho_v + \rho_l + \rho_i , \\ R &= \frac{\rho_d R_d + \rho_v R_v + \rho_l R_l + \rho_i R_i}{\rho} , \\ c_v &= \frac{\rho_d c_{vd} + \rho_v c_{vv} + \rho_l c_{vl} + \rho_i c_{vi}}{\rho} .\end{aligned}\quad (4)$$

The total mixture density is ρ and the subscripts d , v , l , and i refer to dry air, water vapor, liquid water, and ice, respectively.

INITIAL AND BOUNDARY CONDITIONS.

Normal velocities are zero at all boundaries. A no-slip boundary condition is applied at the ground and free-slip conditions are used at the axis of symmetry, upper boundary, and outer radius. It is assumed that the upper boundary is isothermal; the lower boundary and centerline are perfect insulators. The atmosphere is initially quiescent, and the temperature is prescribed by the U.S. Standard Atmosphere [1962]. The initial lapse rate is stable everywhere and constant ($-6.45 \times 10^{-3}^\circ\text{C/m}$) from the ground to an altitude of 10 km in the troposphere, isothermal (-56°C) in the tropopause from 10 to 20 km, and constant ($1.06 \times 10^{-3}^\circ\text{C/m}$) from 20 to 30 km in the stratosphere. The stable stratospheric layer at the top and the large radial extent of the computation domain isolate the flow from the top and outer boundaries. An initial vertical distribution of relative humidity [Manabe and Wetherald, 1967] is assumed:

$$\phi(y) = \frac{\phi_o}{0.98} \left(\frac{p(y)}{p_o} - 0.02 \right) . \quad (5)$$

At the ground, ϕ_0 is 77 percent and p_0 is the ambient surface pressure.

HEAT AND SMOKE SOURCE TERMS.

The three energy source/sink terms (fire heat release, radiative cooling, and latent heat release) control the system dynamics. The fire is modeled as a 100 m-high, volume heat source. The heating rate increases linearly in time from $\dot{q}_f = 0$ to a constant value at $t = 900$ s and thereafter. Radius and heating rate are varied to test the effects of fire size and intensity. Initially, all properties are horizontally homogeneous, except within the fire volume where eddy viscosity and eddy thermal conductivity are set an order of magnitude larger than outside the fire volume ($K_{M,T} = 10^3 \text{ m}^2/\text{s}$, as opposed to $K_{M,T} = 10^2 \text{ m}^2/\text{s}$). The larger values account for fire-generated turbulence and effective surface roughness associated with urban features. Smoke generation and transport are described by:

$$\frac{\partial S}{\partial t} + \frac{1}{r} \frac{\partial}{\partial r} (ruS) + \frac{\partial}{\partial y} (vS) = \dot{S}; \quad \dot{S} = 1.66 \times 10^{-6} \dot{q}_f, \quad (6)$$

where S is the smoke concentration, and \dot{S} is the source function based on a 3 percent smoke emission rate and heat release rate \dot{q}_f (see Appendix A). The combustion of $2 \text{ g/cm}^2/\text{h}$ of fuel is assumed to release 100 kW/m^2 . Heat release increases as fuel loading increases; the total smoke mass input to the atmosphere depends on the burnable fuel loading. During the time of significant heat release (roughly 0.5 to 4 h), smoke transport is primarily determined by large-scale features of the velocity field, and therefore, is modeled as an advective process [see Eq. (6)]. Diffusion becomes a significant transport process only at much later times.

Our use of a volume heat source to model the distribution of fires results in an average temperature, in the region of heat release, considerably lower than that of the individual fires. Accordingly, the radiative loss \dot{q}_r is modeled by:

$$\dot{q}_r = \frac{\alpha \sigma}{H} \left[(\beta T)^4 - T_o^4 \right]. \quad (7)$$

Here, α is the ratio of actual burning area to the total area, H is the height of the fire region, T_o is the far-field ambient temperature, and σ is the Stefan-Boltzmann constant. In general, structures occupy less than 30 percent of the land in dense urban areas. Not all the area burns at one time, nor does all of the area contain accessible combustible material. Thus $\alpha < 1$. The ratio β of actual fire temperature to average region temperature is roughly 3. Temperature decays rapidly above the fire as a result of radiative cooling.

WATER PHASE TRANSITIONS.

A significant amount of heat is released by water phase transitions in the plume well above the fire; the effect of latent heat release becomes increasingly important for lower fire heating rates. At each time step in the calculation, moist air is first transported by the flow without phase change. The saturation vapor density is then compared to the new water vapor density at each grid point. A phase transition then occurs, bringing the vapor density as close as possible to saturation by means of evaporation, condensation, melting, freezing, or sublimation, depending on temperature (see Appendix B). For temperatures warmer than 0°C , the process requires that, first, all ice melts, and then, either liquid water evaporates or water vapor condenses, contingent on whether the air is subsaturated or supersaturated with respect to liquid water. At temperatures lower than -15°C , liquid water first freezes, and then ice sublimates or vapor accretes, depending on whether the air is subsaturated or supersaturated with respect to ice.

For the temperature range 0° to -15°C , liquid water and ice are allowed to coexist to simulate the supercooled water condition observed in naturally occurring clouds. A deficit in water vapor density relative to saturation over ice is first corrected by evaporating water, since the saturation vapor pressure over water is higher than that over ice, and then any further subsaturation is made up for by

sublimating ice. Alternatively, an excess water vapor density relative to saturation over water is corrected by the accretion of vapor to ice. If the water vapor pressure is subsaturated with respect to liquid water but saturated with respect to ice, no change in vapor density takes place. Thus, liquid water may be advected into regions where the temperature is in the range 0° to -15° C but does not form in these regions. This is consistent with the fact that the vapor pressure over water is greater than that over ice within this temperature range. All temperature changes due to latent heating or cooling are assumed to occur at constant pressure and are incorporated in the energy equation at the next time step [δt is, at most, $O(10^{-1})$ s].

Upon condensation (or freezing), one-third (or one-half) of the condensate is removed from the atmosphere to simulate precipitation. Details of the precipitation process, particularly scavenging of smoke particles, are not included in this preliminary study. This modeling of precipitation, although it is rudimentary, does reproduce the irreversible process found in naturally occurring clouds of moist adiabatic ascent followed by dry adiabatic descent, warming the cloud region.

Combustion of the hydrogen component of the fuel in the presence of atmospheric oxygen produces a mass of water approximately half the fuel mass. This water vapor is also drawn up into the plume, where it condenses and releases latent heat. However, the mass of water vapor produced by combustion is generally at least an order of magnitude lower than that present in the atmosphere or entrained by the fire winds. Except for a very dry atmosphere, it has a negligible effect on the plume dynamics (see Appendix C).

SECTION 3 RESULTS

INPUT PARAMETERS.

The test matrix of input conditions covered a range of fire sizes, fire intensities, and atmospheric moisture conditions (see Table 1). Area fires of radii 5, 7, and 10 km were considered. They correspond either to cities completely involved in fire but of different sizes, or to fires started by weapons of different yields. Heating by the fire does not take place directly at the surface, but is distributed across a volume of finite depth as a result of combustion of fuel vapors within the volume, and conduction and radiation of heat away from localized fire regions. A 100-m depth was assumed. Combustion of 2 g/cm^2 (1 to 2 g/cm^2 is a typical fuel loading for residential areas) in 1 h releases 100 kW/m^2 , or 1 kW/m^3 throughout the heat release volume. One- to four-hour burn times are reasonable; higher fuel loadings and longer burn times are plausible. A 7-km radius, 0.5-kW/m^3 fire would be typical for most city sizes, fuel loadings, and expected burning rates.

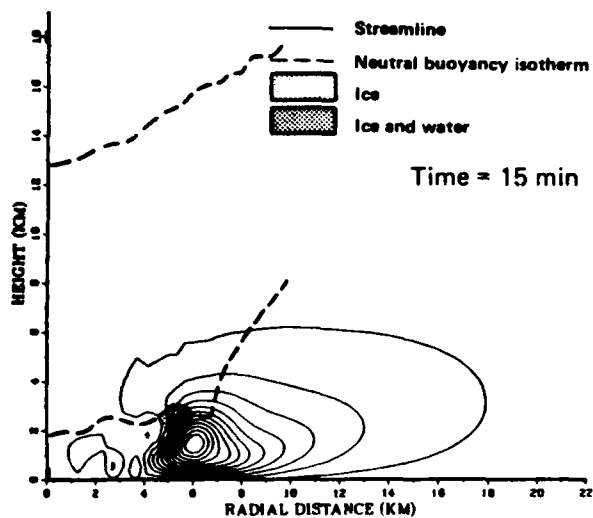
Table 1. Test matrix and summary of input conditions.

Case		Heating Rate (kW/m^3)	Fire Radius (km)
Moist	1	1.00	10
	2	0.50	10
	3	0.25	10
	4	1.00	7
	5	0.50	7
	6	0.25	7
	7	0.50	5
Dry	8	0.50	7
Grid	9	0.50	7

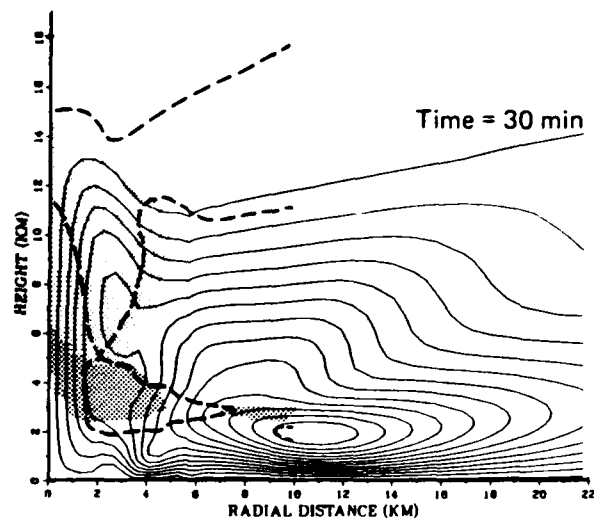
Simulations were also performed for fire intensities of 0.25, 0.50, and 1.00 kW/m³. These values represent either different fuel loadings or burn times. With the exception of one simulation in a dry atmosphere, all cases had identical atmospheric temperature and moisture structure. In addition, one case tested the effect of grid resolution. Results include smoke concentrations, distributions of liquid water and ice, and velocity, pressure, temperature, and density fields.

BASELINE WATER CLOUD.

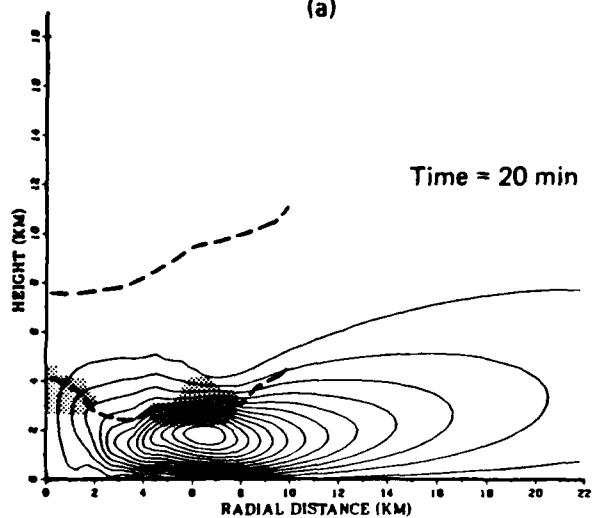
Many features of plume evolution are similar for all the fire intensities and sizes tested. Figures 1 and 2 show the development of the moisture and smoke clouds for a baseline case (7-km radius fire, 0.5-kW/m³ heat release rate). Initially, there is a warming of the lowest 2 km of the atmosphere above the fire. Air drawn radially inward toward the fire produces an upward mass flux. That, in turn, produces subsidence, slightly warming the entire troposphere at larger radii. The inflowing air initially turns up sharply near the outer perimeter of the fire and forms a small cloud (Fig. 1a). The cloud base forms at 2 km but rises slightly as the fire (heat release) warms the lower atmosphere. Gradually, the converging radial inflow establishes a strong updraft at the centerline (Fig. 1c). Later, as the buoyant air gains momentum, it is lofted considerably above its level of neutral buoyancy and becomes colder and more dense than the ambient air surrounding the plume (Figs. 1c-f). This cold air diverges radially at the top of the plume, falls downward, again overshoots equilibrium, and becomes warmer than the surrounding air. The process may continue several times at successively larger radii. Thus, the cloud consists of a warm core, sheathed by alternating cold and warm regions. The core is cloud free near the base because the air is sufficiently warm to be subsaturated. Similar cloud-free vaults are commonly observed in large thunderstorms. The low pressure caused by the heat of the fire produces subsidence and warming at high altitudes. Local thickening of the stratosphere may result.



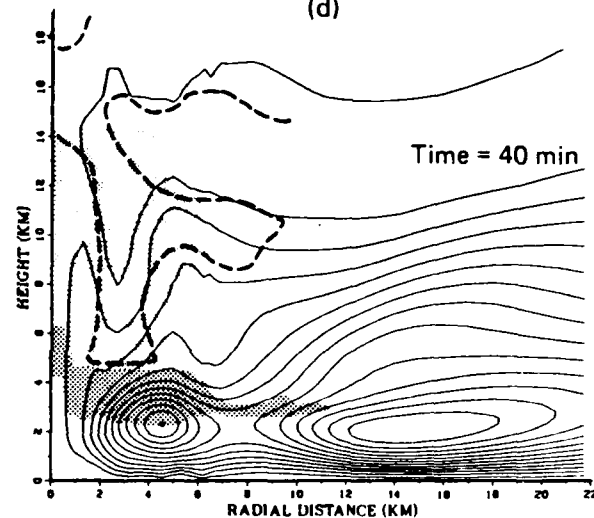
(a)



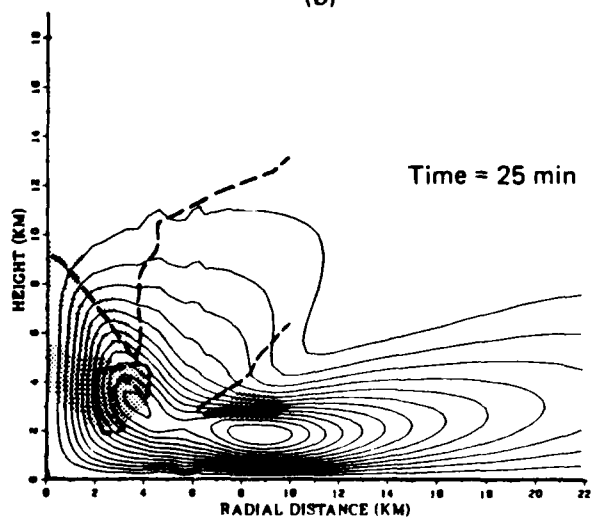
(d)



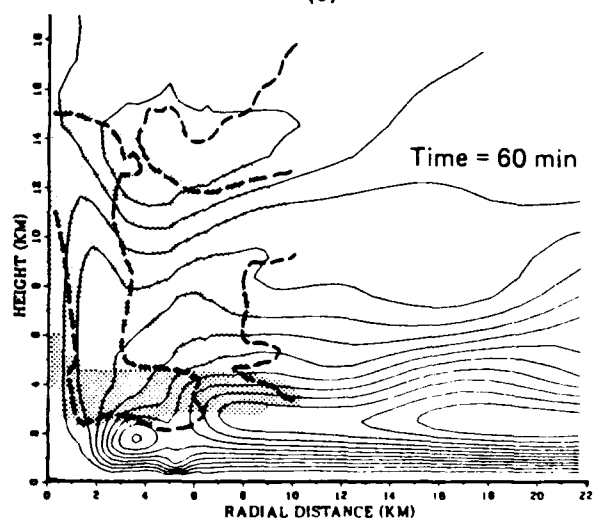
(b)



(e)

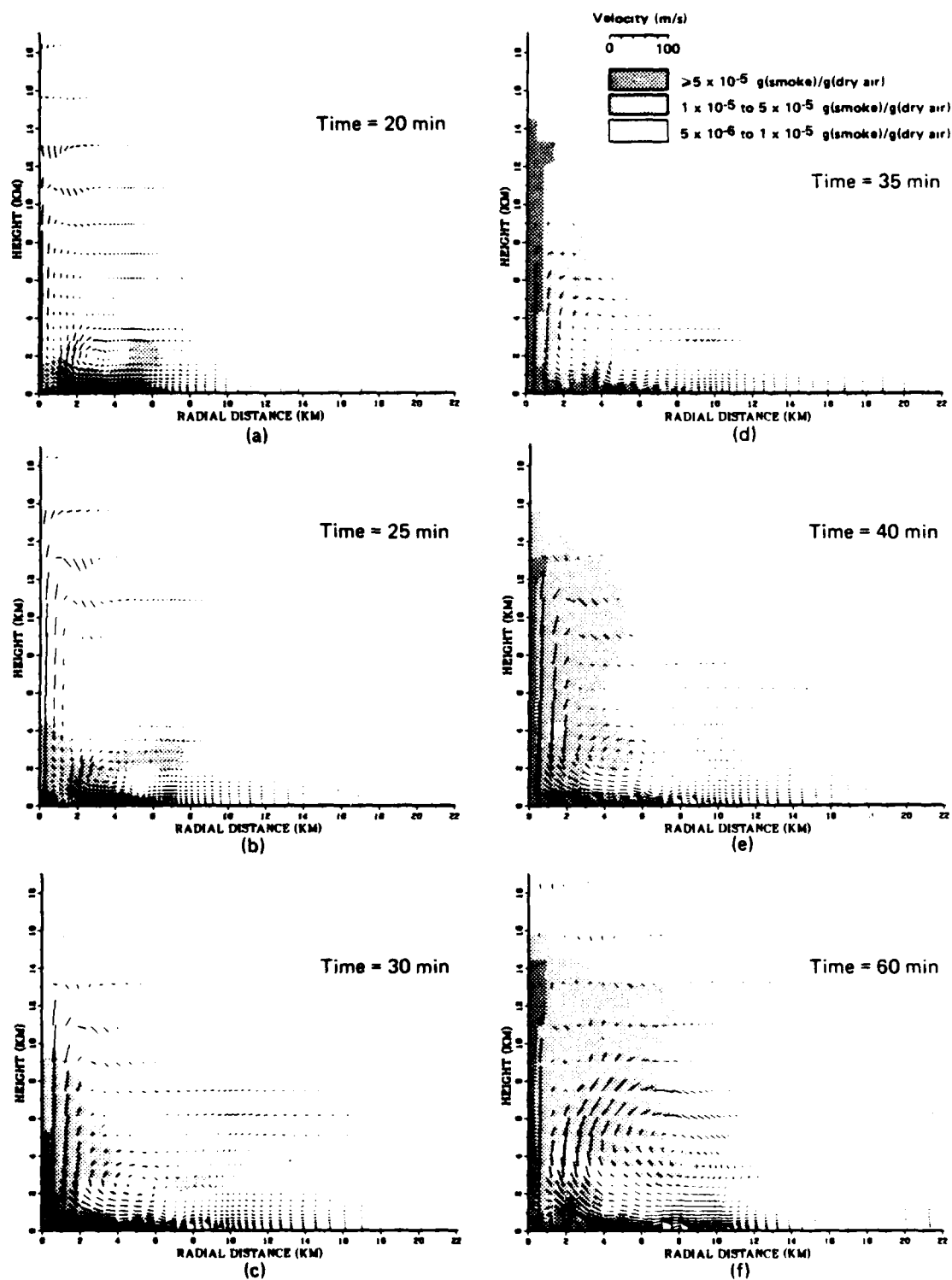


(c)



(f)

Figure 1. Moisture cloud simulation for 0.5-kW/m^3 heating rate and 7-km radius fire.



Note: Line segments denote velocity vectors.

Figure 2. Smoke cloud simulation for 0.5-kW/m^3 heating rate and 7-km radius fire.

Early (less than 20 min) in the evolution of the flow field, a small vortex develops at the fire edge. Vertical velocities in the plume core are influenced by the inward translation of that vortex. The sharp thermodynamic gradients at the fire edge cause a periodic reforming of the vortex near the fire perimeter, reducing the flow to the centerline. As a result, the vertical velocity of the plume core oscillates. Between 25 and 40 min, the plume top remains relatively stationary at about 14.5 km as a new, secondary circulation forms near the perimeter of the fire (Figs. 1c-e). When this pattern breaks down, allowing increased inflow to the centerline, the plume top rises to 17 km (not shown in Figs. 1 or 2) at 55 min. Later, as the outer secondary circulation reemerges, plume core velocities decrease and the top drops to about 15.5 km. The centerline oscillations cause large amplitude gravity waves that propagate radially outward (Fig. 1c-f).

BASELINE SMOKE CLOUD.

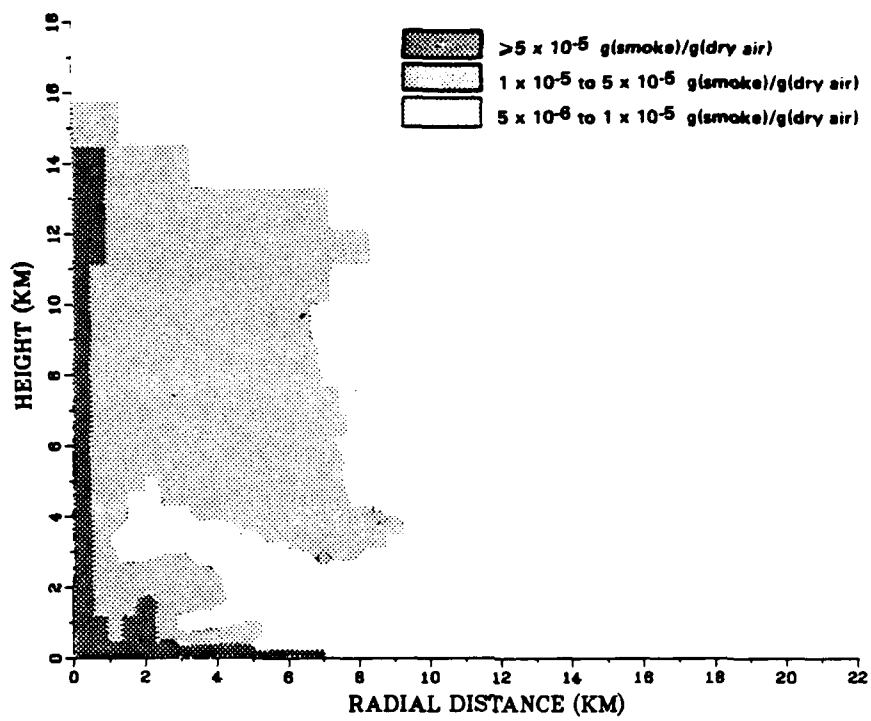
Figure 2 shows the smoke plume evolution for the same radius and heating rate as the moisture cloud sequence in Fig. 1. The smoke and moisture clouds coincide, except near the ground and centerline, where the rising warm air is subsaturated, and near the lower, outer edge, where smoke detrains from the moisture cloud (see Figs. 1f and 2f). The top of the smoke cloud approximately coincides with the top of the ice cloud at the top of the dome of cold air capping the warm plume core. The cold dome represents the maximum vertical extent reached by air from the surface, before its density excess causes it to fall back to lower altitudes. There is a well-defined boundary between the smoke cloud and the clear air outside it. The strongest concentrations of smoke lie near the source region and the plume core. The axisymmetric geometry of the simulation must be taken into account when considering smoke distribution. In Fig. 2f, over 70 percent of the total smoke mass lies outside the 4-km radius, despite the higher concentrations for smaller radii.

Large-scale mixing processes spread the smoke out from the plume core at higher altitudes. The vortex above the outer edge of the fire

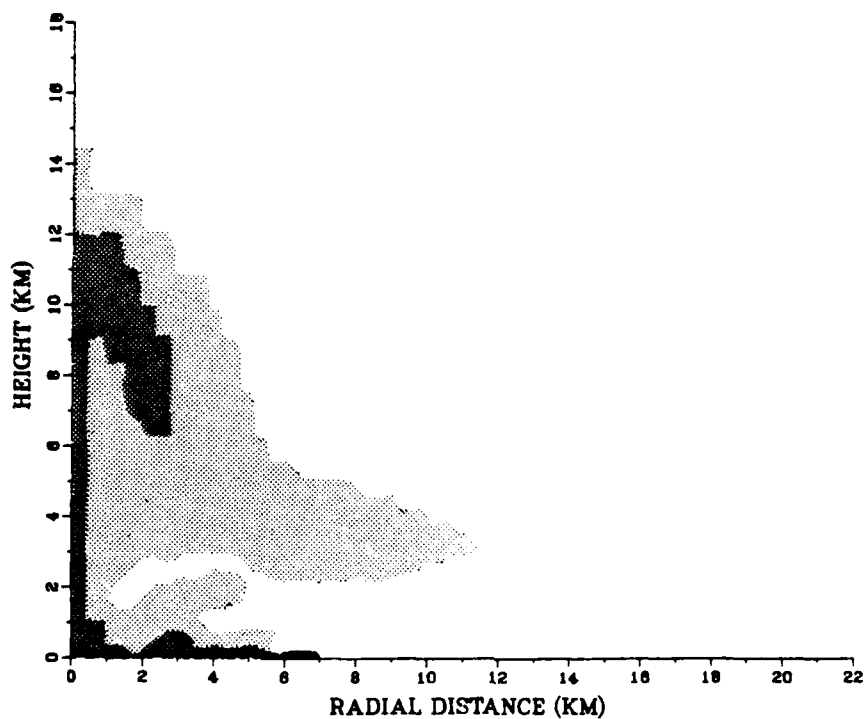
appears to fold pockets of clear ambient air into the smoke cloud (Fig. 2e). The vortex also seems to produce a downward rolling motion near the outer edge. Such features are consistent with observations of actual fire plumes. Except for the largest, most intense fires, smoke does not appear to be injected into the stratosphere. The maximum altitude reached by the smoke from a 0.5-kW/m^3 , 7-km fire was 17 km at 55 min. Simulations of more intense fires (1 kW/m^3) result in correspondingly higher plume rises (discussed later); lower heat release rates (0.25 kW/m^3) result in lower plume heights. The outcome is more or less independent of fire area, although a threshold size presumably exists [Small and Larson, 1984/5]. Comparable plume heights have been observed in nature [Manins, 1985]. The radial spreading of the smoke is independent of fire radius or heat release rate, and is roughly confined to a region less than twice the radius of the fire at 60 min. Upper-level winds would presumably transport smoke downwind, or diffusion would spread smoke radially, at later times. However, the large radial spread predicted by Penner, Haselman, and Edwards [1986] in quiescent atmospheres is not reproduced in these simulations.

COMPARISON BETWEEN DRY AND MOIST ATMOSPHERE.

Comparison of plume growth in a moist atmosphere to that in a dry atmosphere shows that smoke deposition is markedly affected by ambient moisture. Figure 3 shows the difference in plume growth after 60 min. The heat release rate is the same as the baseline case shown in Figs. 1 and 2 (0.5 kW/m^3 , 7-km radius). When plume motions reach the level of condensation and latent heat is released, buoyancy increases. Comparison of the maximum centerline velocities shows the effect of moisture. The velocity for the moist case (Fig. 3a) is 117 m/s and for the dry case (Fig. 3b) it is 81 m/s. Condensation produces high-velocity motions early in the development of the plume, carrying large concentrations of smoke to high altitudes. The smoke spreads out radially initially by advection and later by diffusion. The maximum vertical and radial extent of the smoke clouds are about the same, but the moist case deposits more smoke in the upper atmosphere.



(a)



(b)

Figure 3. Comparison of moist and dry smoke clouds for 0.5-kW/m³ heating rate and 7-km radius fire at 60 min.

The simulations clearly show condensation early in the plume evolution. Figure 1 shows initial condensation at 15 min (Fig. 1a) and shows ice developing within 25 min (Fig. 1c). Ice formation is generally indicative of the onset of precipitation. Although not explicitly modeled, precipitation early in the plume development suggests that some of the dense sooty smoke released by the fire in its early stages may be scavenged. That appears to be consistent with observations of rain generated by wildland fires and of black rain generated by several fires during World War II [Committee for the Compilation of Materials on Damage Caused by the Atomic Bombs in Hiroshima and Nagasaki, 1981]. The efficiency of smoke particles, however, as cloud condensation nuclei, is not well known, and only a small fraction may actually be scavenged [Pittock, et al., 1986].

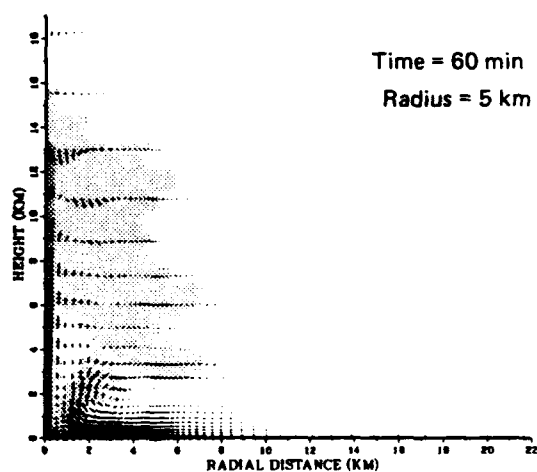
EFFECT OF FIRE AREA AND HEATING RATE.

Clouds produced by fires of three different radii but equal heat release rates are shown in Figs. 4a through 4c, and clouds produced by fires of constant radii but three different heat release rates are shown in Figs. 4d through 4f. Figure 4 shows that a concentrated heat source deposits smoke much higher in the atmosphere than does a source of equal volume-integrated magnitude that is spread over a larger surface area. Figure 4a through 4c shows that plume height at 60 min is roughly the same (it actually decreases slightly from 17.5 to 15.5 km) as the fire radius increases, even though total heat release increases by a factor of 4. In contrast, Figs. 4d through 4f show that plume height increases (from 9 to 23 km) in direct response to increased heat release rate for fires of the same radius. Clearly, classical plume theories are unsuitable for modeling large-scale fires--they use a point source, rather than distributing energy across a finite area.

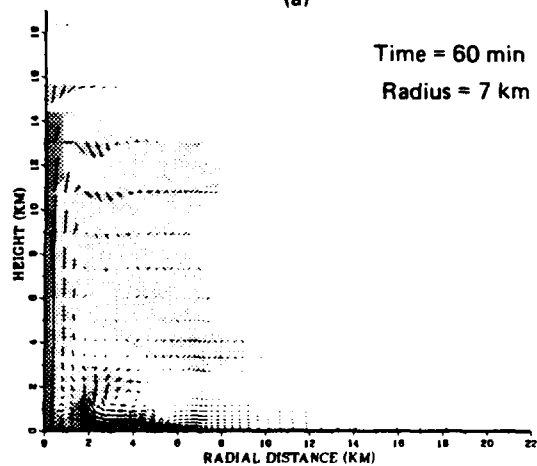
FIRE WINDS.

Figure 5 shows the fire wind velocity at 8 km for the 7-km baseline radius (1 km outside the fire volume) and the three heating rates. Maximum inflow velocities occur at early times and near the

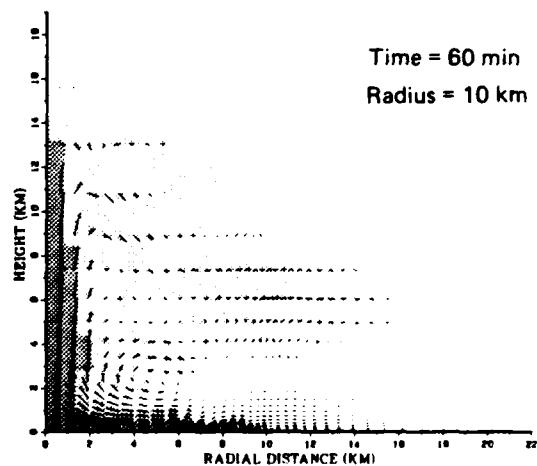
VARIABLE FIRE RADIUS
(Heating rate = 0.5 kW/m^3)



(a)

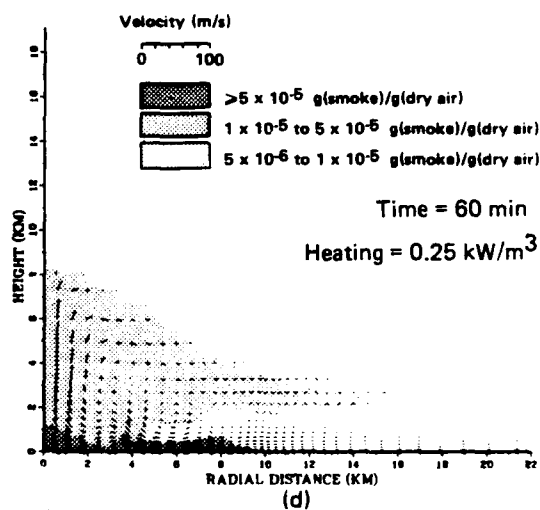


(b)

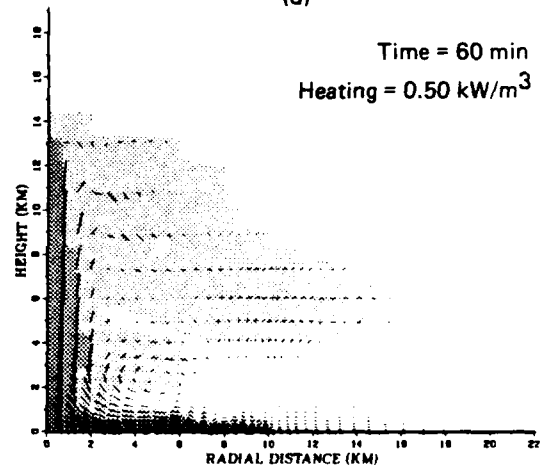


(c)

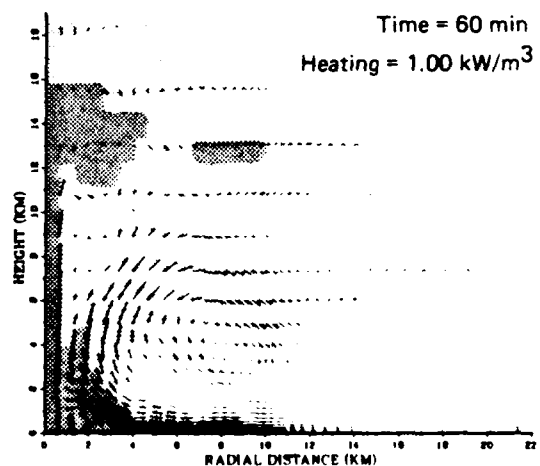
VARIABLE HEATING RATE
(Fire radius = 10 km)



(d)



(e)



(f)

Figure 4. Comparison of smoke clouds obtained at 60 min for constant heating and variable radius and for constant radius and variable heating.

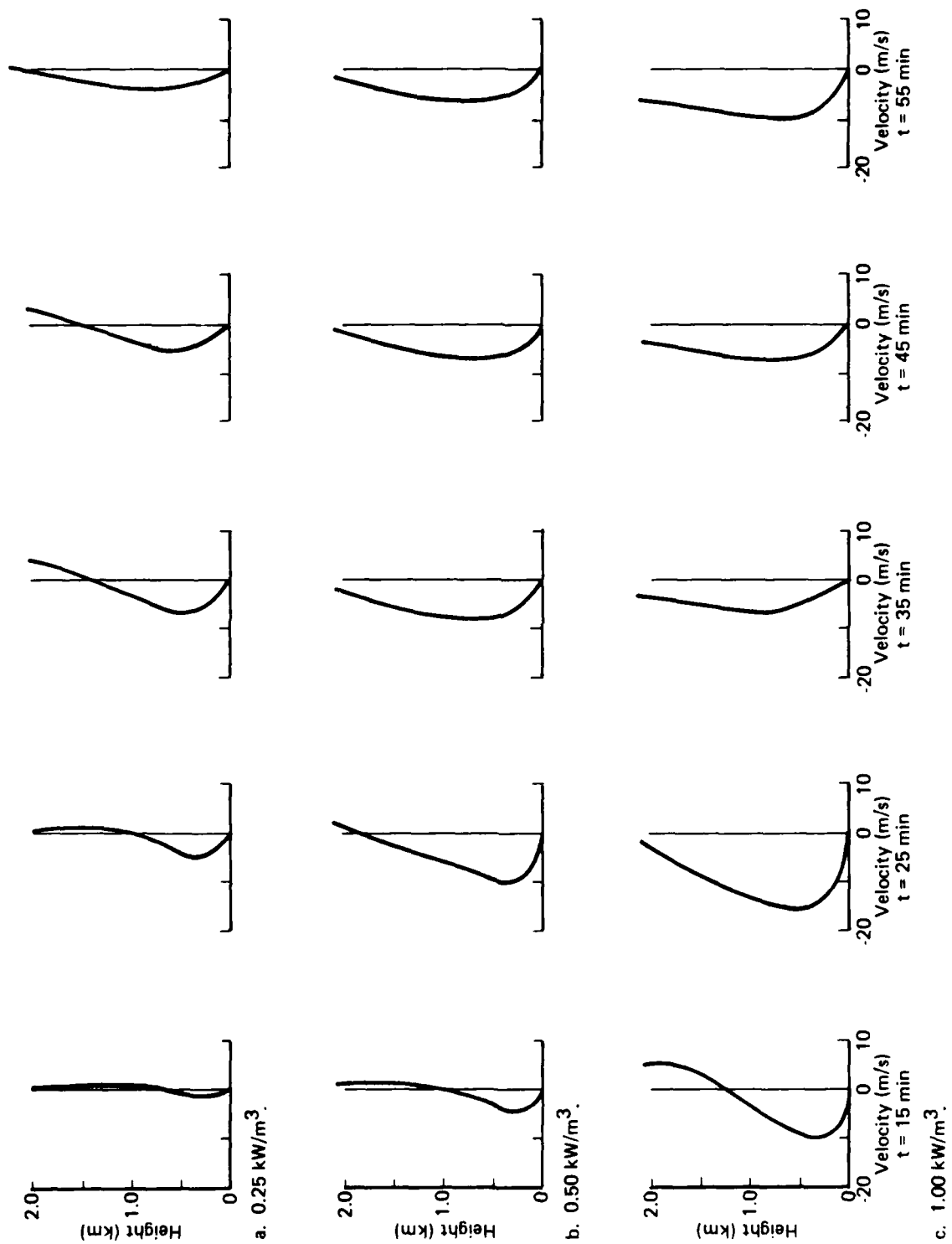
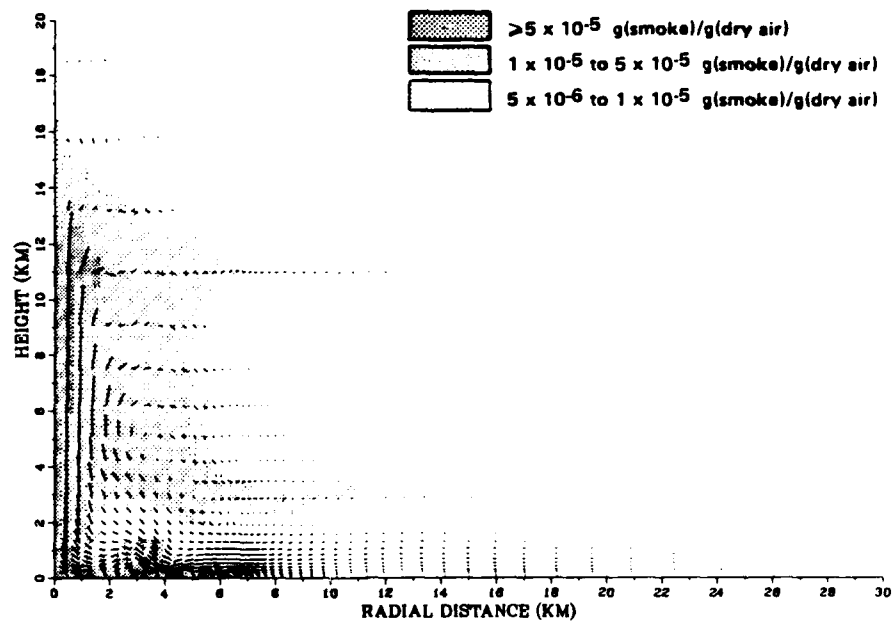


Figure 5. Radial velocity at 8-km radius for three heating rates for 7-km radius fire at 10 min intervals.

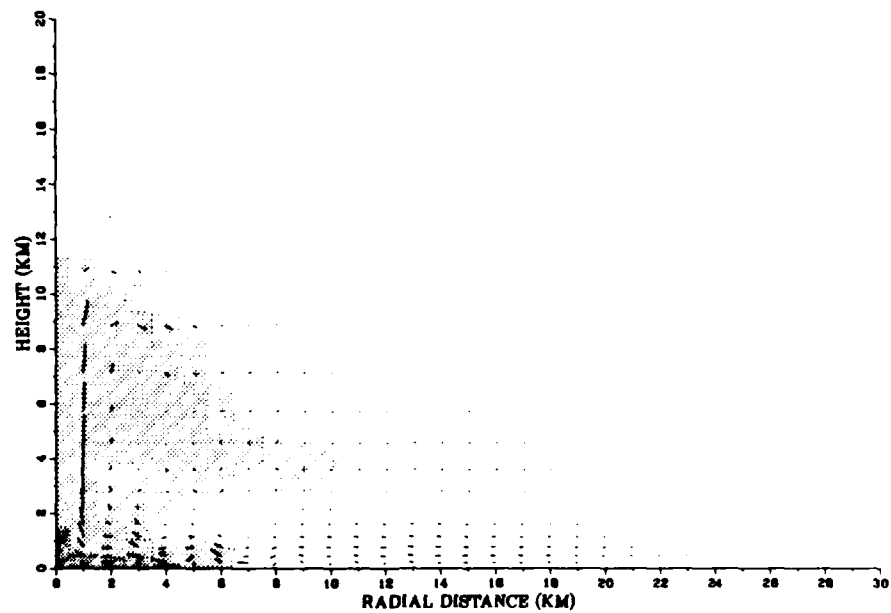
ground. Later, the inflow wind speed is lower but occupies a deeper layer, so the depth-integrated inflow remains nearly constant after 25 min. There is outflow aloft associated with the return circulations shown in Fig. 1. The outflow is most intense at early times when the azimuthally aligned vortex lies just over the heating volume circumference. The mean fire wind velocities near the ground are surprisingly low in comparison to observations of fire winds associated with large urban fires [Committee for the Compilation of Materials on Damage Caused by the Atomic Bombs in Hiroshima and Nagasaki, 1981; Small and Larson, 1984]. The maximum is 20 m/s but the average is approximately 10 m/s. Observations of fire winds are highly subjective and reported wind speeds are not usually based on instrumented measurements. Winds may be channeled by streets and structures--such winds may not be representative of the mean flow. Moreover, the model is two-dimensional and does not simulate channeled winds nor those associated with local concentrations of vorticity.

EFFECT OF GRID RESOLUTION.

The effect on the baseline case of a reduction of grid resolution was tested by changing the radial spacing from an average spacing of about 270 m near the centerline (increasing by 15 percent for successive grid points in the positive radial direction) to a constant 1 km. The vertical spacing was changed from 100 m near the ground, (increasing by 20 percent for successive grid points above the ground) to 1000 m (increasing by 20 percent for successive grid points above the ground). The lower resolution case is comparable to that used in three-dimensional simulations. Figure 6 shows the effect of reduced resolution on the baseline smoke cloud (Fig. 6a). Clearly, smoke is not lofted as high in the low-resolution case as it is in the high-resolution case for identical heating and fire size. There appears to be a greater concentration of smoke at low altitude for the low-resolution case. The reasons for such dramatic differences are unclear, but the higher resolution is expected to more accurately simulate the thermodynamics of smoke-cloud evolution. Lower resolution, two- and three-dimensional results [Penner, Haselman, and Edwards,



a. Fine grid.



b. Coarse grid.

Figure 6. Smoke clouds at 45 min for fire 7 km in radius with 0.50 kW/m^3 volume heating rate.

1986; and Tripoli and Kang, 1987] in fact, do sometimes show greater horizontal smoke spreading and lower lofting.

INDIVIDUAL CASES.

In addition to the general comparisons of cases with differing heating rates, radii, and moisture content in this section, we highlight some features of the individual moist-atmosphere simulations. Plots of water and smoke clouds are shown in Figs. 7 through 15 and 16 through 24, respectively.

Case 1: High Heating Rate (1.00 kW/m^3), Large Radius (10 km).

A strong circulation initially occurs at the fire edge and lasts 20 min. During that period, there is little penetration radially to the centerline and little vertical motion to the condensation level. Maximum lofting into the tropopause occurs at 35 min. After that time, two low-level, azimuthally aligned vortices appear within the troposphere and divert the flow from the centerline. The fire initially heats the lower levels. The rising air overshoots its level of equilibrium and becomes cooler than the surrounding air. Due to adiabatic compression, air in the downward leg of the circulation becomes warmer than ambient. The fire continually heats the lower levels, particularly near the centerline. Shear stress appears to carry air aloft (despite its negative buoyancy) at the plume edge. A weak secondary circulation within the upper tropopause and lower stratosphere carries air downward near the centerline and is associated with the low pressure caused by the fire heat near the surface.

Case 2: Medium Heating Rate (0.50 kW/m^3), Large Radius (10 km).

Streamline gradients near the ground indicate large mass flux and high wind into the fire region. Cloud formation begins at 20 min. The cloud base is elevated near the centerline, forming a cloud-free vault after 30 min. Again, the formation of the double azimuthally oriented vortex configuration corresponds to a decrease in radial inflow to the centerline. The temperature perturbation from ambient

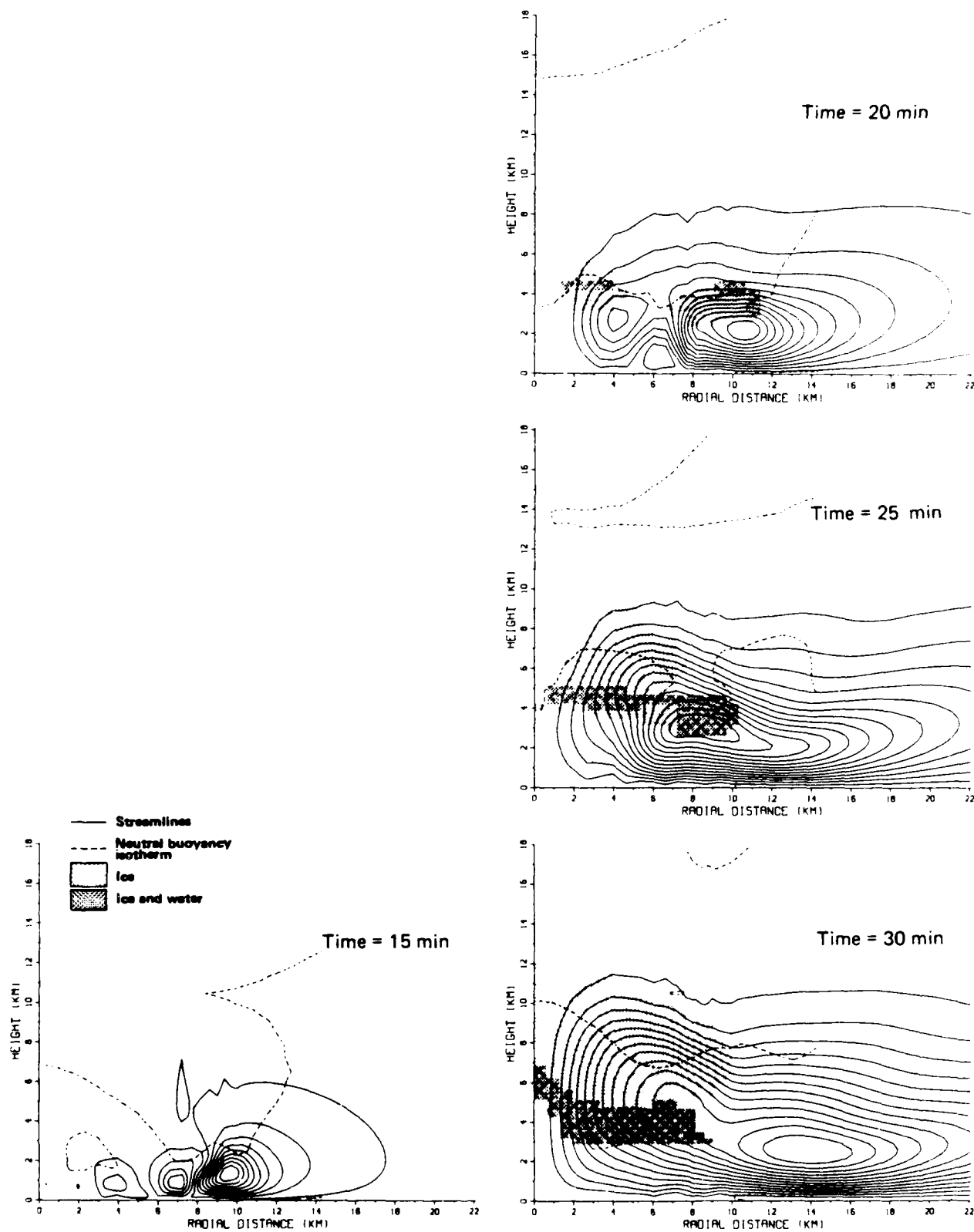


Figure 7. Moisture cloud, streamlines, and neutral buoyancy isotherms for case 1--high heating rate (1.00 kW/m^3), large radius (10 km).

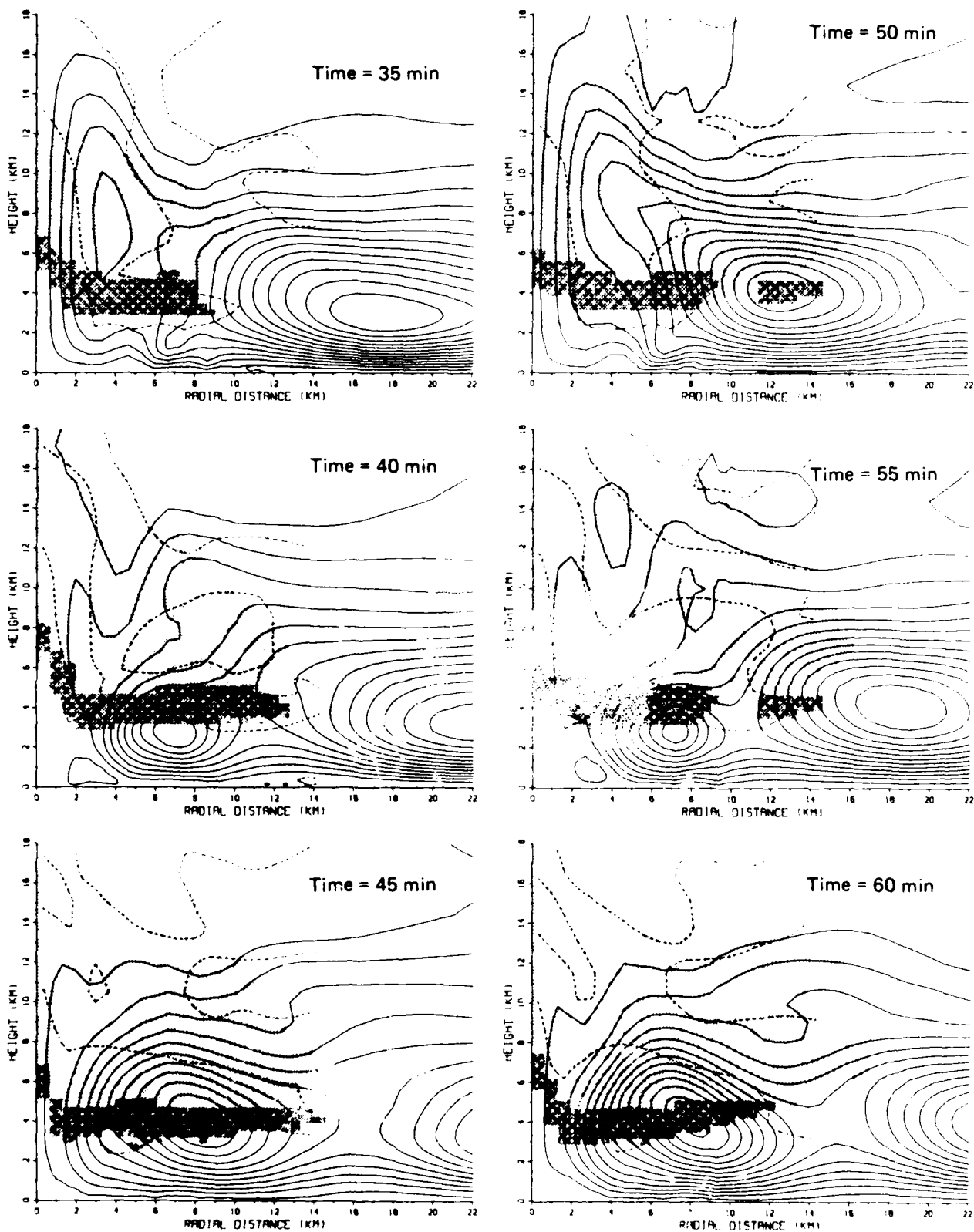


Figure 7. Moisture cloud, streamlines, and neutral buoyancy isotherms for case 1--high heating rate (1.00 kW/m^3), large radius (10 km) (Concluded).

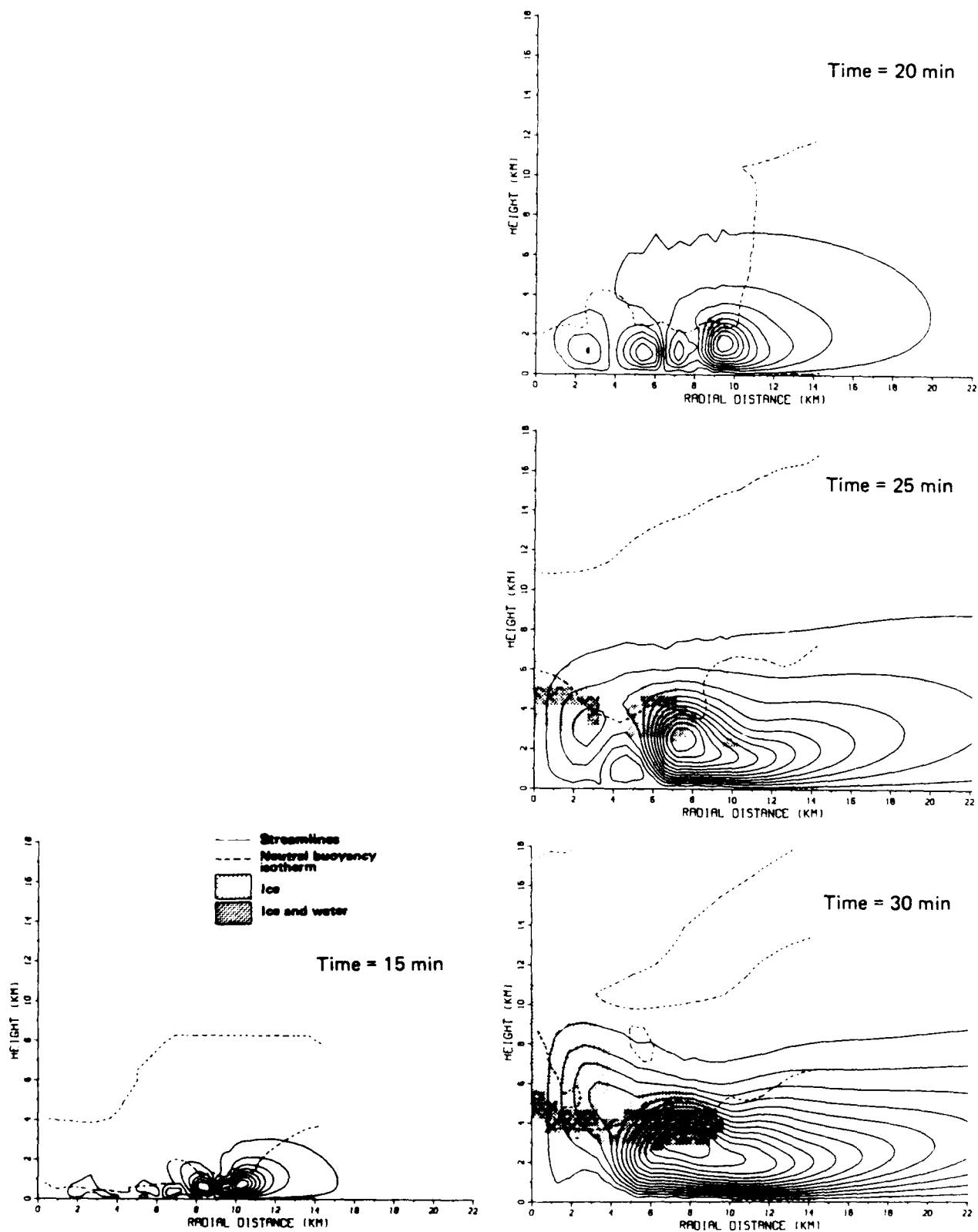


Figure 8. Moisture cloud, streamlines, and neutral buoyancy isotherms for case 2--medium heating rate (0.50 kW/m^3), large radius (10 km).

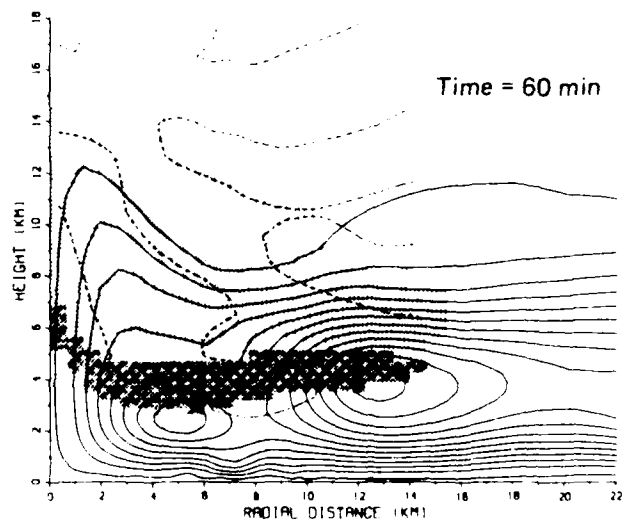
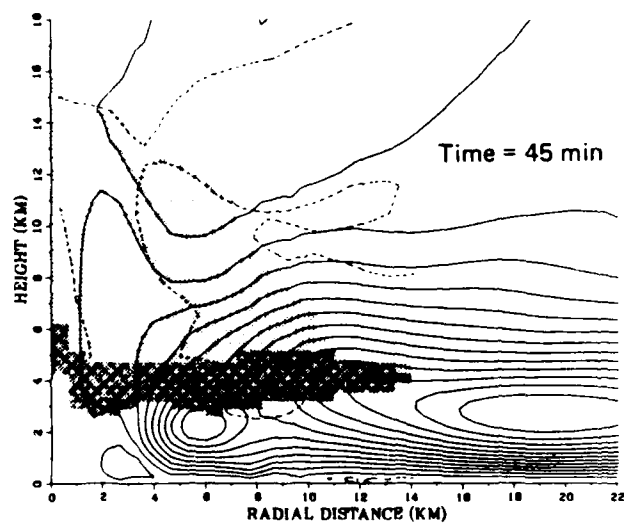
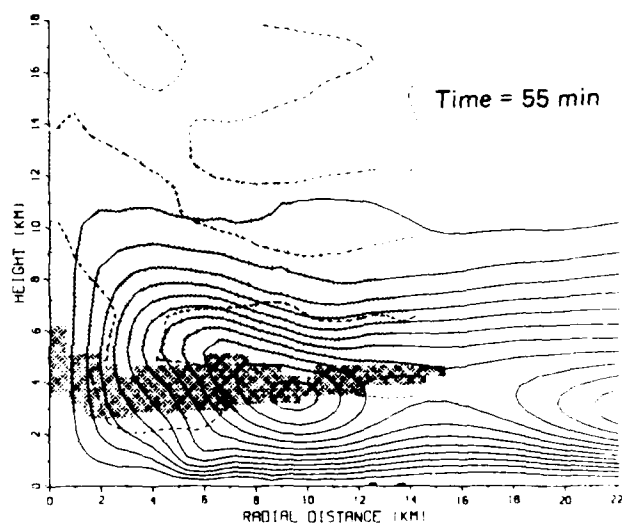
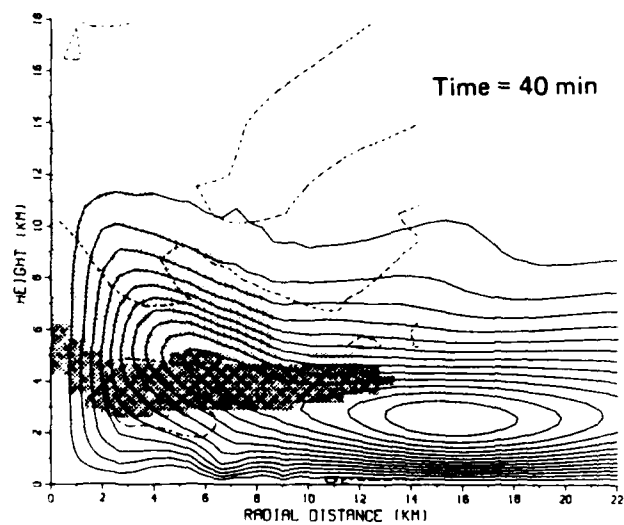
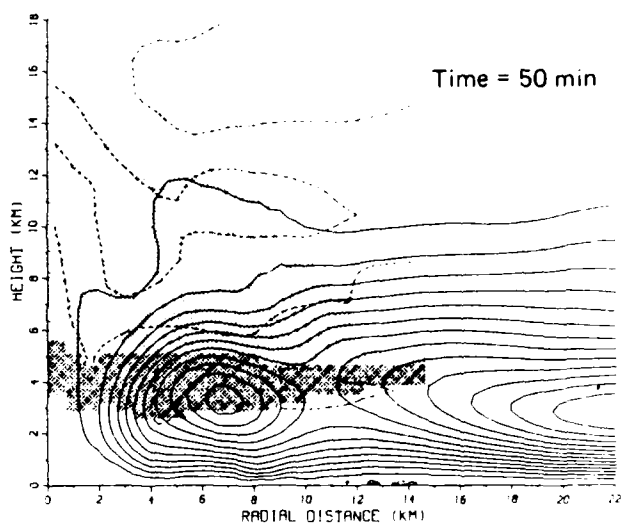
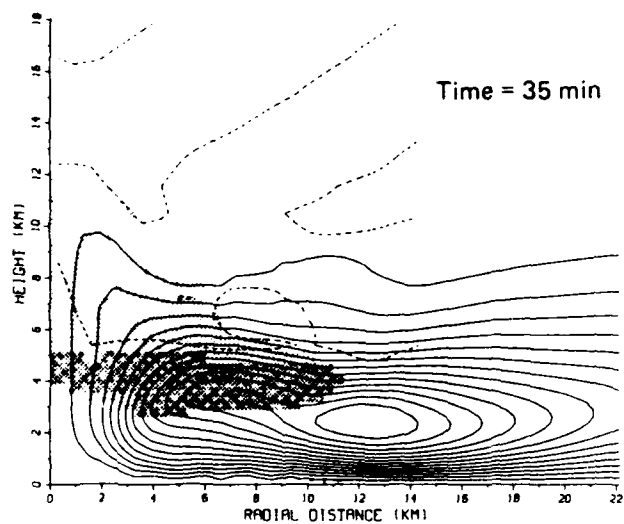


Figure 8. Moisture cloud, streamlines, and neutral buoyancy isotherms for case 2--medium heating rate (0.50 kW/m^3), large radius (10 km) (Concluded).

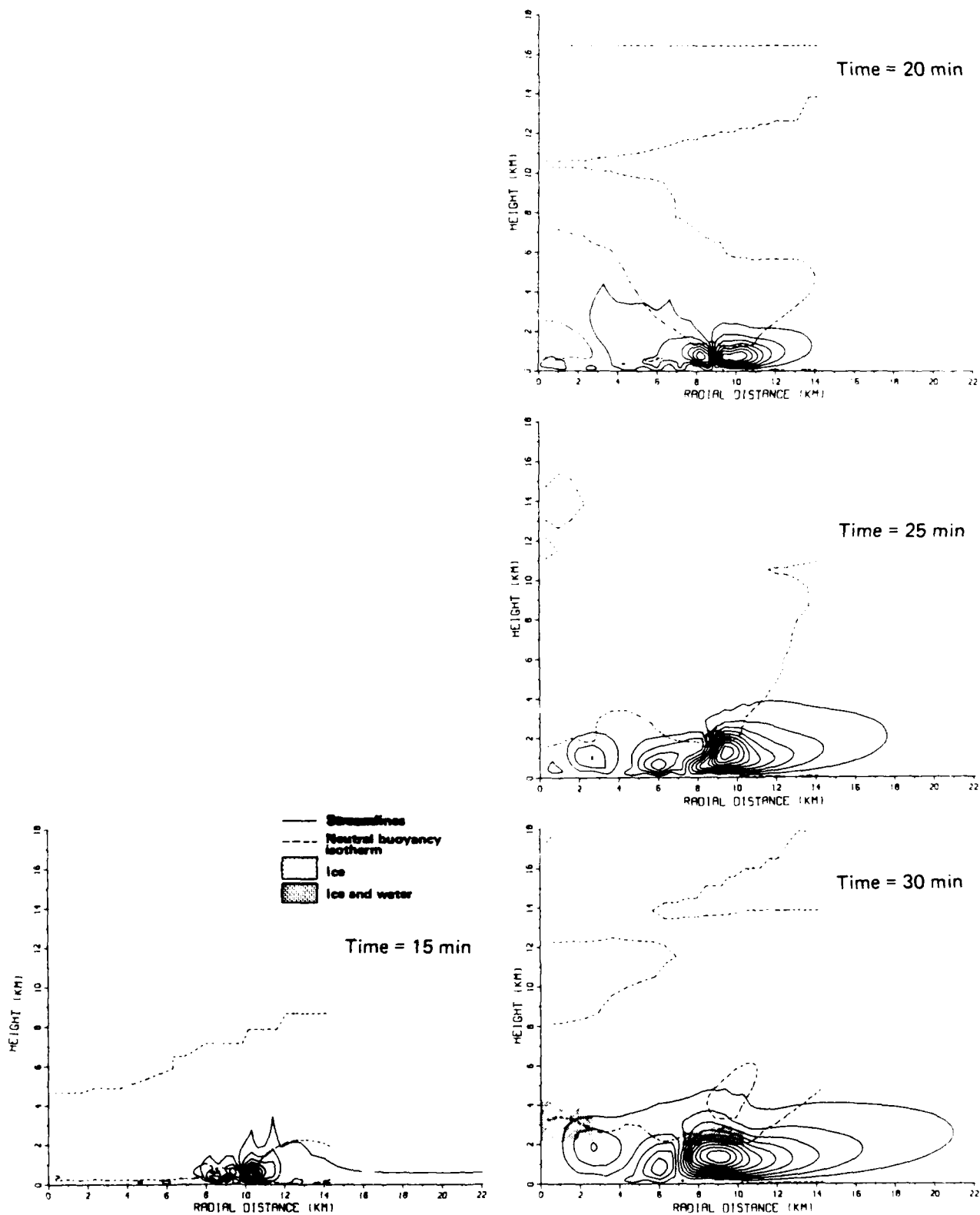


Figure 9. Moisture cloud, streamlines, and neutral buoyancy isotherms for case 3--low heating rate (0.25 kW/m^3), large radius (10 km).

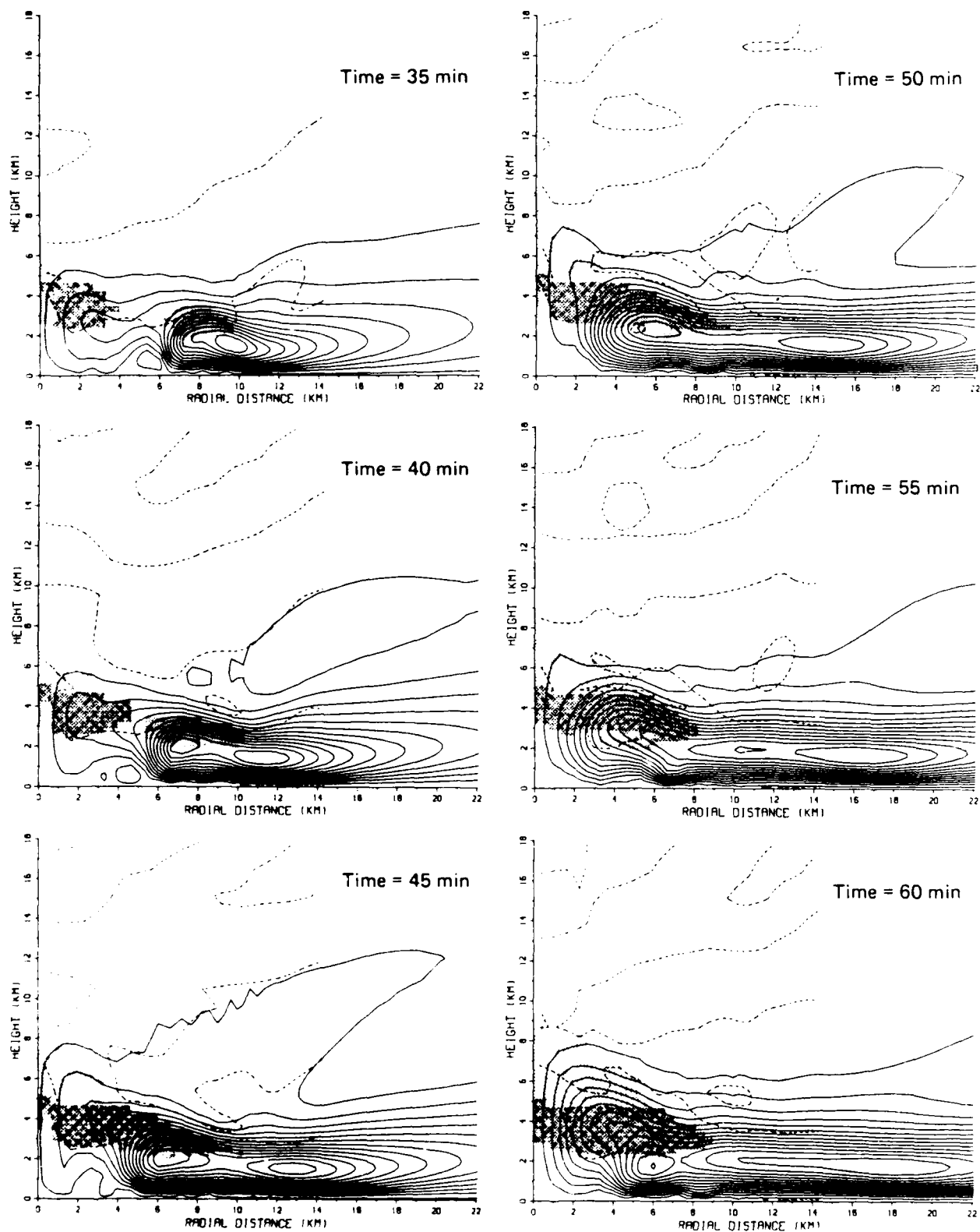


Figure 9. Moisture cloud, streamlines, and neutral buoyancy isotherms for case 3--low heating rate (0.25 kW/m^3), large radius (10 km) (Concluded).

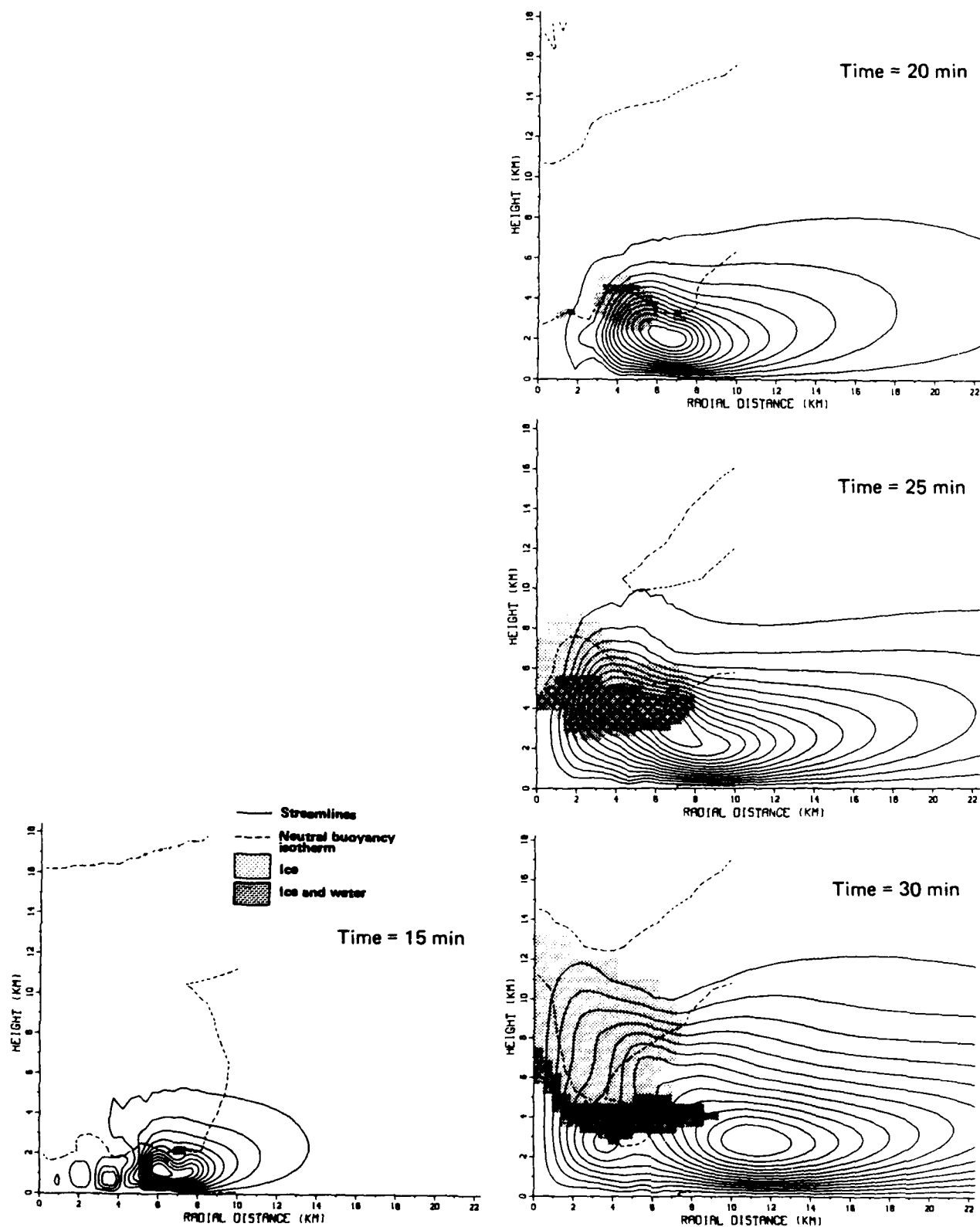


Figure 10. Moisture cloud, streamlines, and neutral buoyancy isotherms for case 4--high heating rate (1.00 kW/m^3), medium radius (7 km).

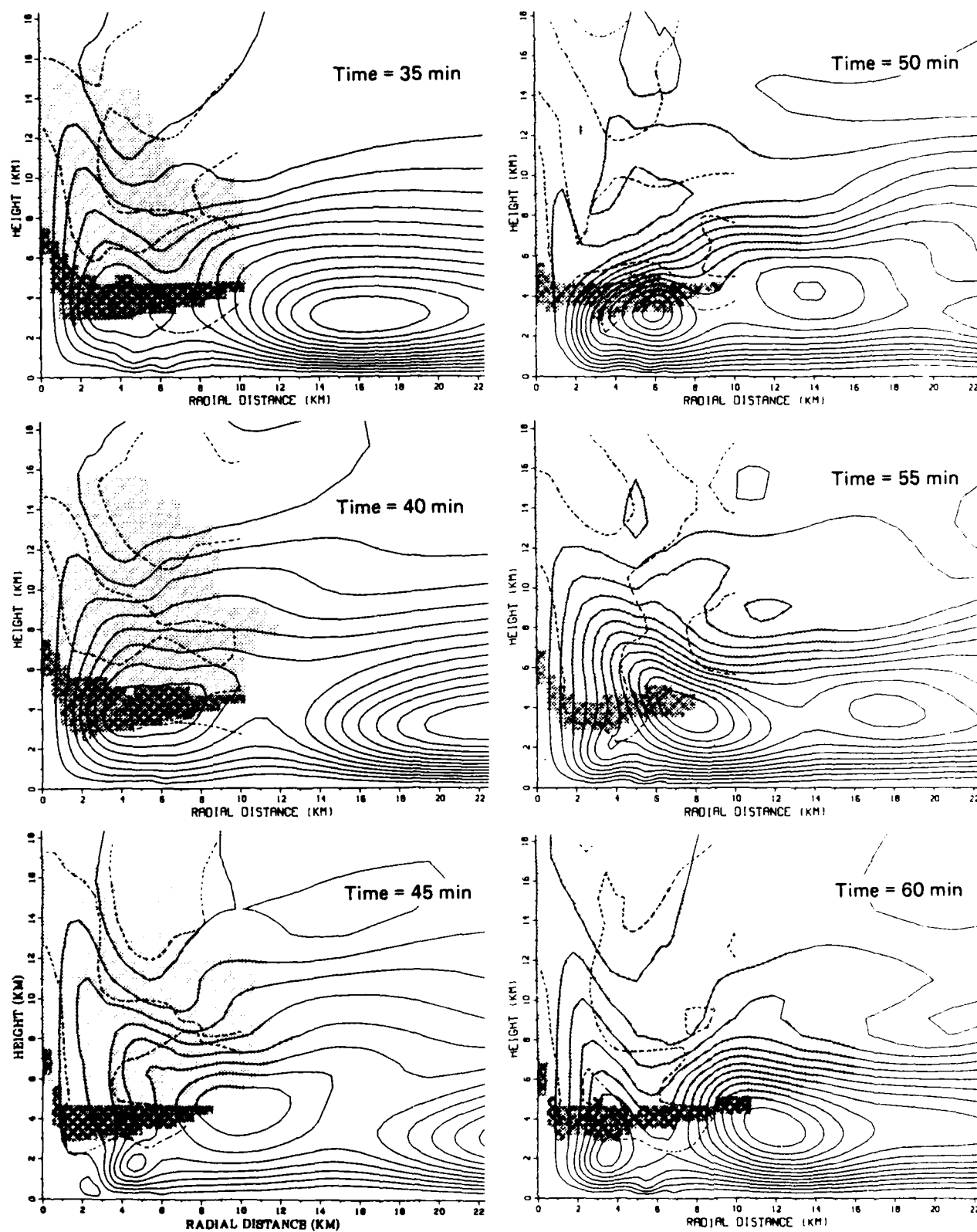


Figure 10. Moisture cloud, streamlines, and neutral buoyancy isotherms for case 4--high heating rate (1.00 kW/m^3), medium radius (7 km) (Concluded).

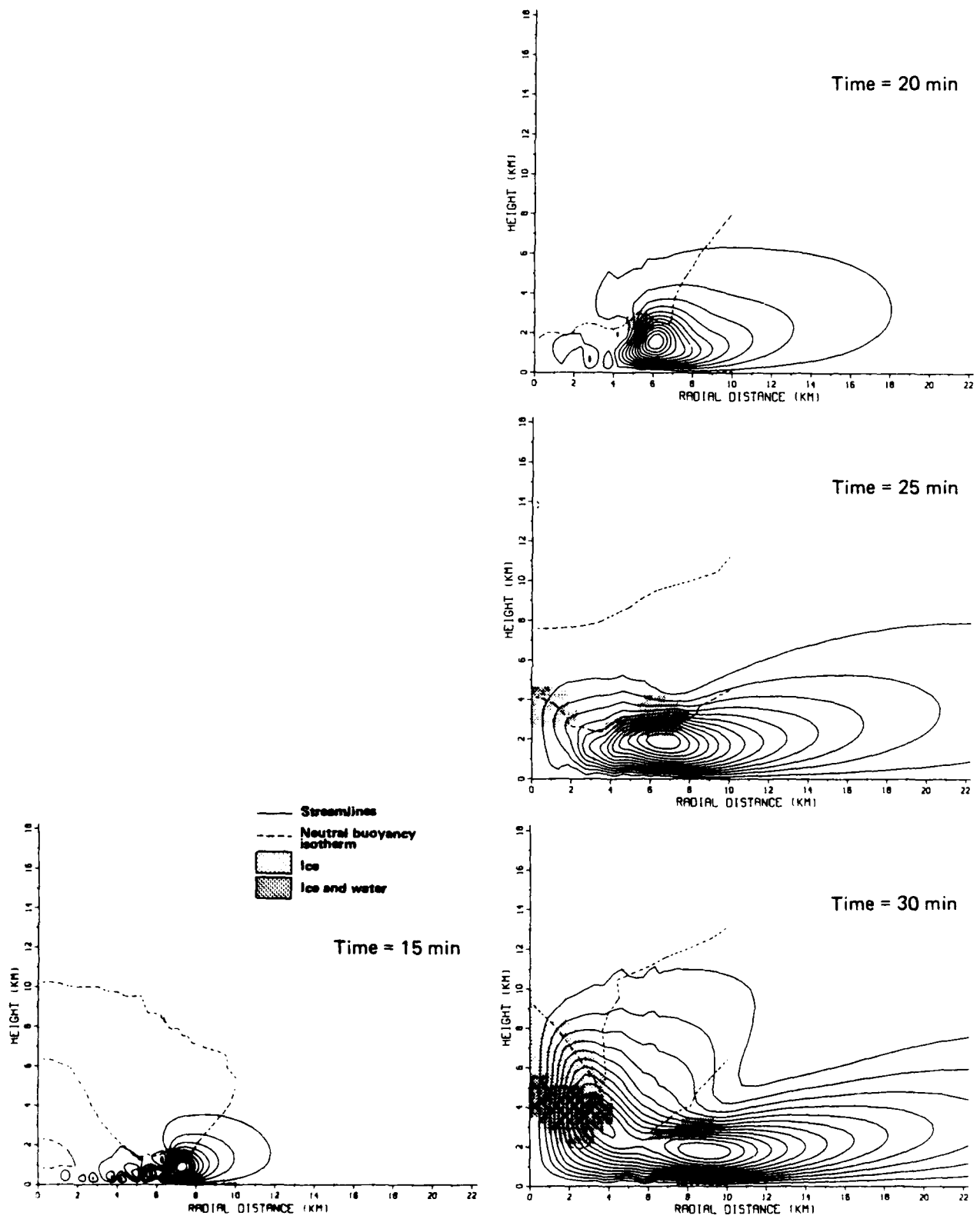


Figure 11. Moisture cloud, streamlines, and neutral buoyancy isotherms for case 5--medium heating rate (0.50 kW/m^3), medium radius (7 km).

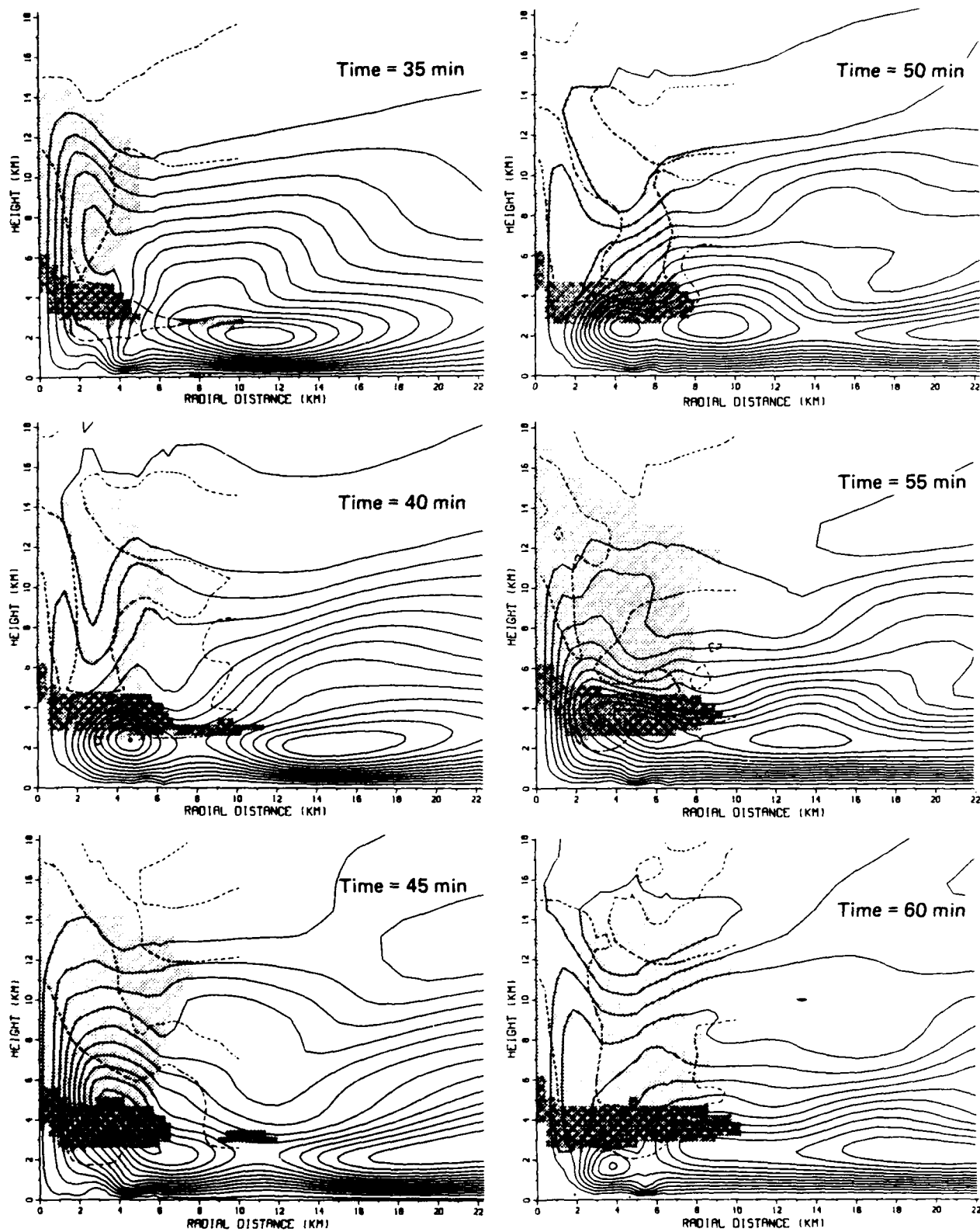


Figure 11. Moisture cloud, streamlines, and neutral buoyancy isotherms for case 5--medium heating rate (0.50 kW/m^3), medium radius (7 km) (Concluded).

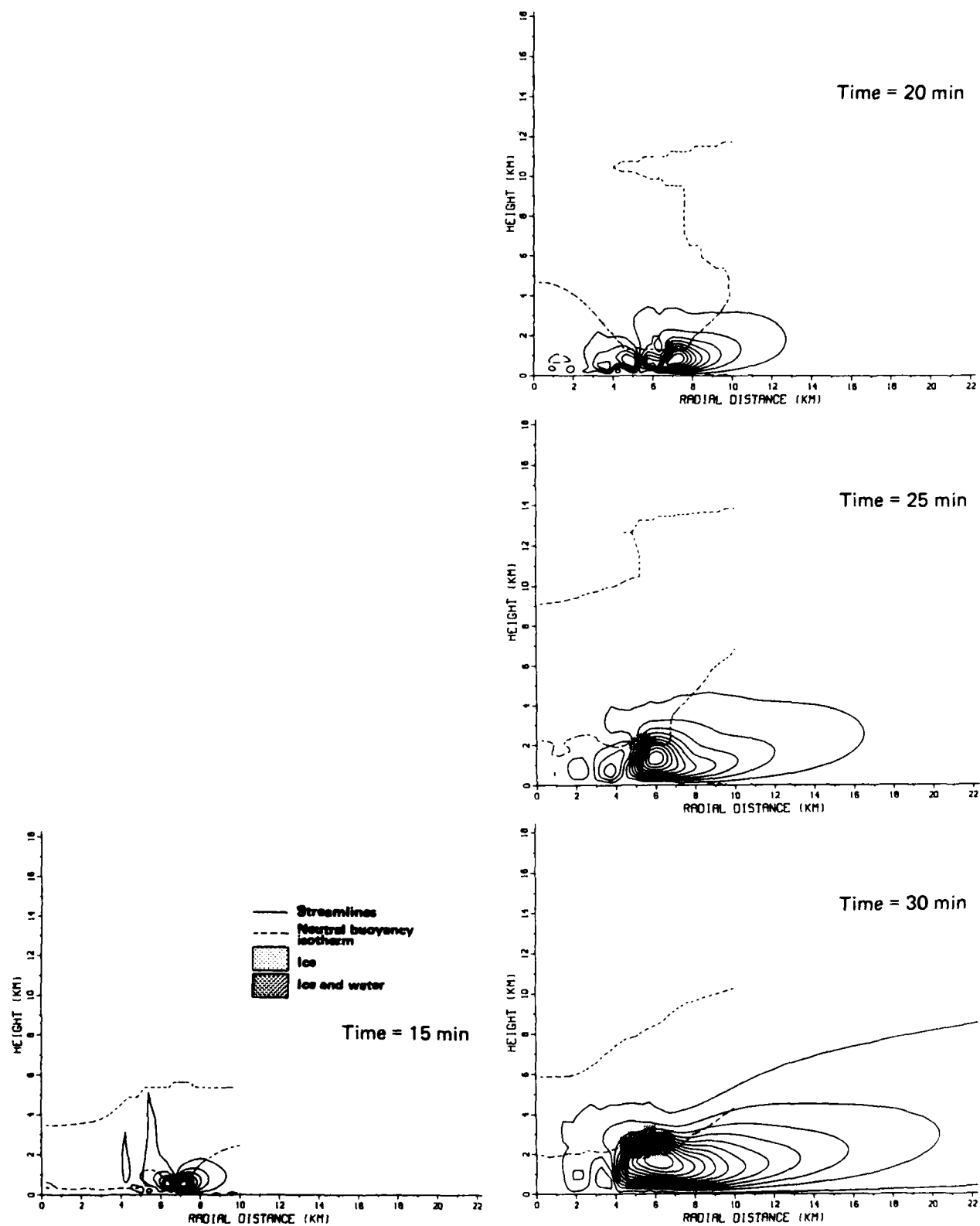


Figure 12. Moisture cloud, streamlines, and neutral buoyancy isotherms for case 6--low heating rate (0.25 kW/m^3), medium radius (7 km).

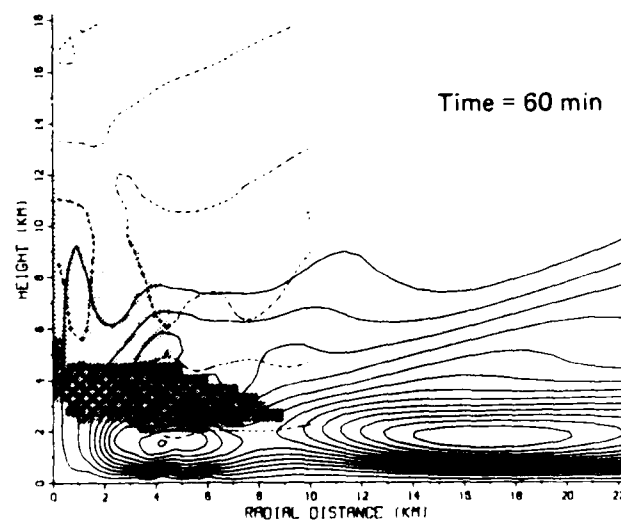
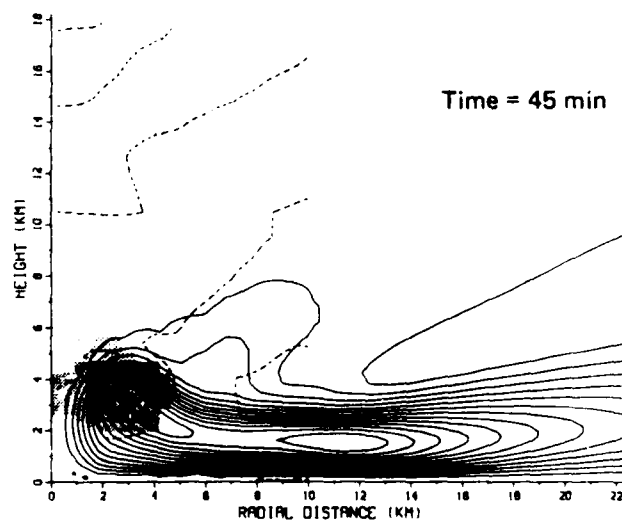
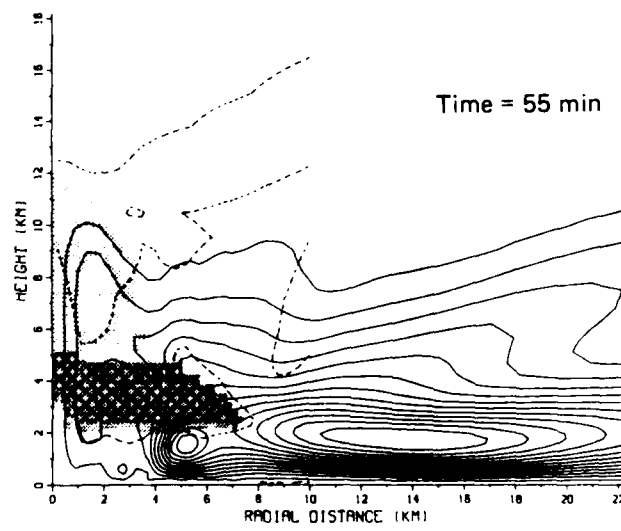
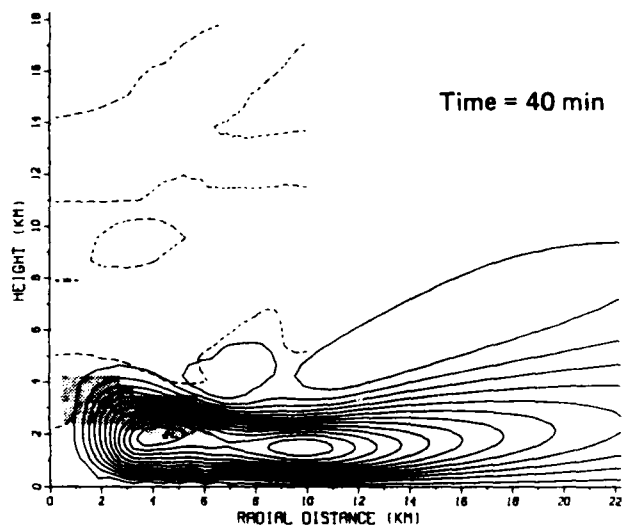
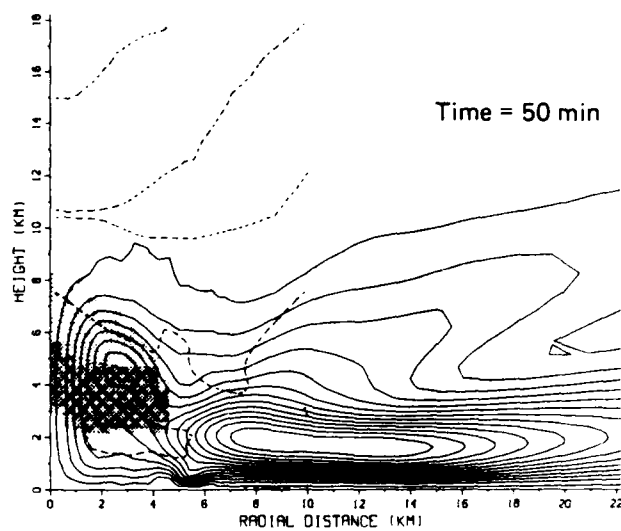
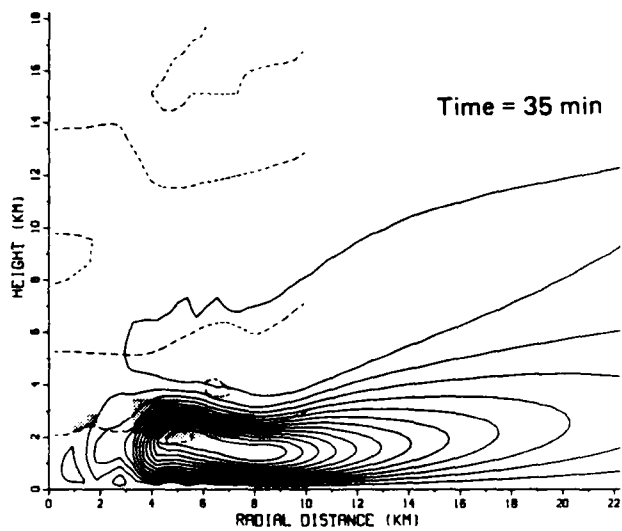


Figure 12. Moisture cloud, streamlines, and neutral buoyancy isotherms for case 6--low heating rate (0.25 kW/m^3), medium radius (7 km) (Concluded).

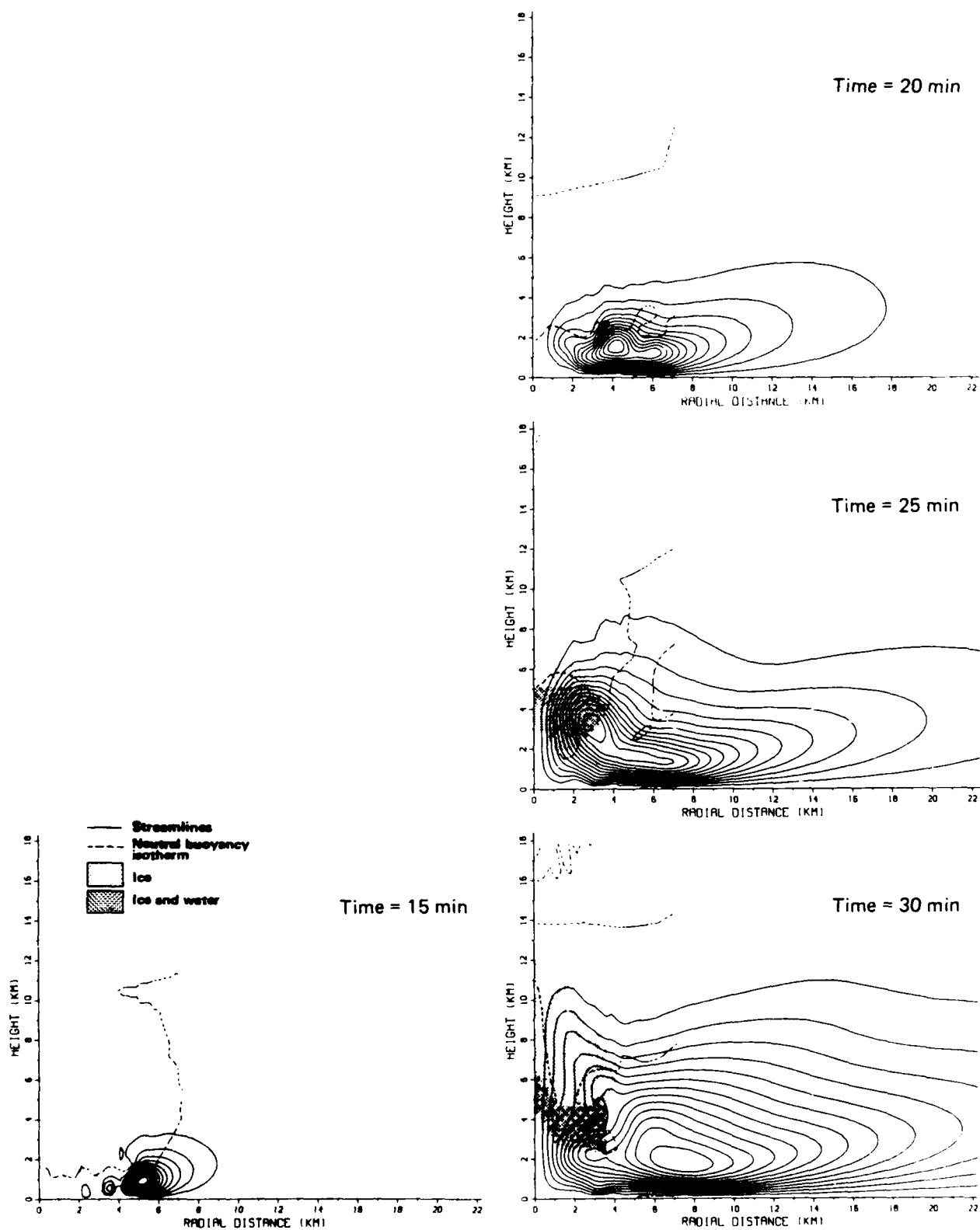


Figure 13. Moisture cloud, streamlines, and neutral buoyancy isotherms for case 7--medium heating rate (0.50 kW/m^3), small radius (5 km).

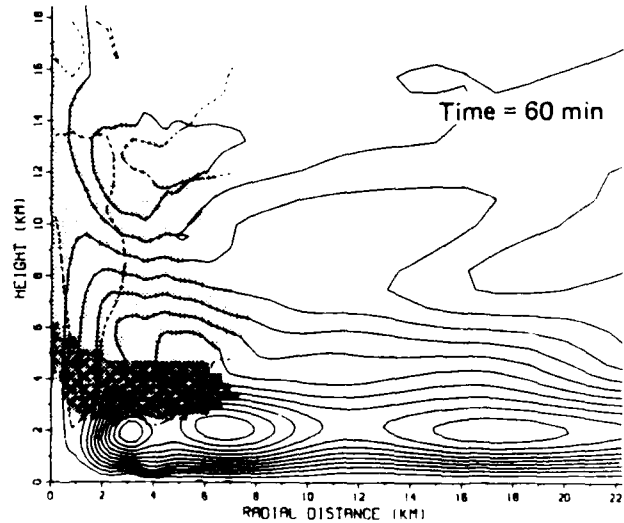
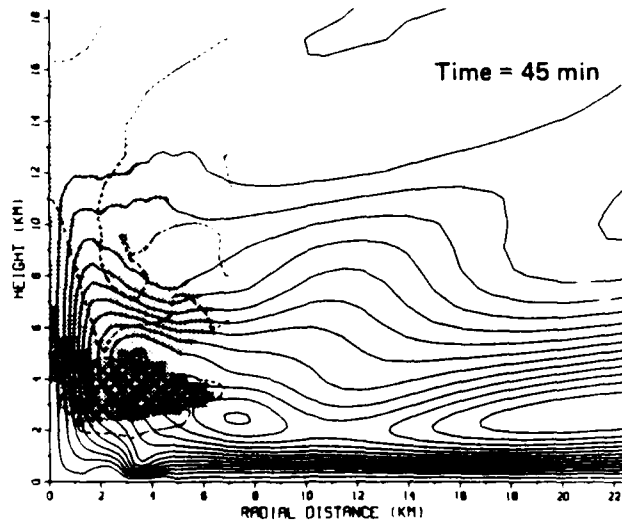
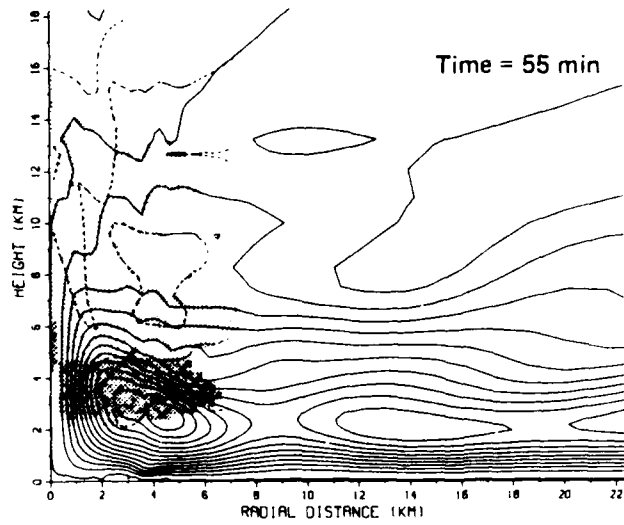
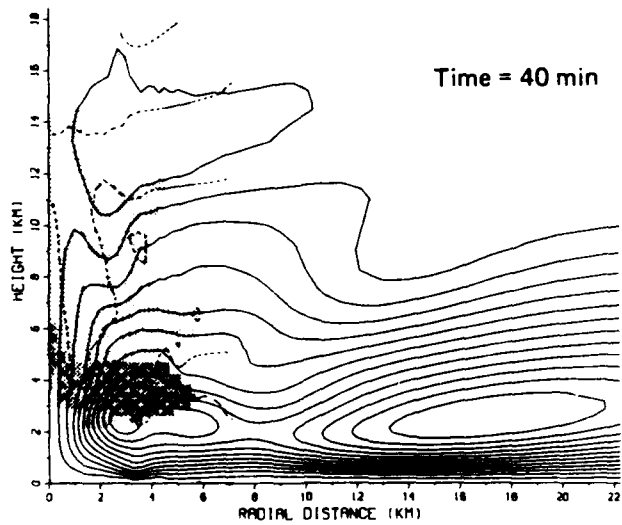
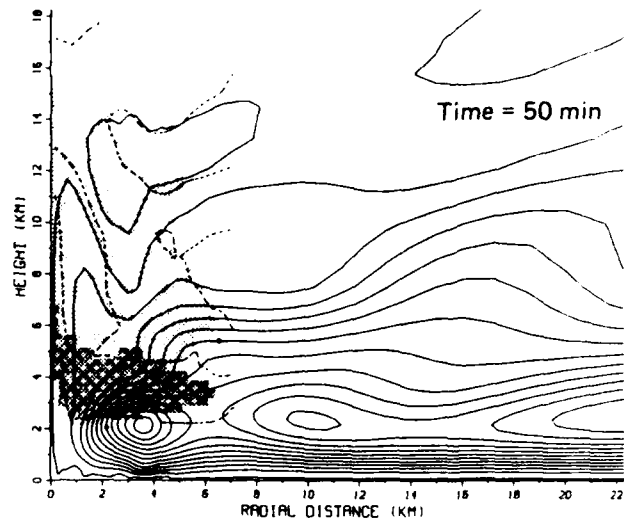
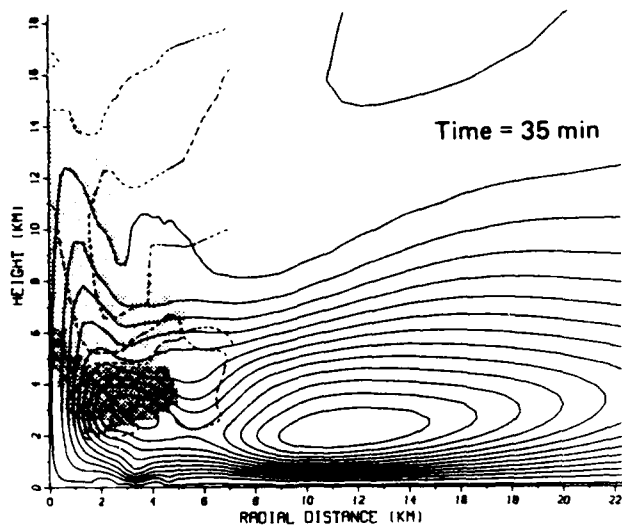


Figure 13. Moisture cloud, streamlines, and neutral buoyancy isotherms for case 7--medium heating rate (0.50 kW/m^3), small radius (5 km) (Concluded).

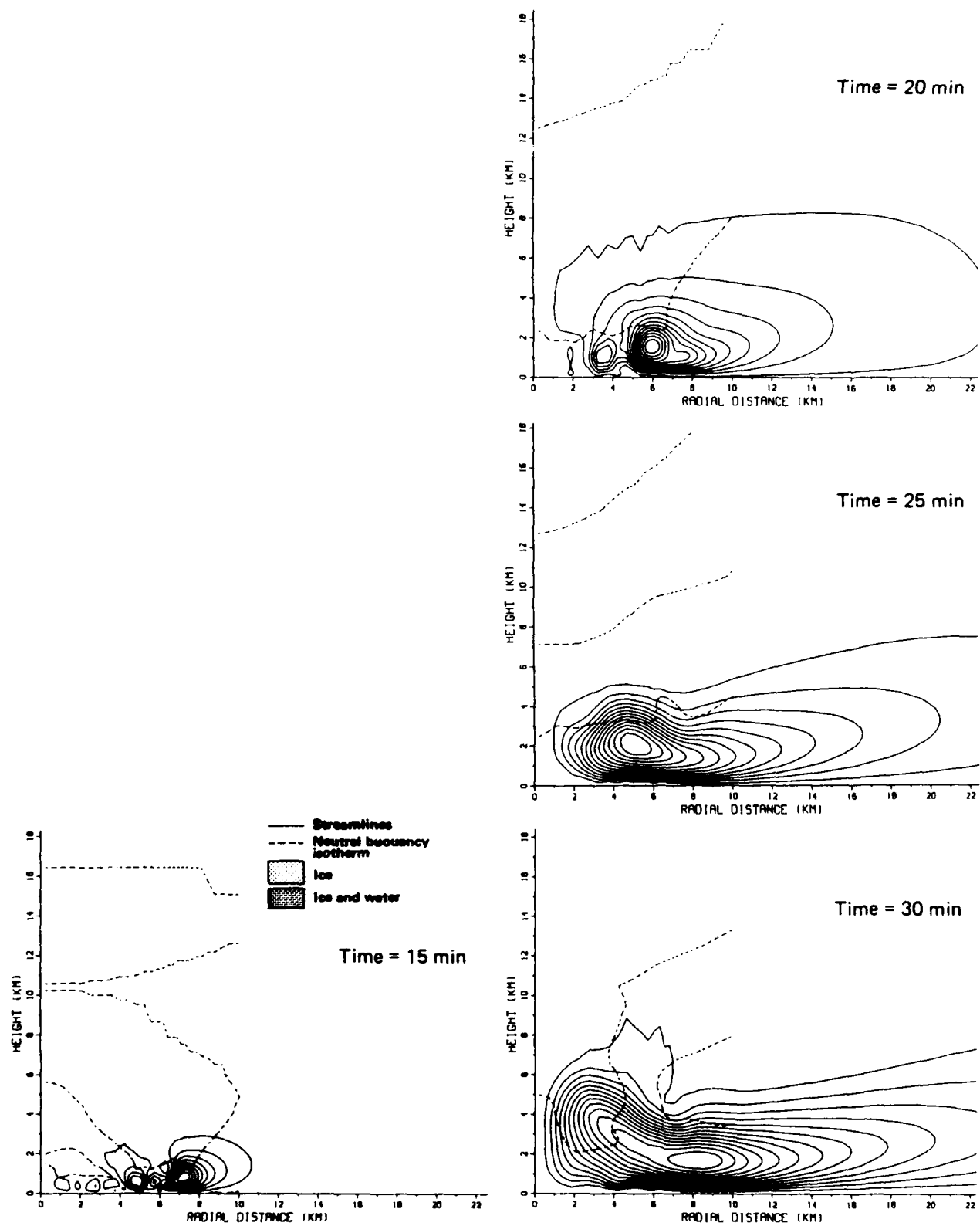


Figure 14. Streamlines and neutral buoyancy isotherms for case 8--dry atmosphere.

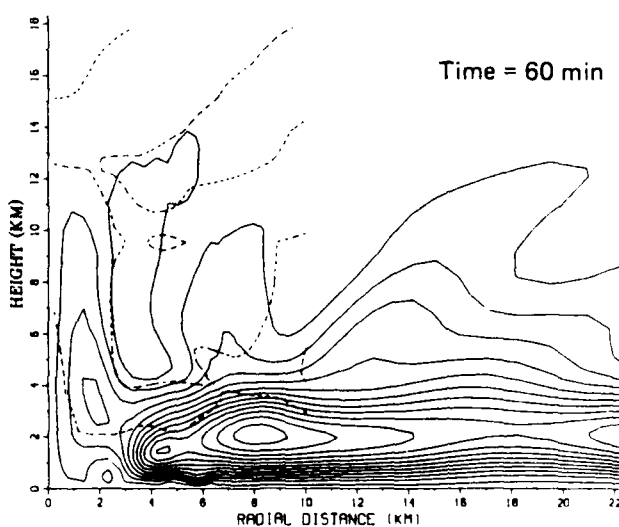
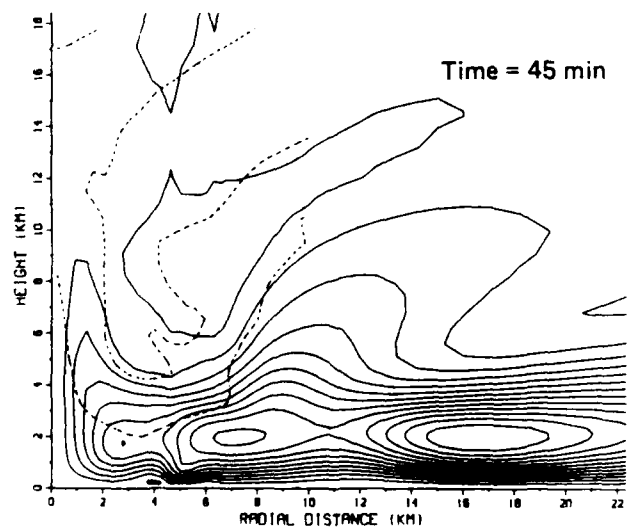
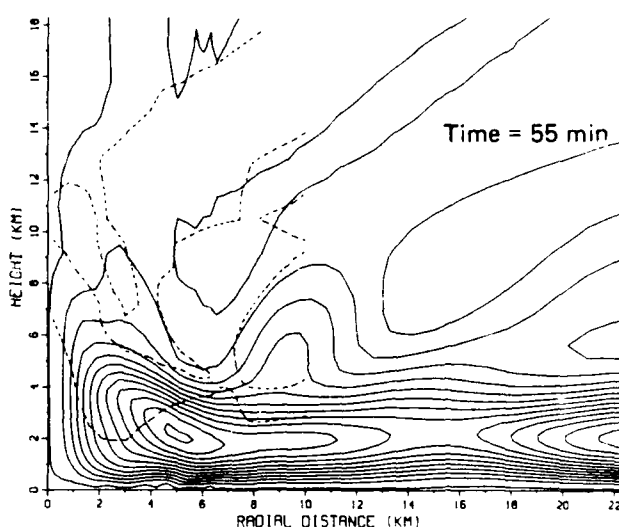
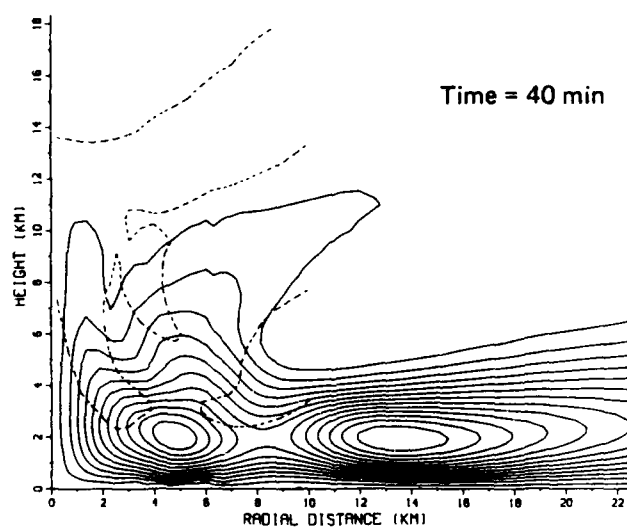
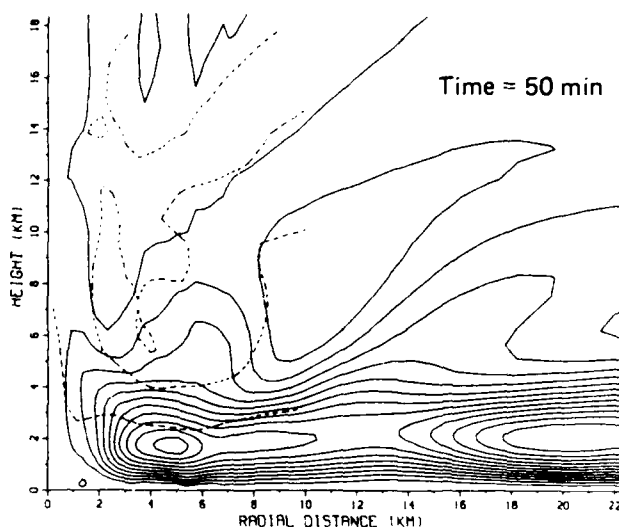
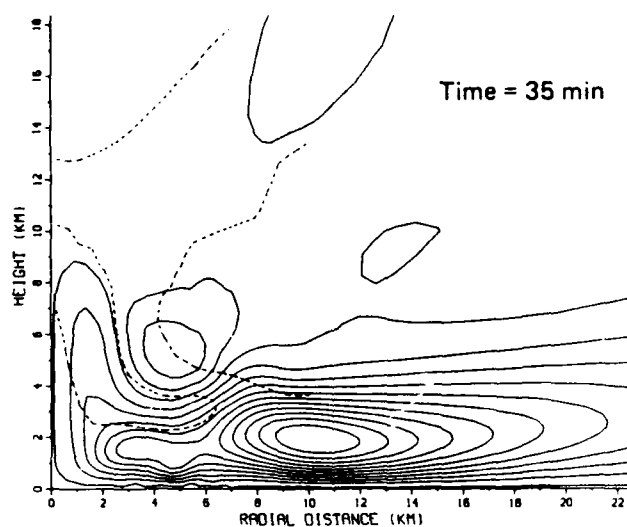


Figure 14. Streamlines and neutral buoyancy isotherms for case 8--dry atmosphere (Concluded).

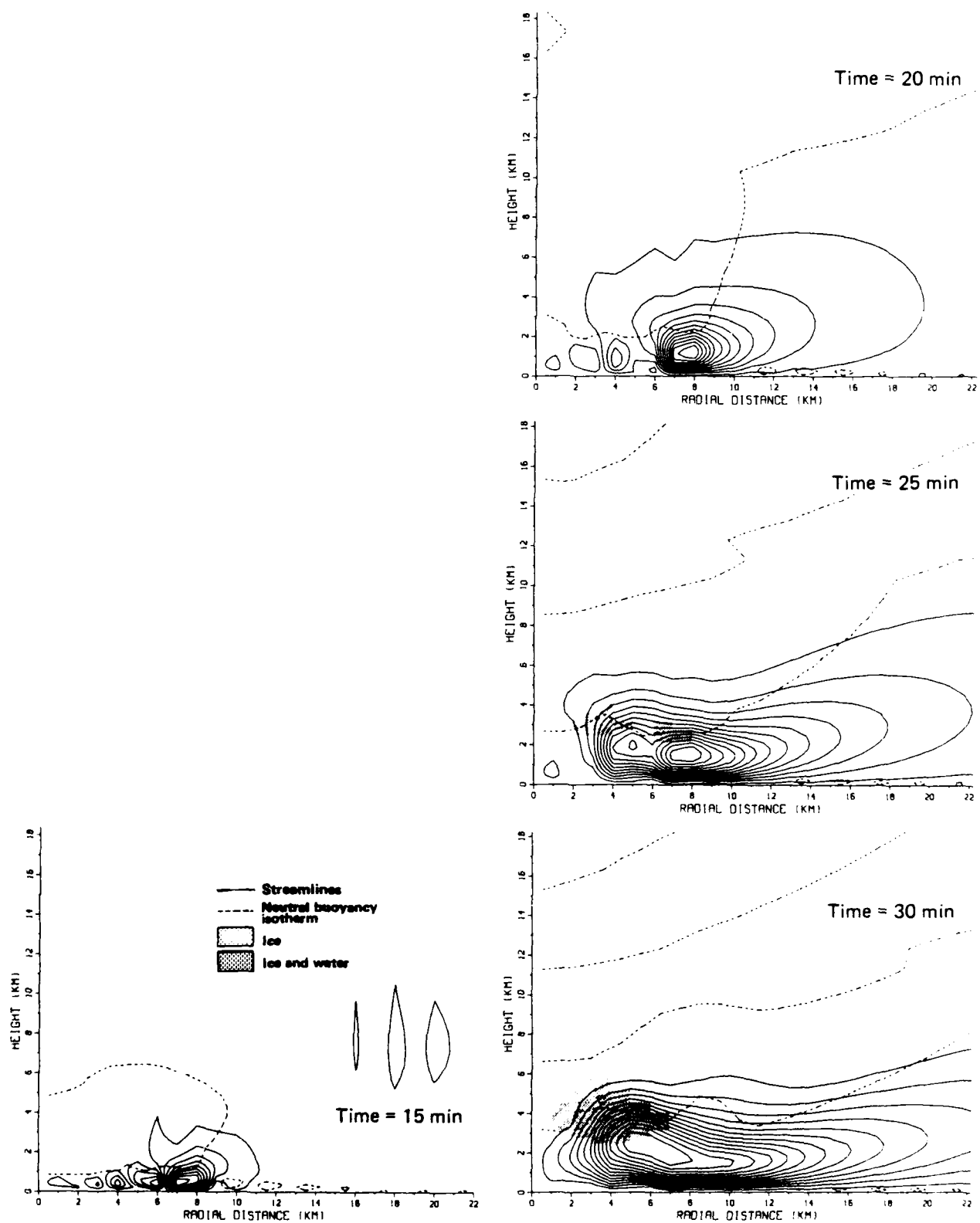


Figure 15. Moisture cloud, streamlines, and neutral buoyancy isotherms for case 9--low-resolution grid.

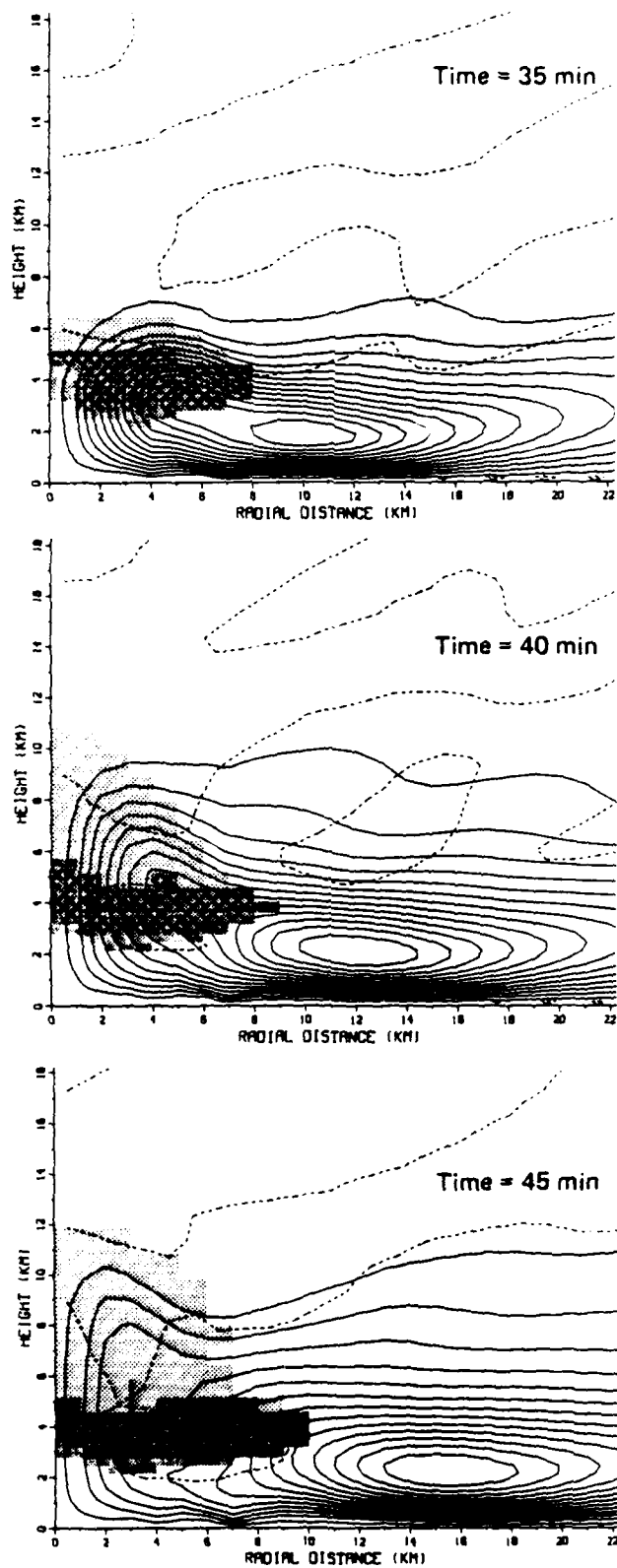


Figure 15. Moisture cloud, streamlines, and neutral buoyancy isotherms for case 9--low-resolution grid (Concluded).

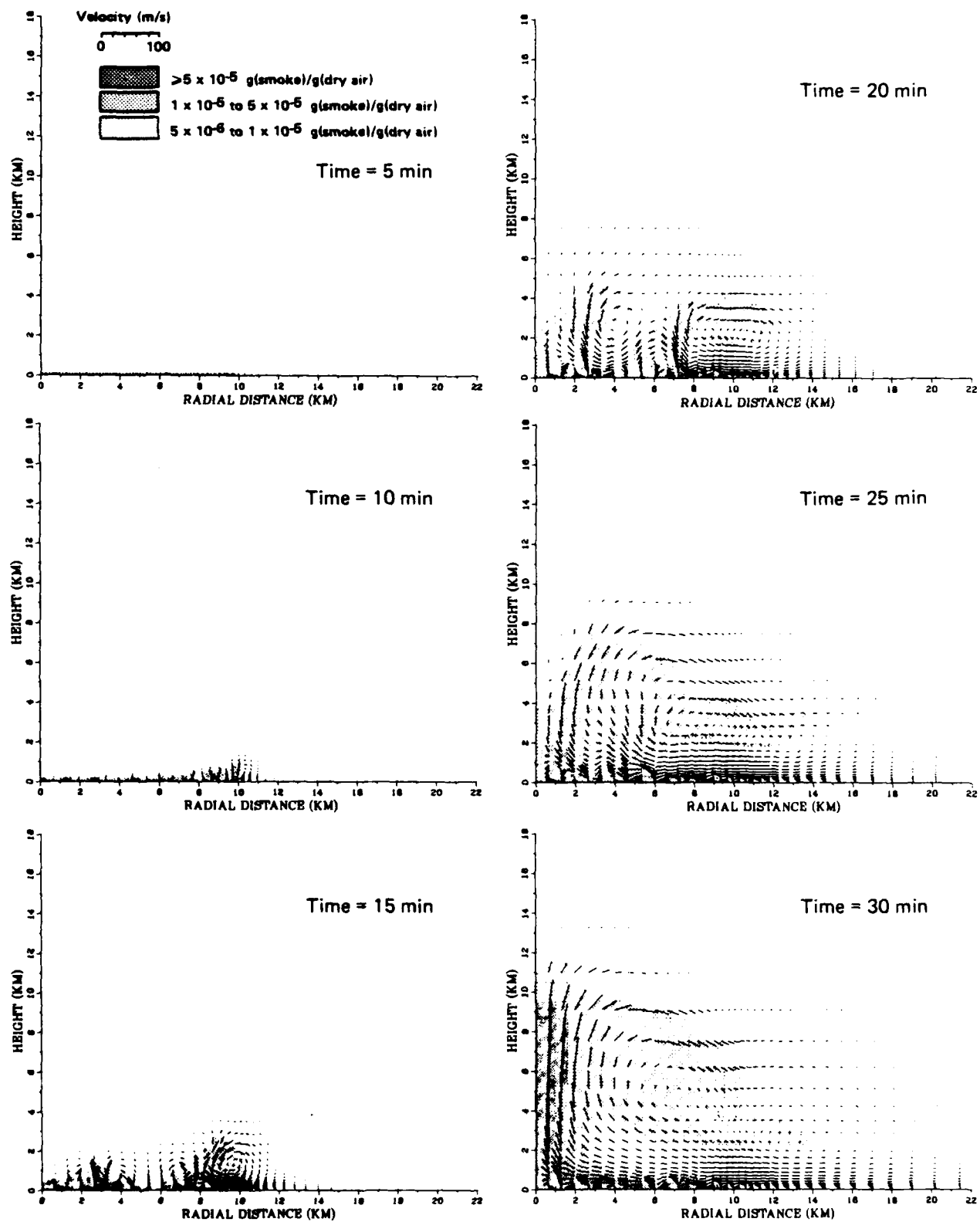


Figure 16. Smoke cloud and velocity vectors for case 1--high heating rate (1.00 kW/m^3), large radius (10 km).

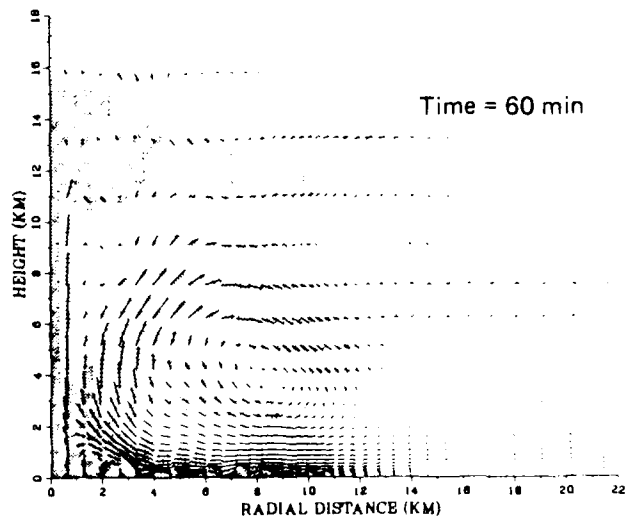
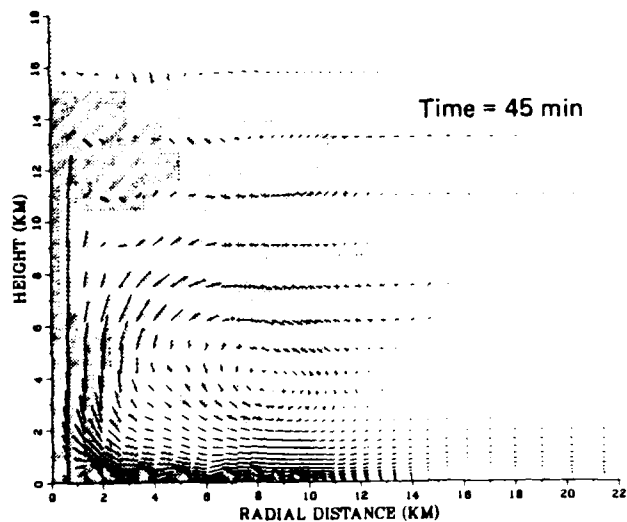
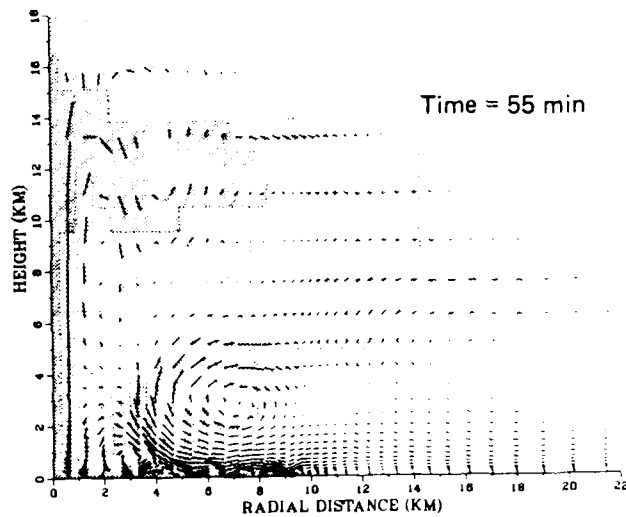
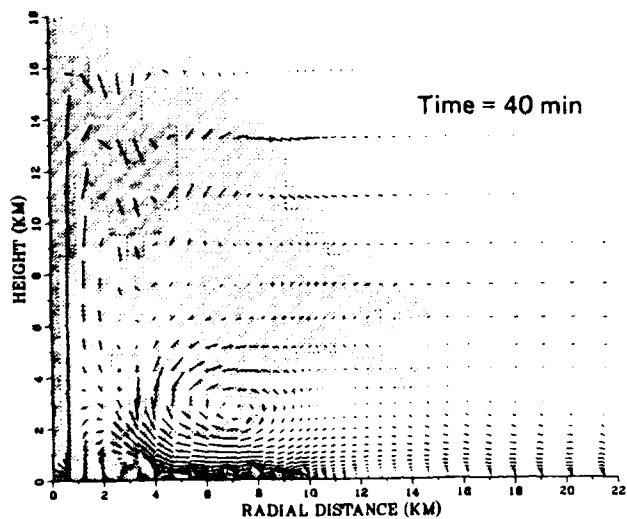
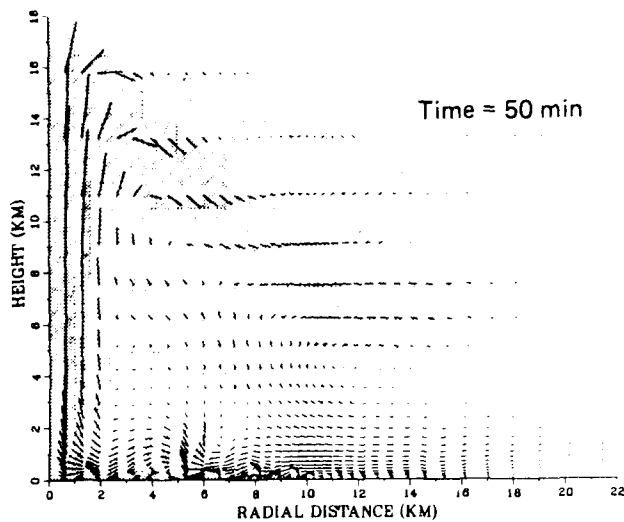
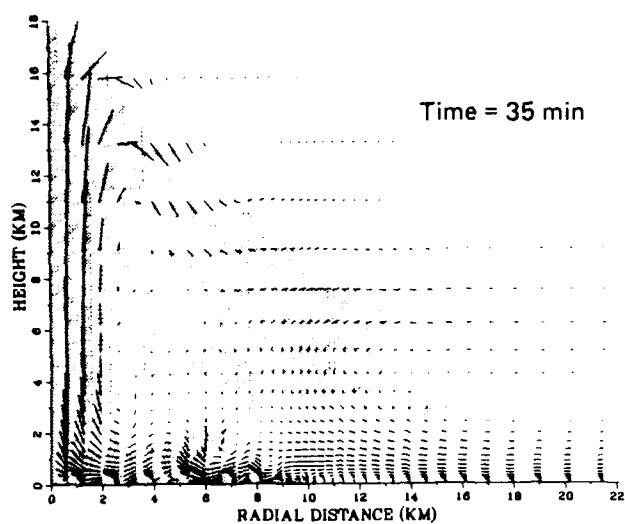


Figure 16. Smoke cloud and velocity vectors for case 1--high heating rate (1.00 kW/m^3), large radius (10 km) (Concluded).

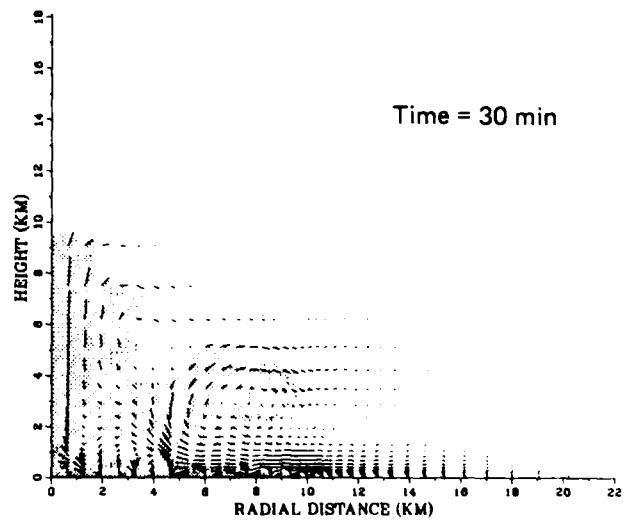
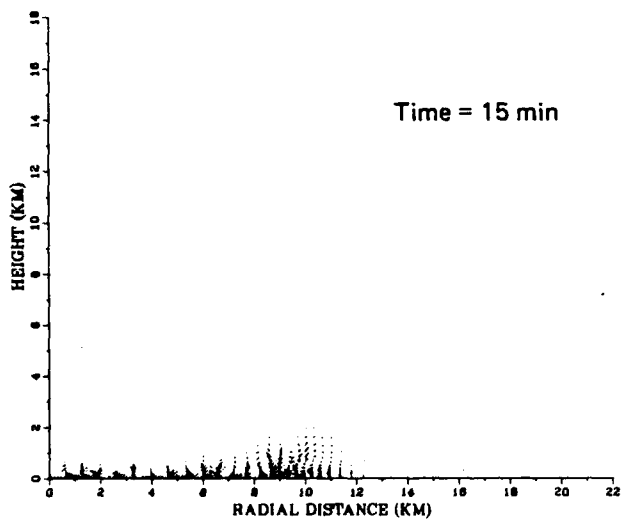
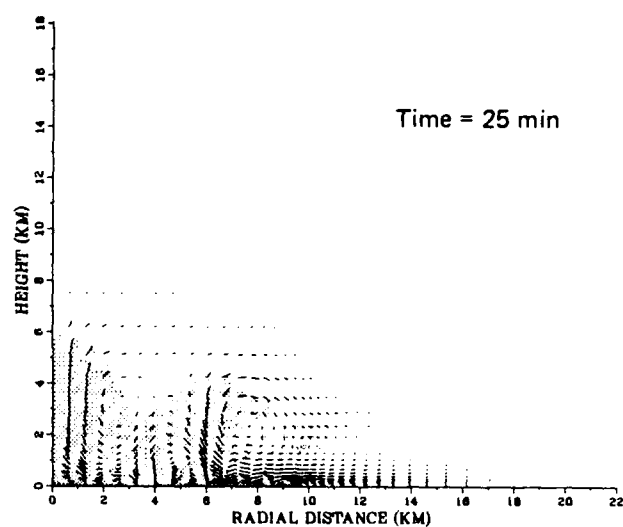
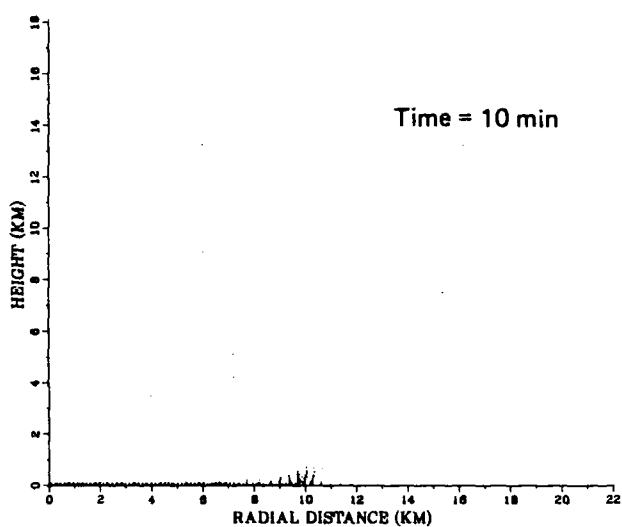
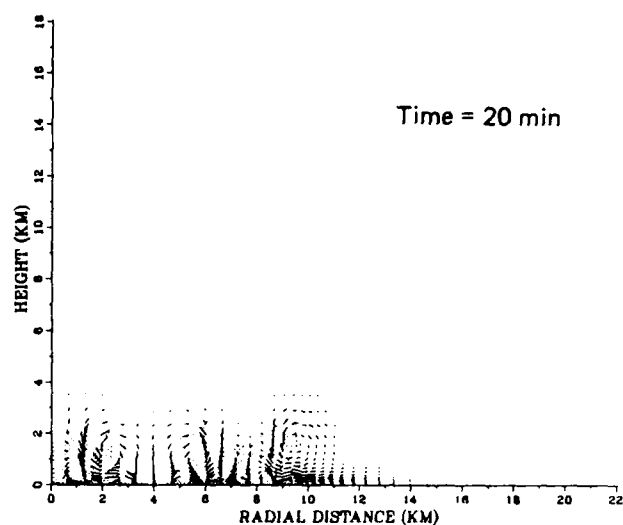
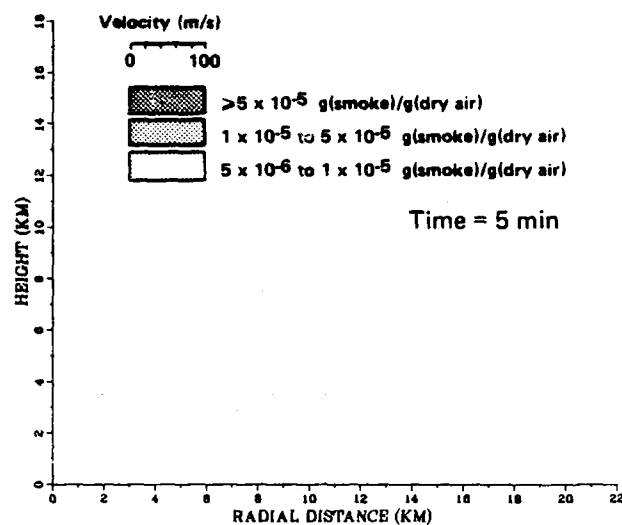


Figure 17. Smoke cloud and velocity vectors for case 2--medium heating rate (0.50 kW/m^3), large radius (10 km).

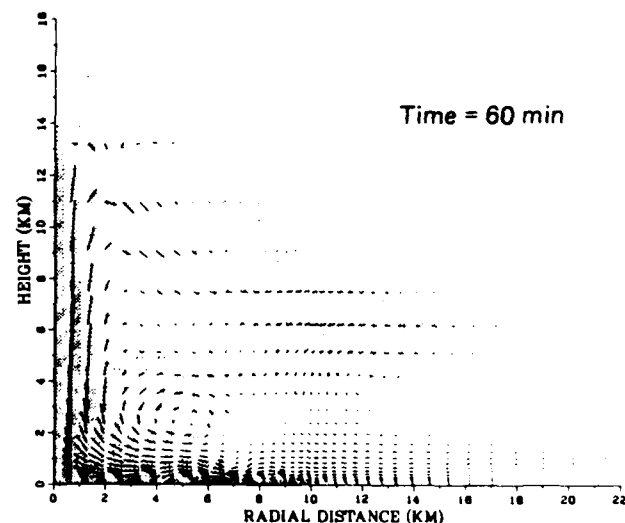
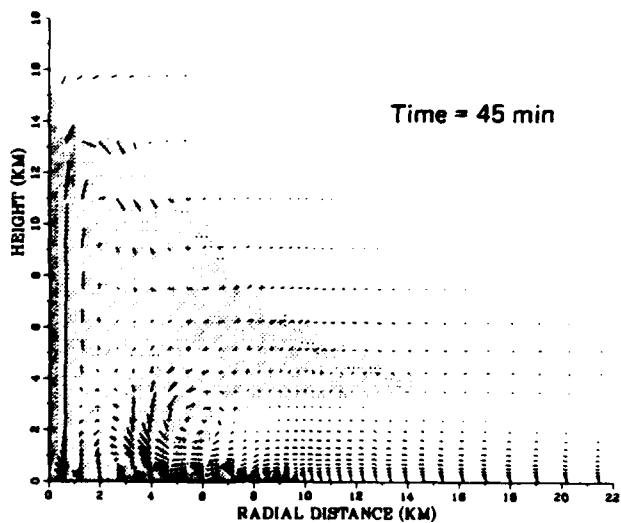
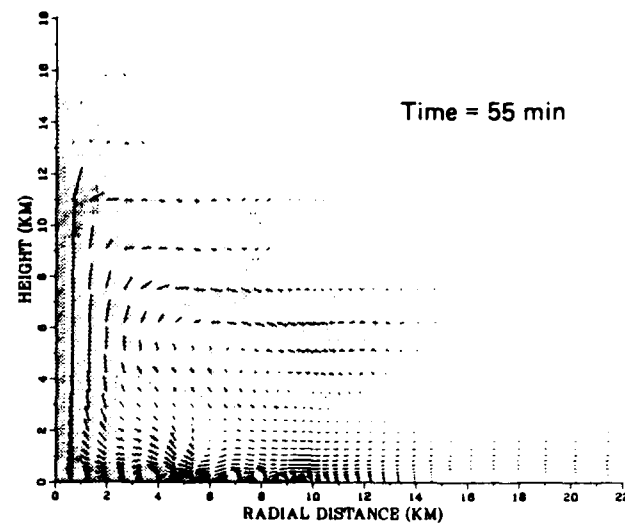
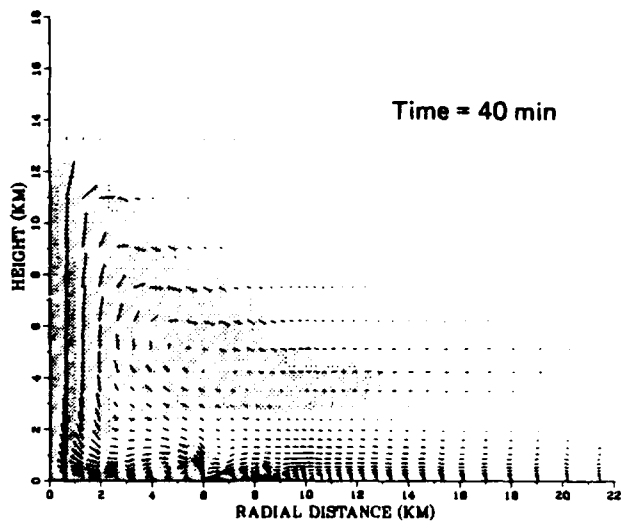
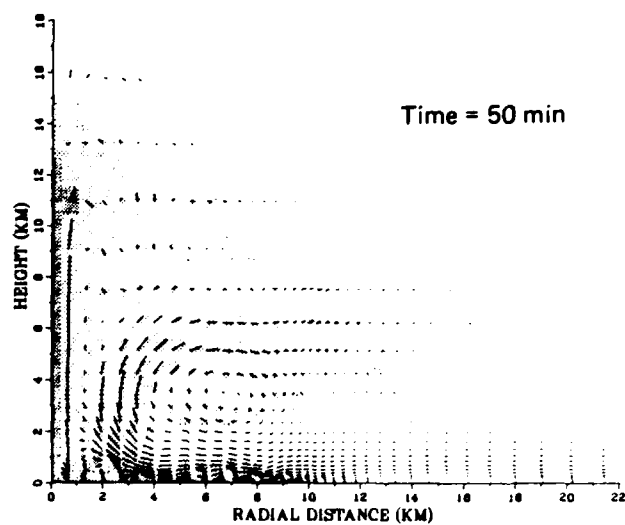
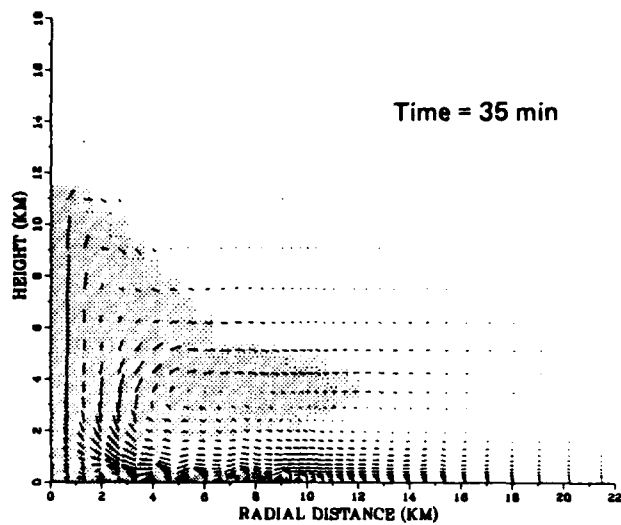


Figure 17. Smoke cloud and velocity vectors for case 2--medium heating rate (0.50 kW/m^3), large radius (10 km) (Concluded).

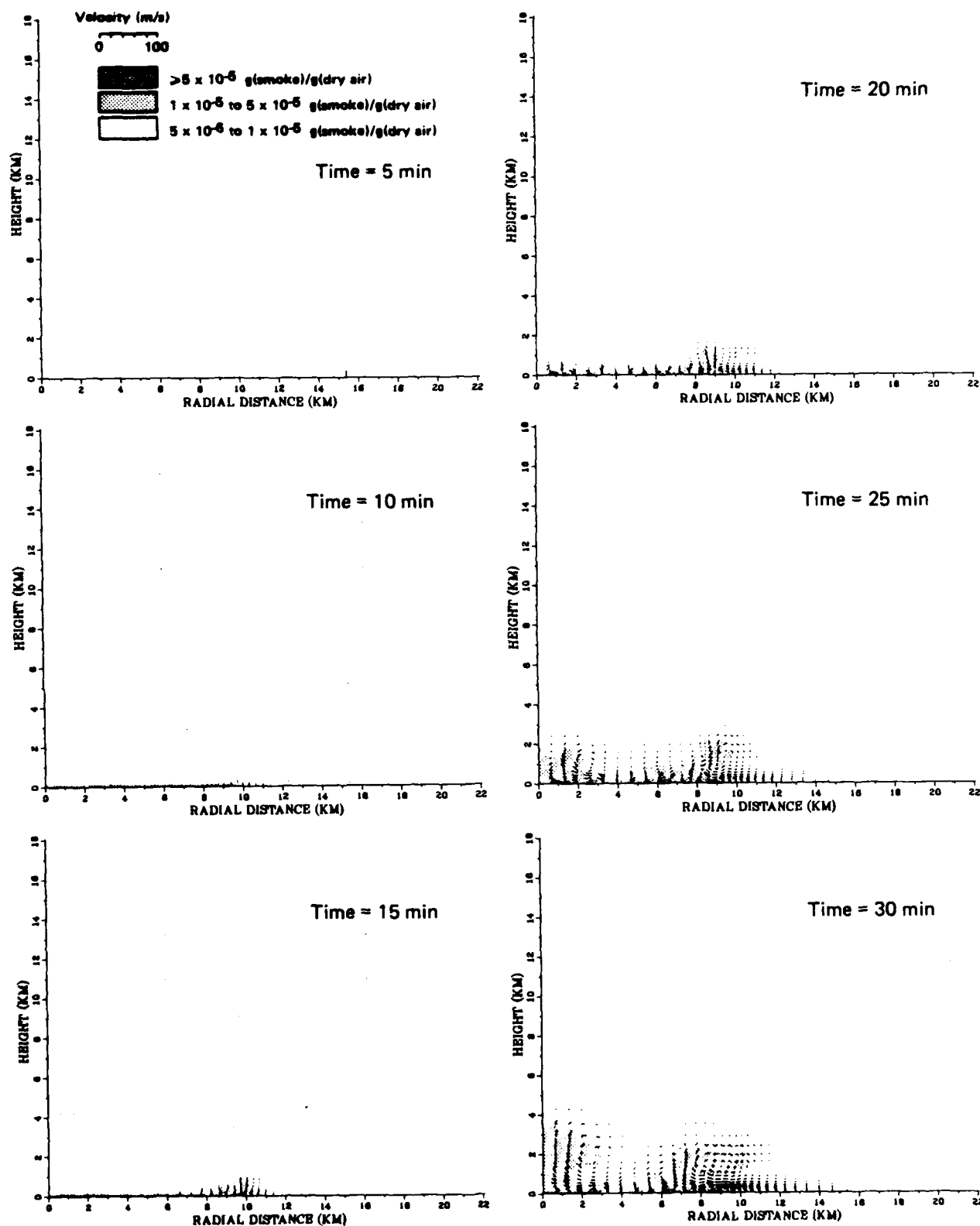


Figure 18. Smoke cloud and velocity vectors for case 3--low heating rate (0.25 kW/m^3), large radius (10 km).

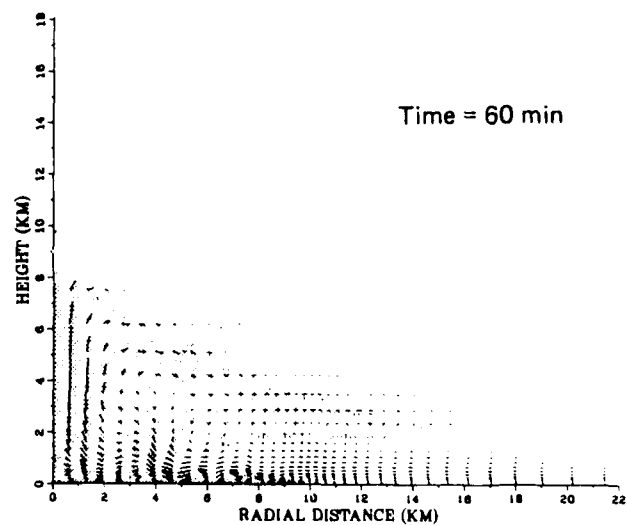
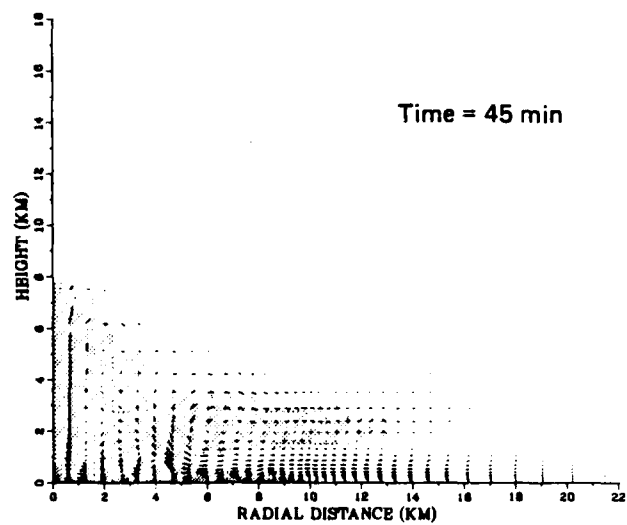
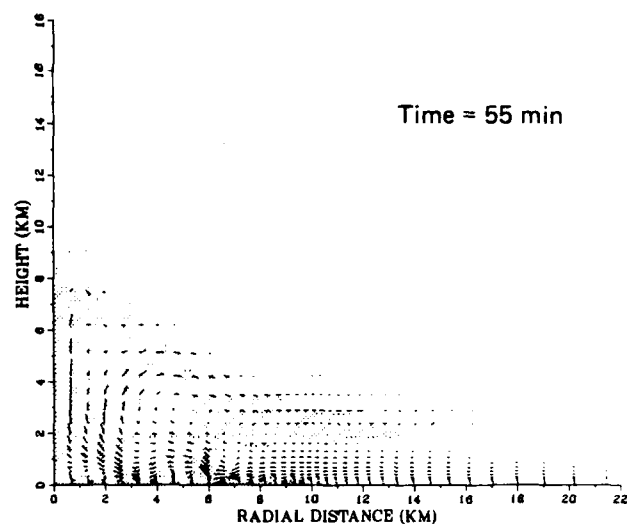
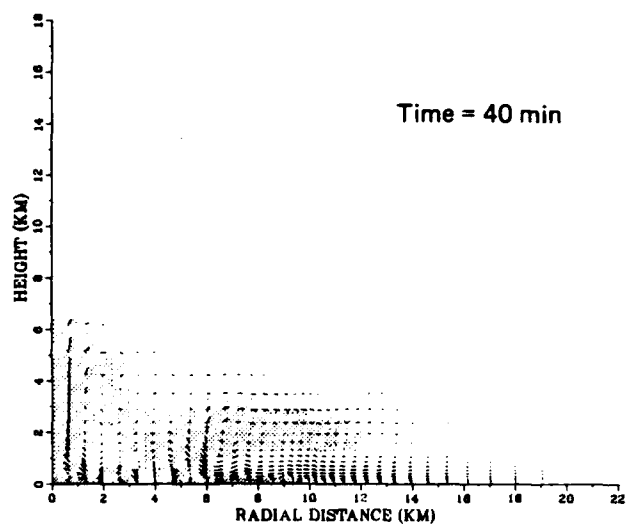
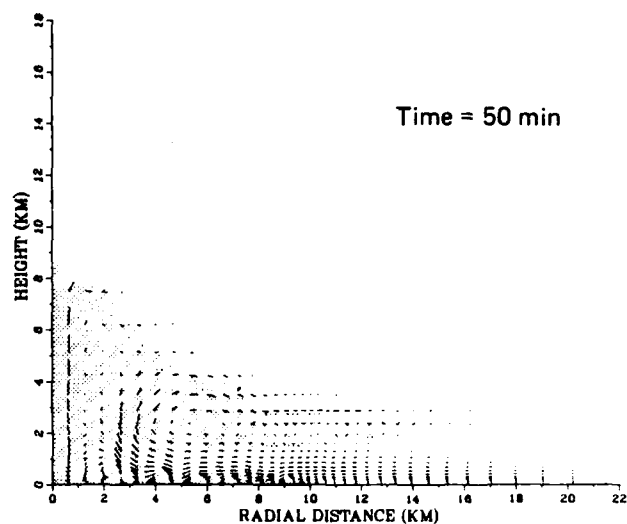
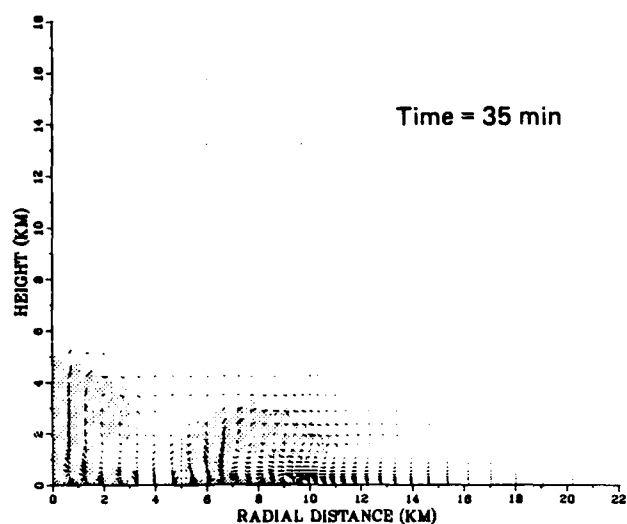


Figure 18. Smoke cloud and velocity vectors for case 3--low heating rate (0.25 kW/m^3), large radius (10 km) (Concluded).

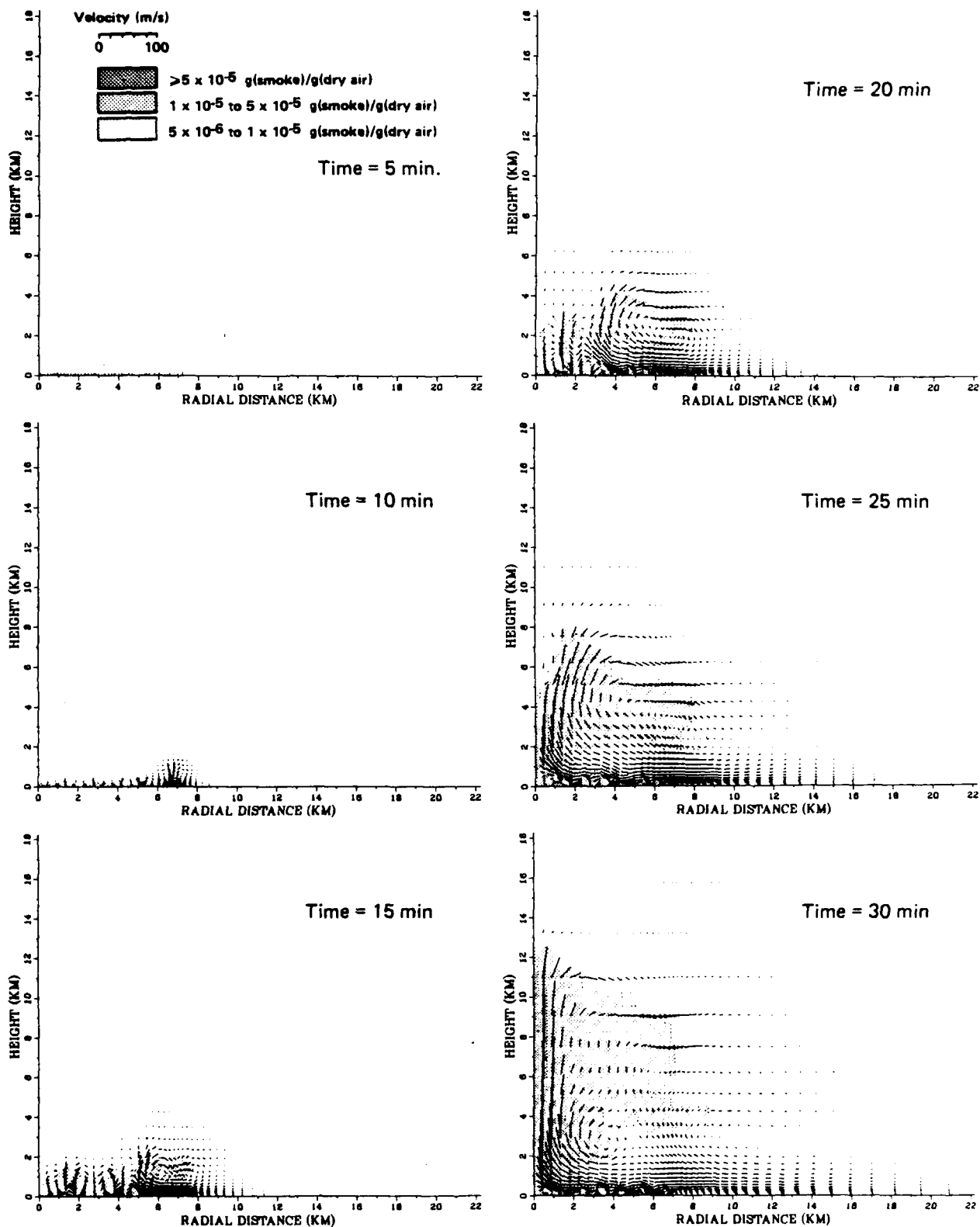


Figure 19. Smoke cloud and velocity vectors for case 4--high heating rate (1.00 kW/m^3), medium radius (7 km).

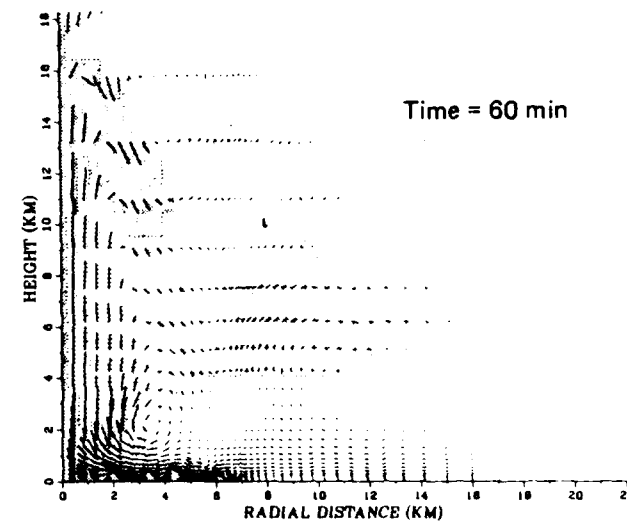
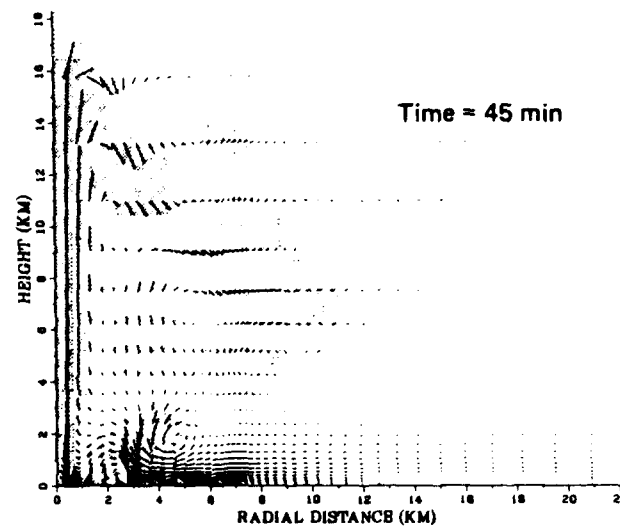
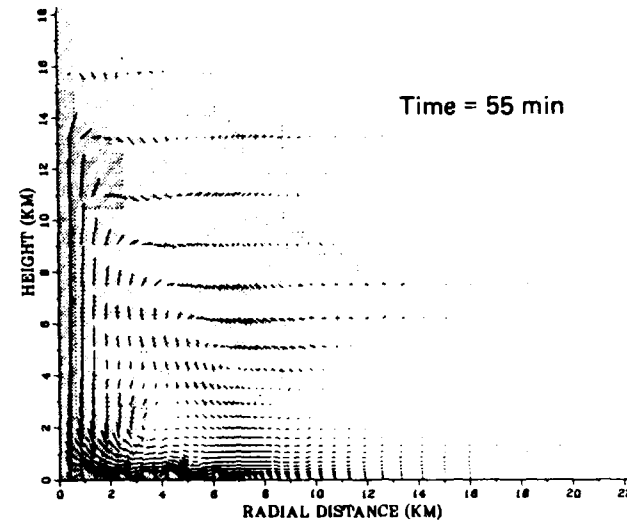
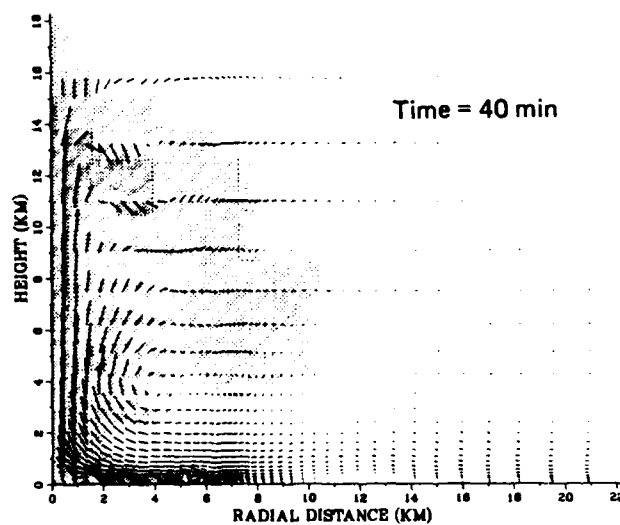
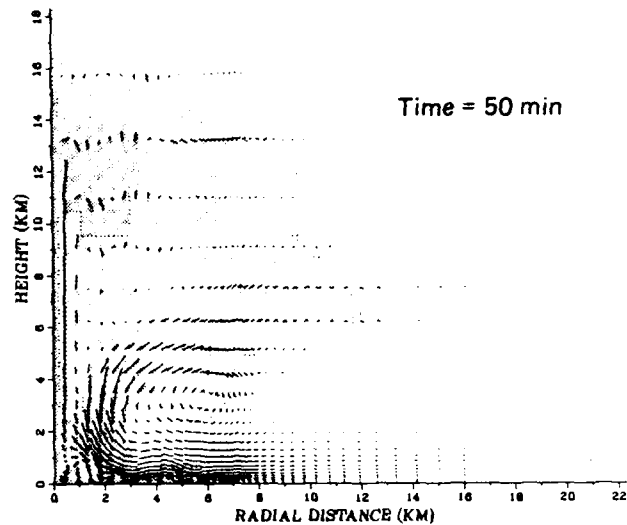
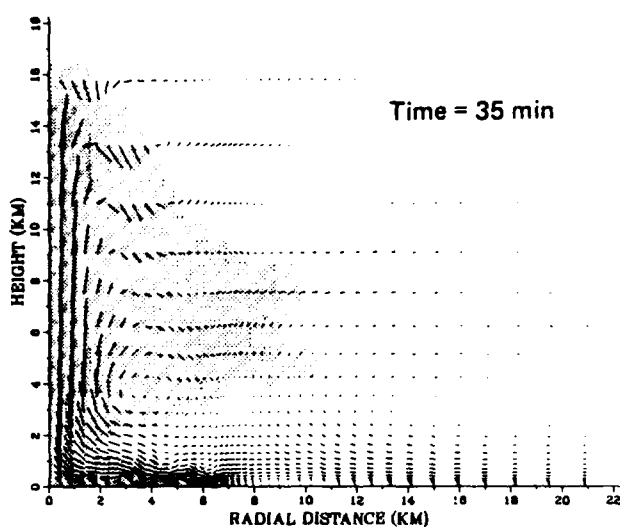


Figure 19. Smoke cloud and velocity vectors for case 4--high heating rate (1.00 kW/m^3), medium radius (7 km) (Concluded).

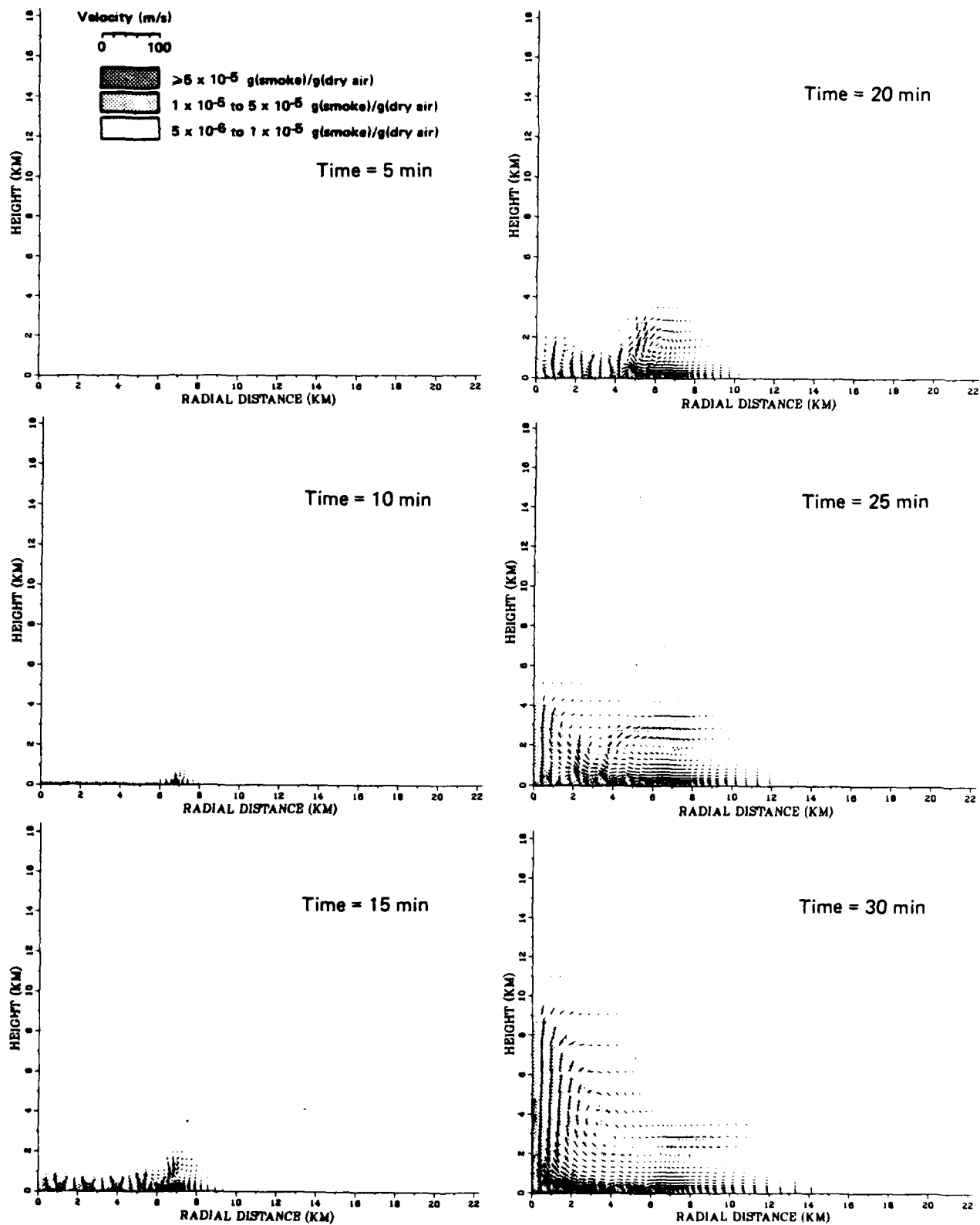


Figure 20. Smoke cloud and velocity vectors for case 5--medium heating rate (0.50 kW/m^3), medium radius (7 km).

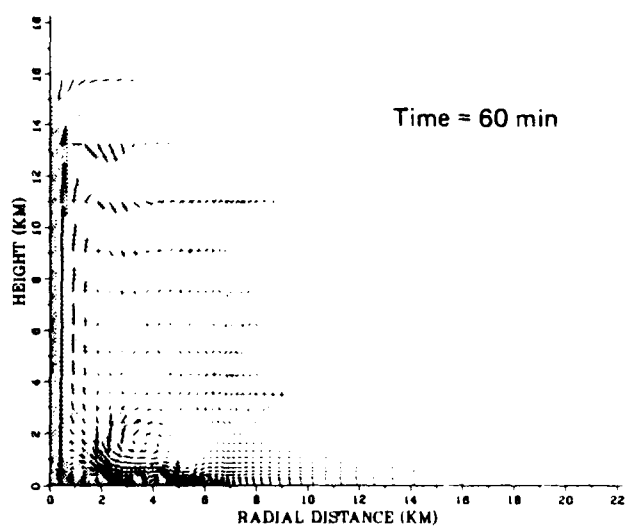
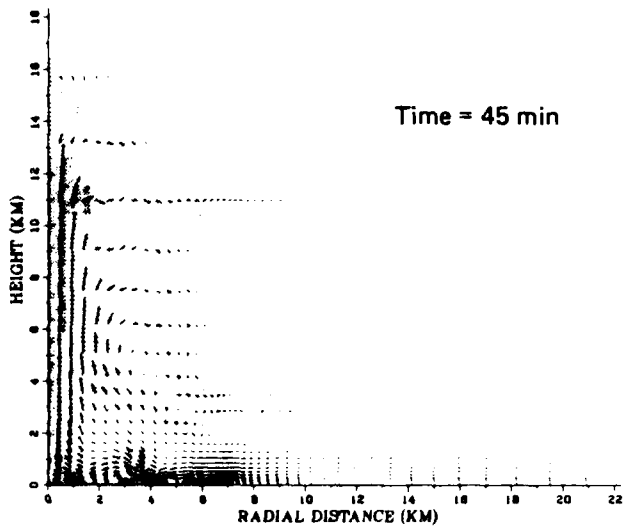
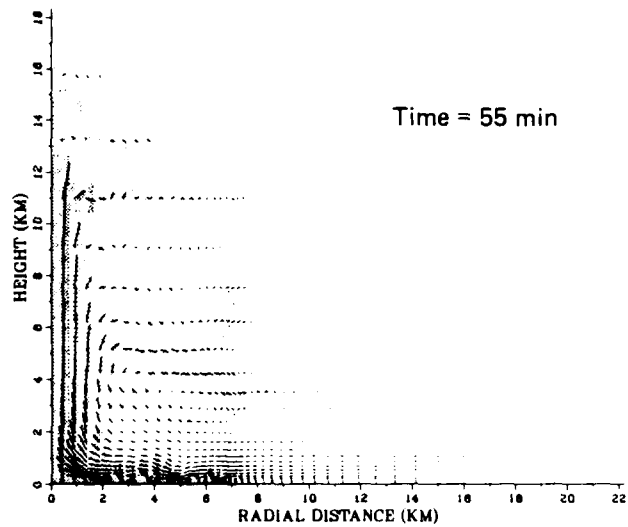
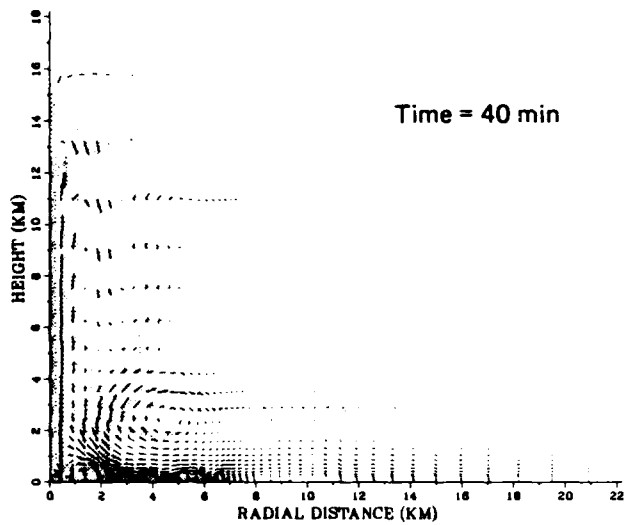
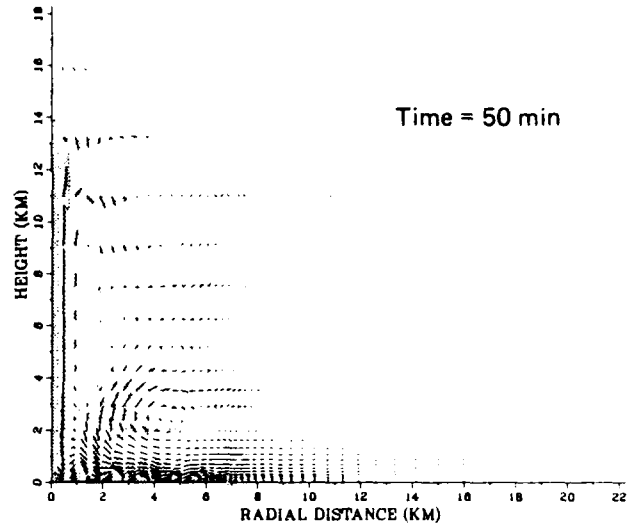
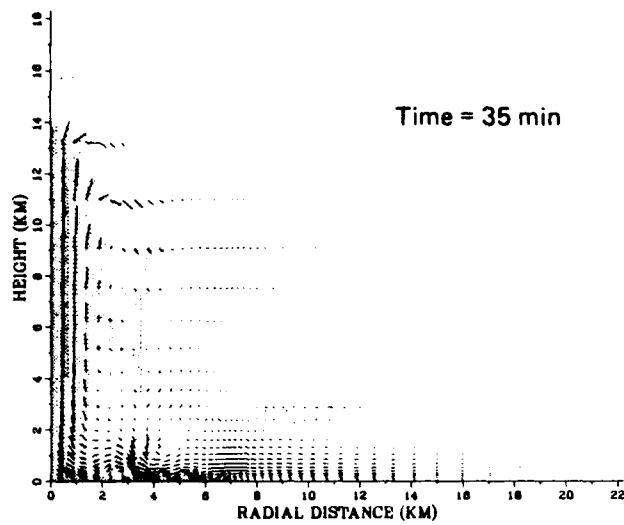


Figure 20. Smoke cloud and velocity vectors for case 5--medium heating rate (0.50 kW/m^3), medium radius (7 km) (Concluded).

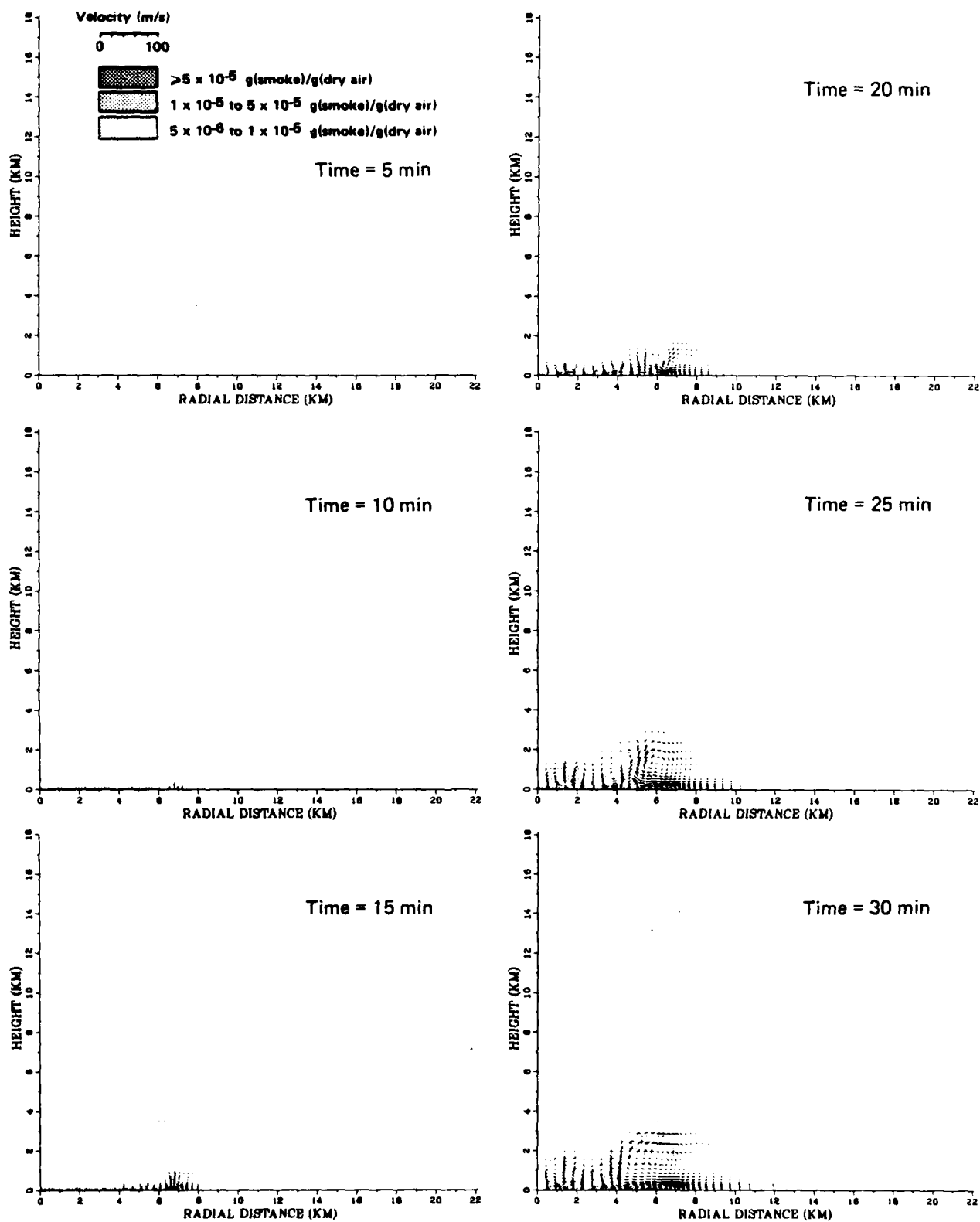


Figure 21. Smoke cloud and velocity vectors for case 6--low heating rate (0.25 kW/m^3), medium radius (7 km).

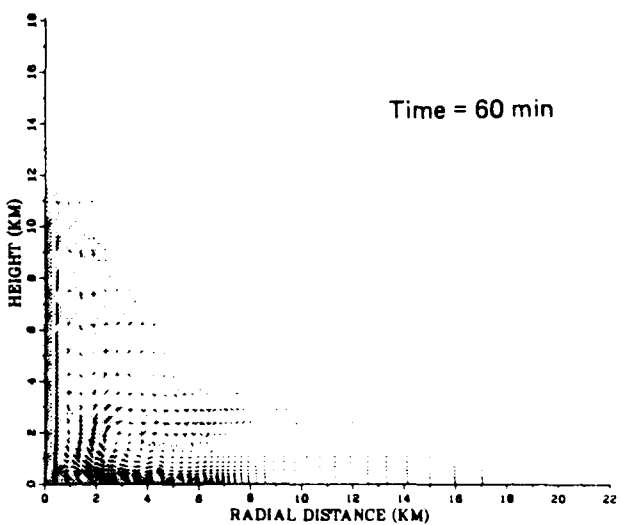
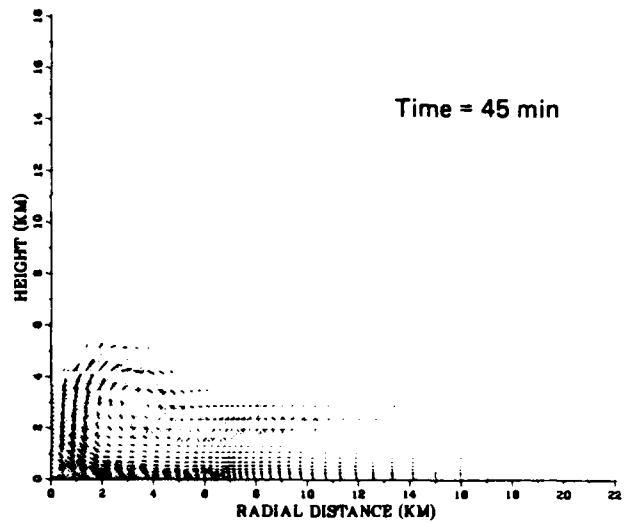
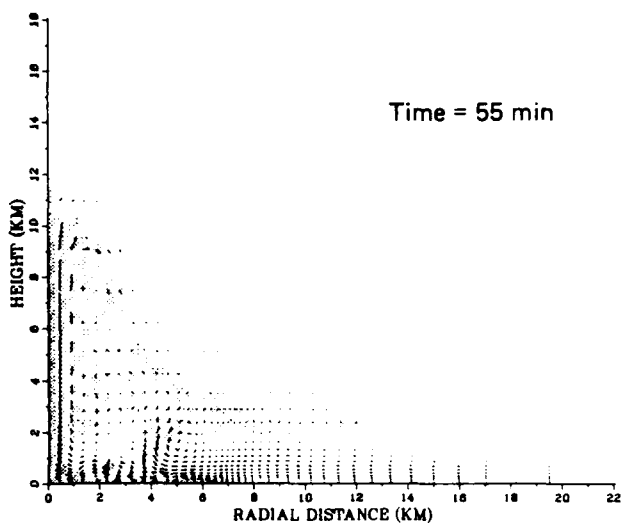
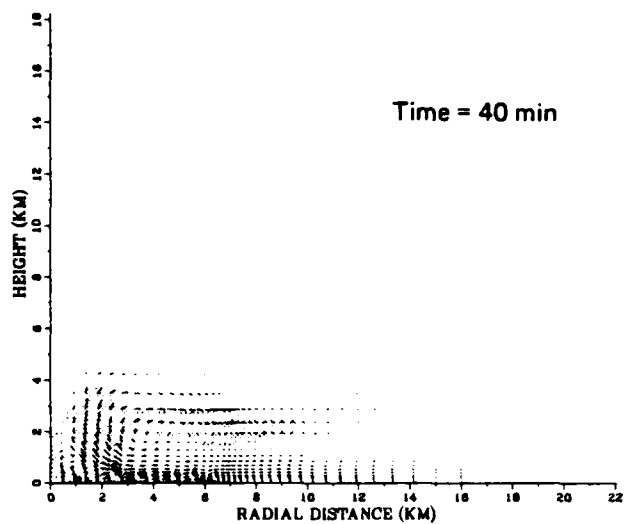
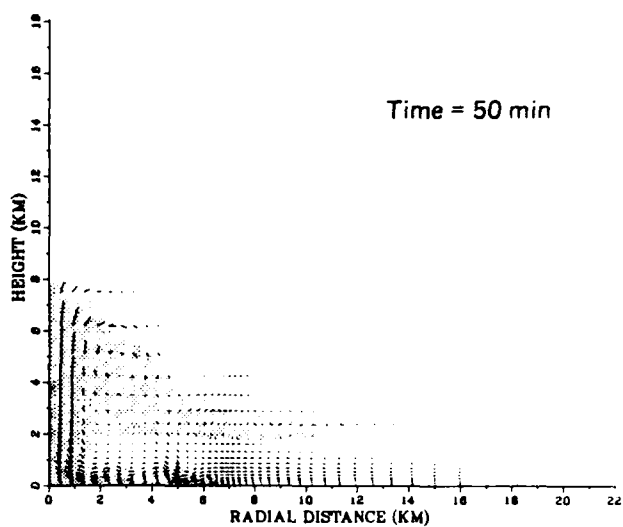
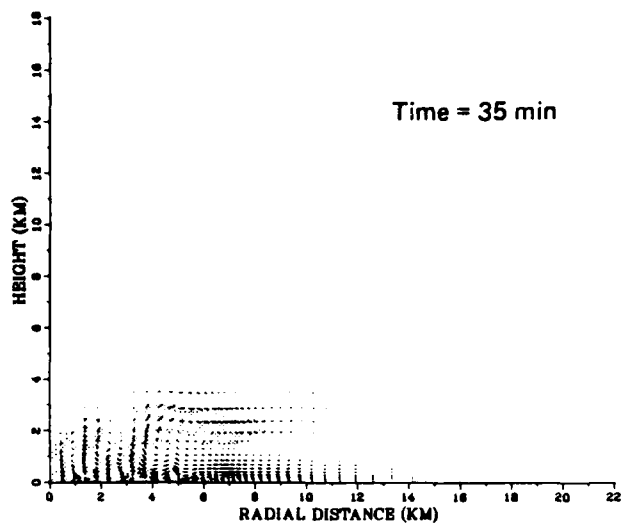


Figure 21. Smoke cloud and velocity vectors for case 6--low heating rate (0.25 kW/m^3), medium radius (7 km) (Concluded).

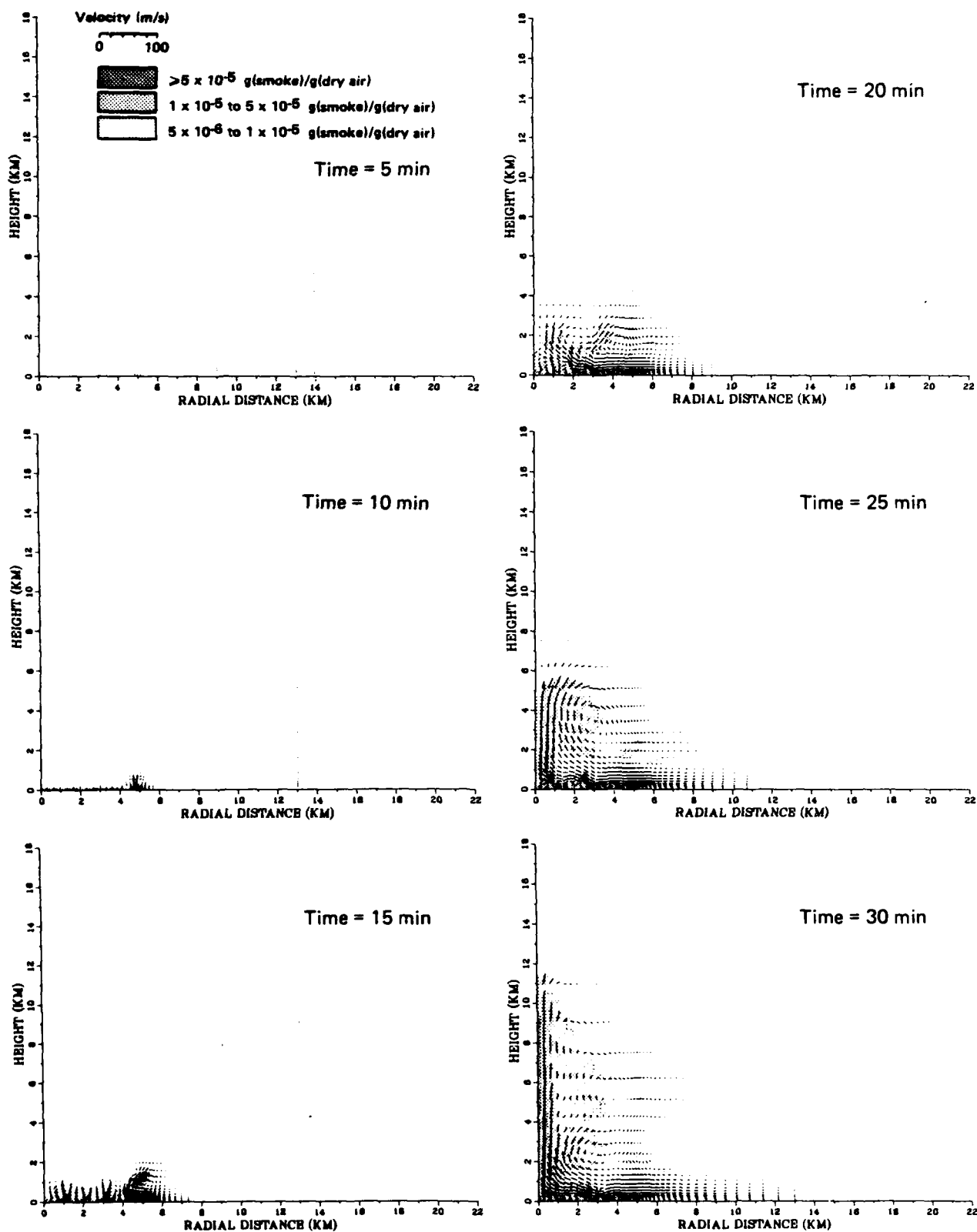


Figure 22. Smoke cloud and velocity vectors for case 7--medium heating rate (0.50 kW/m^3), small radius (5 km).

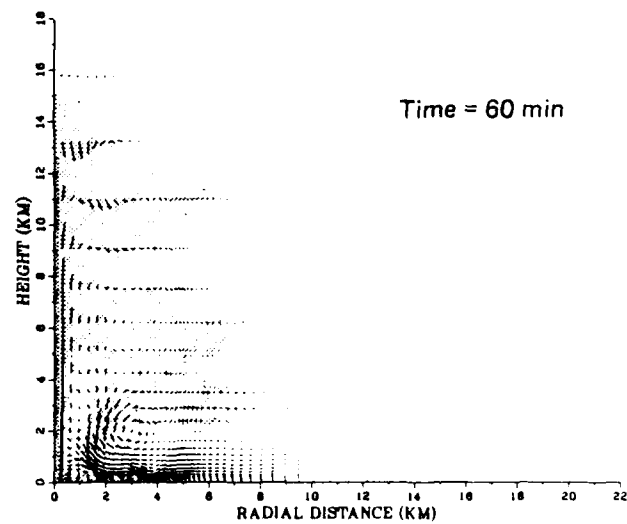
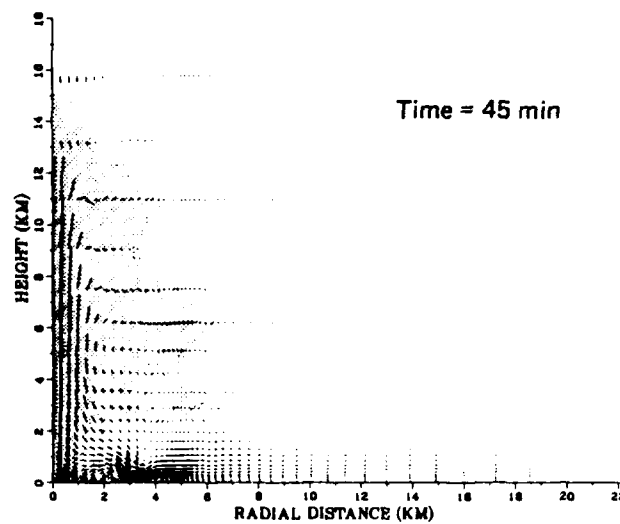
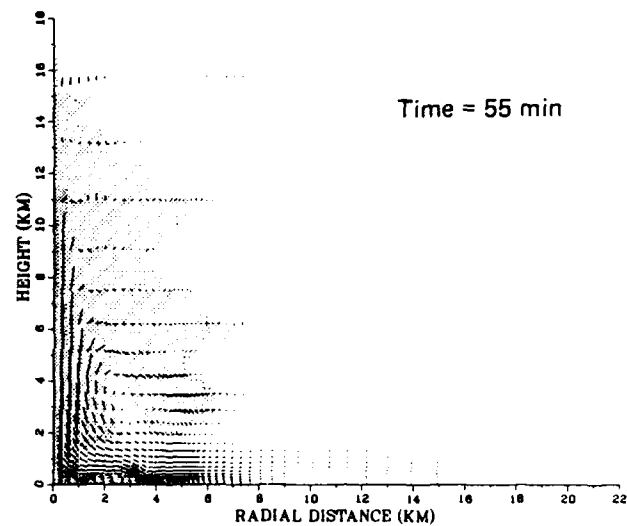
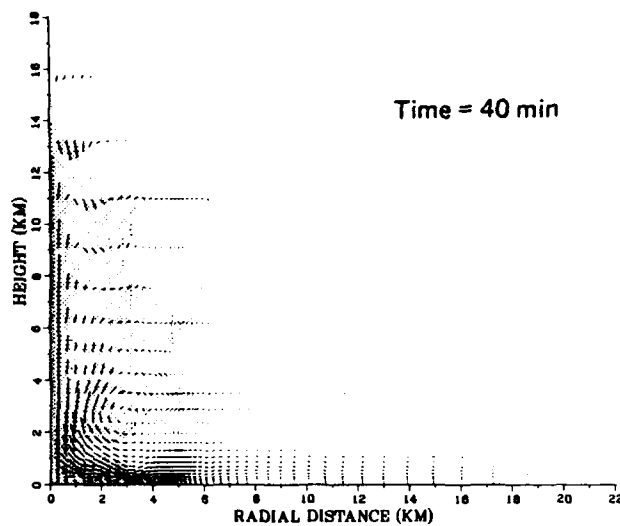
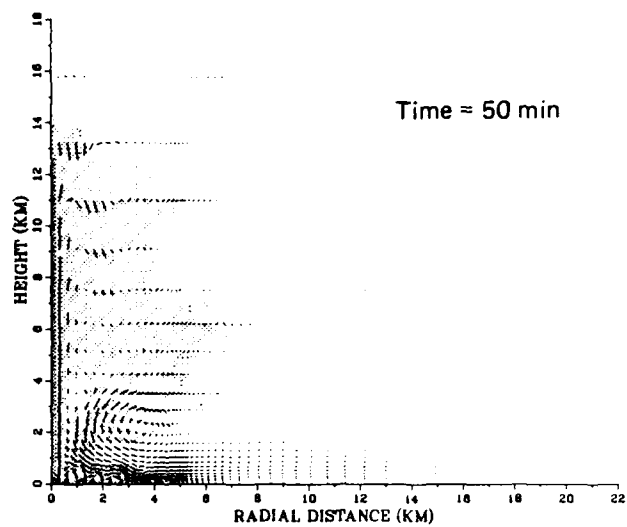
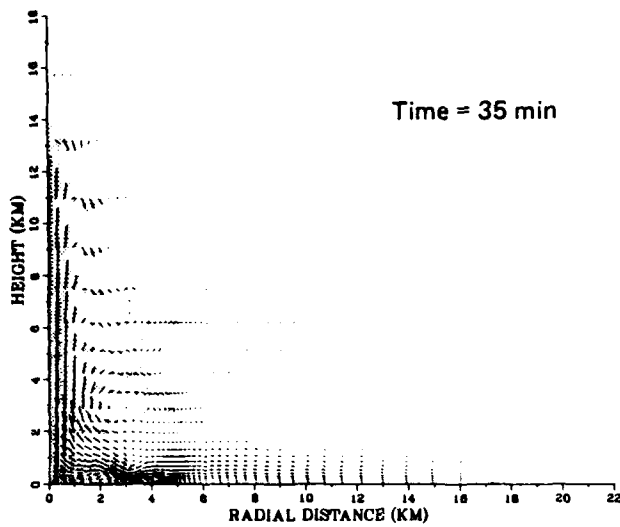


Figure 22. Smoke cloud and velocity vectors for case 7--medium heating rate (0.50 kW/m^3), small radius (5 km) (Concluded).

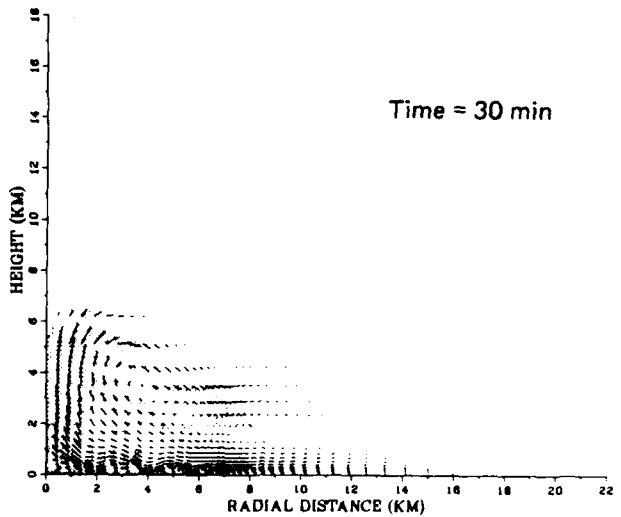
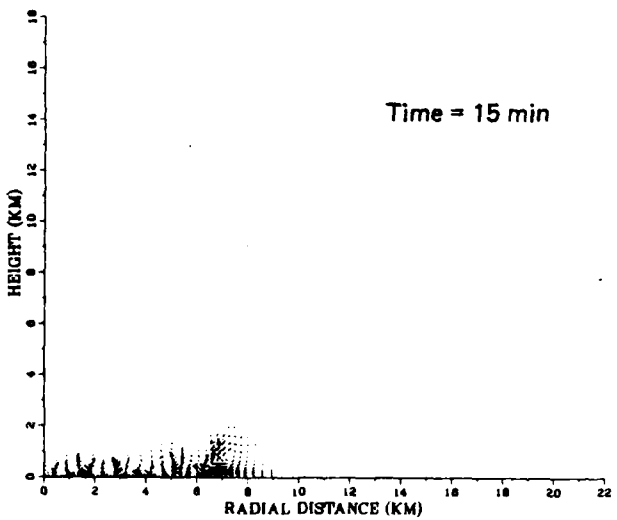
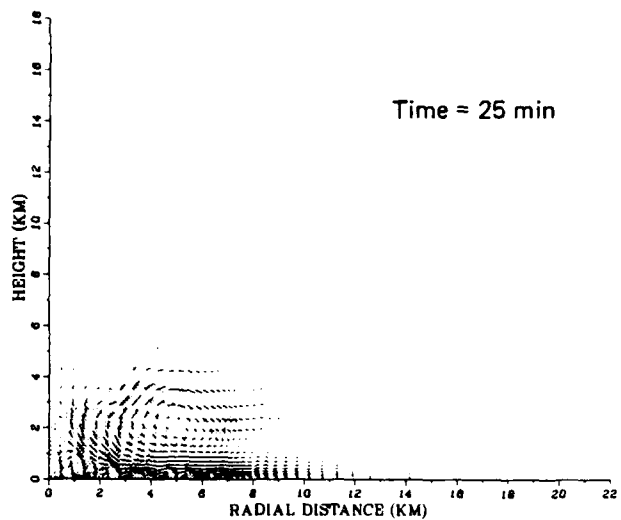
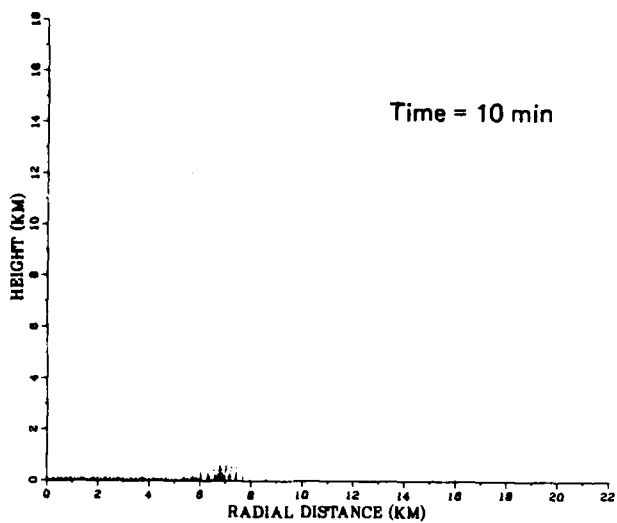
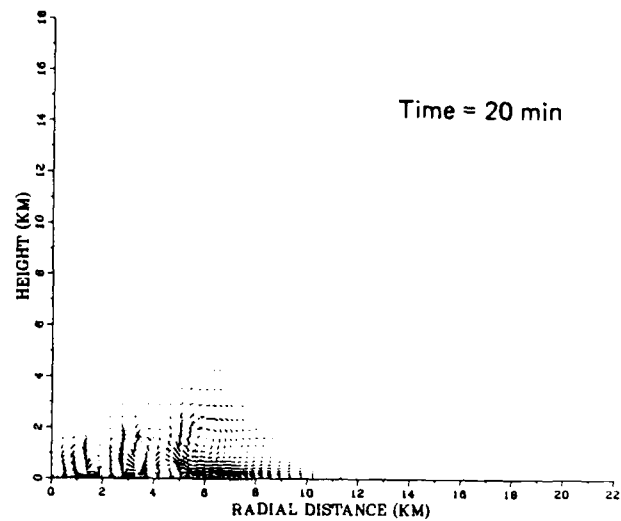
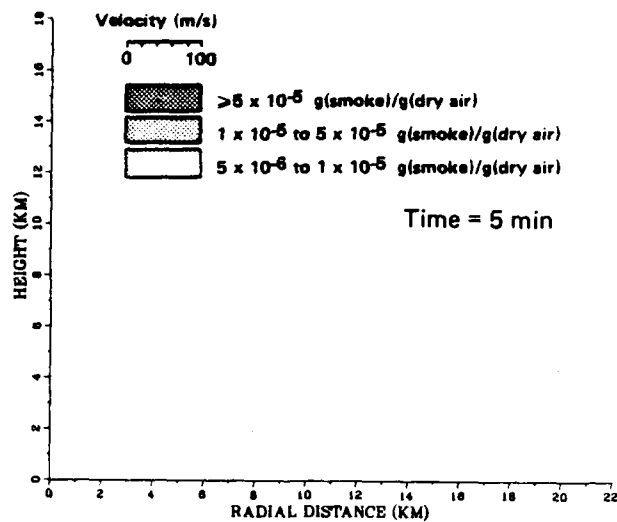


Figure 23. Smoke cloud and velocity vectors for case 8--dry atmosphere.

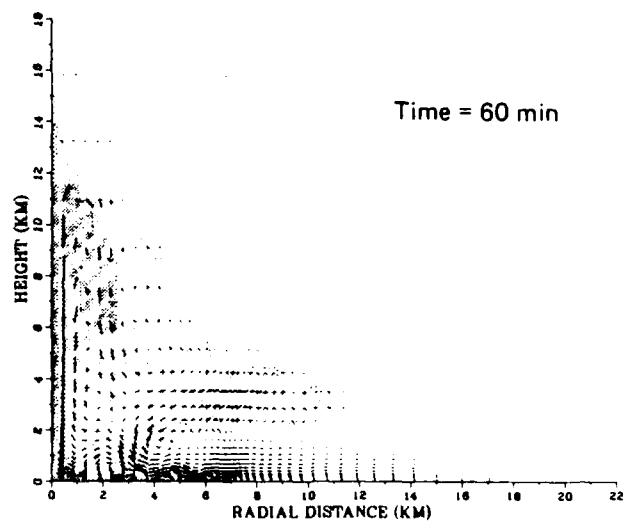
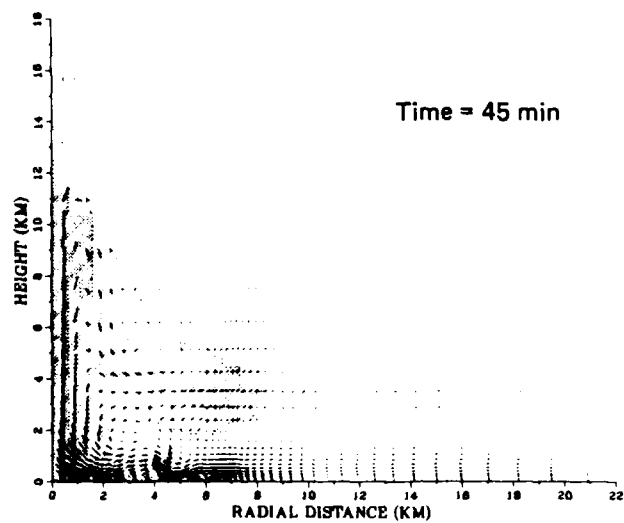
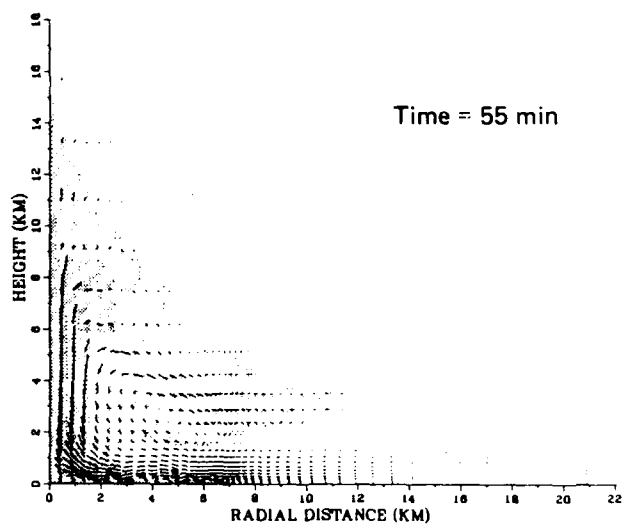
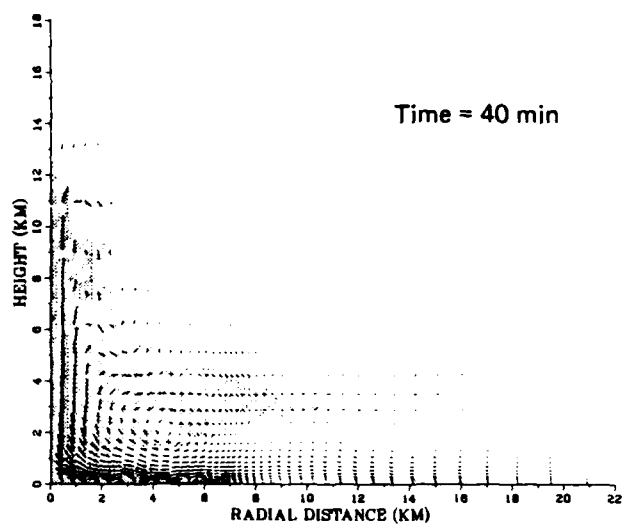
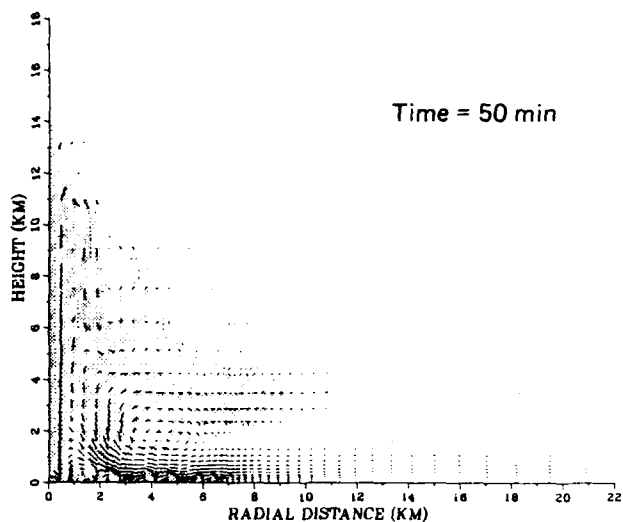
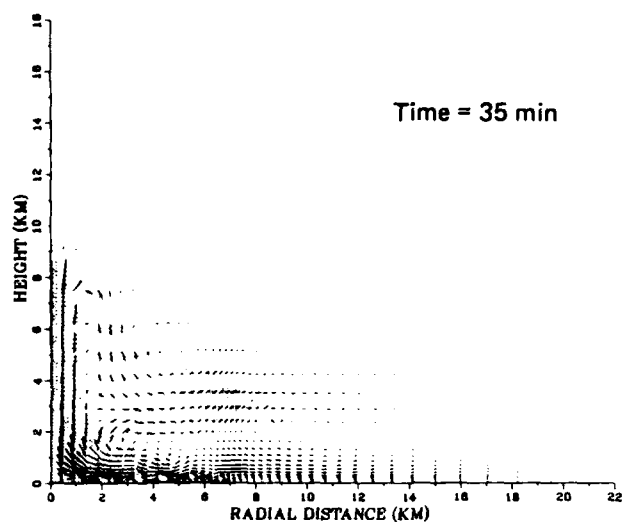


Figure 23. Smoke cloud and velocity vectors for case 8--dry atmosphere (Concluded).

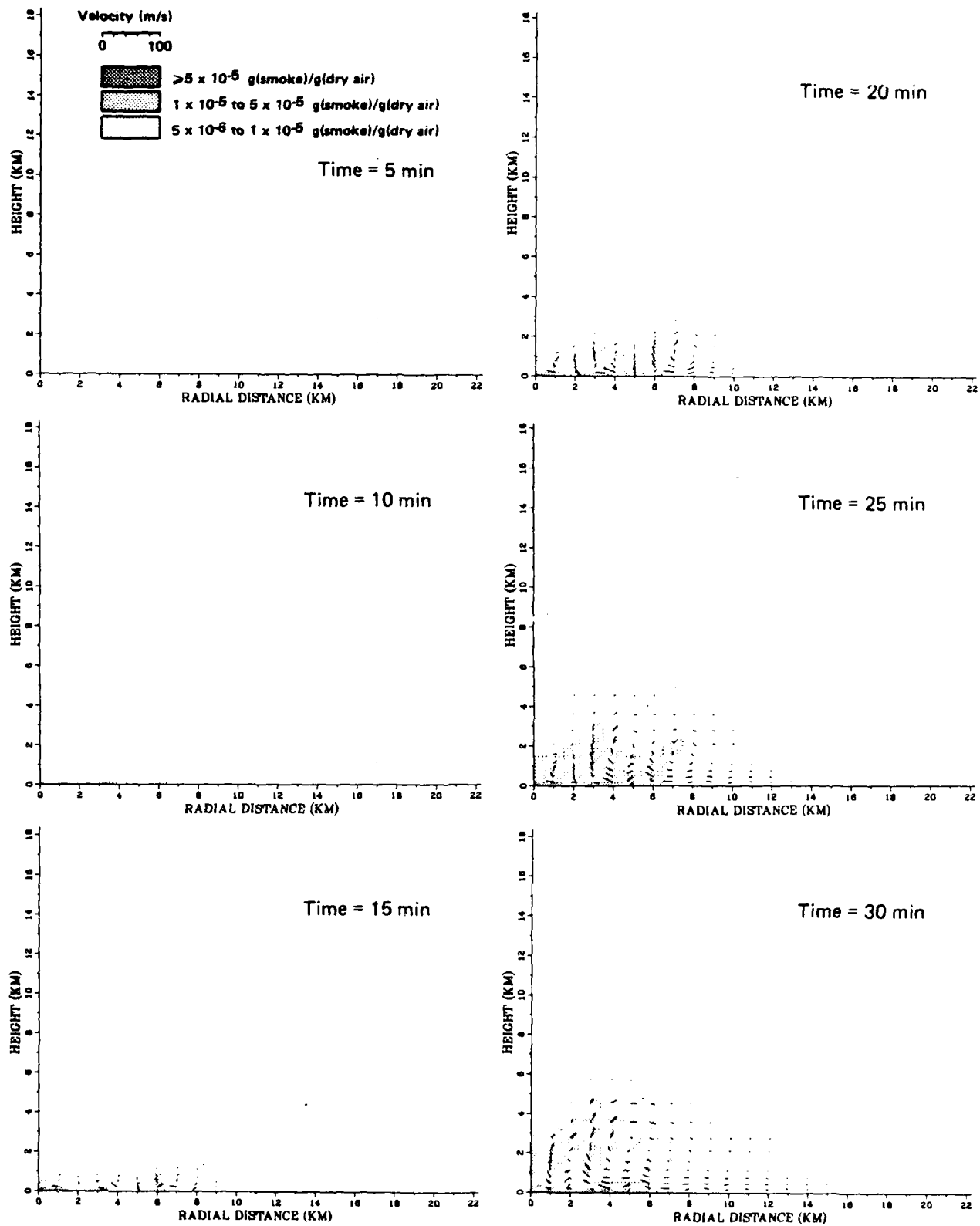


Figure 24. Smoke cloud and velocity vectors for case 9--low-resolution grid.

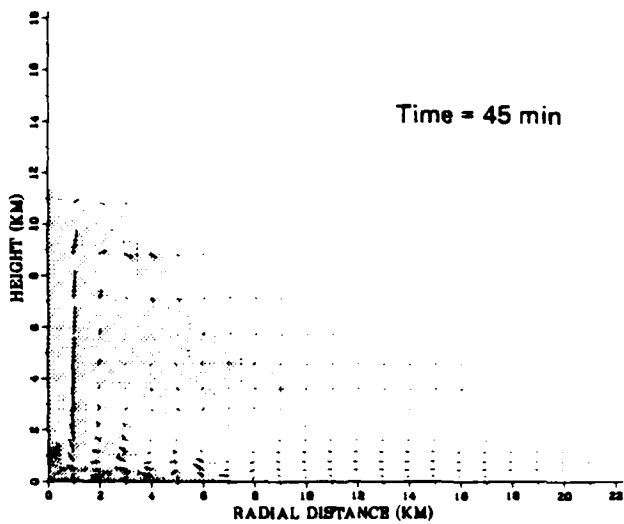
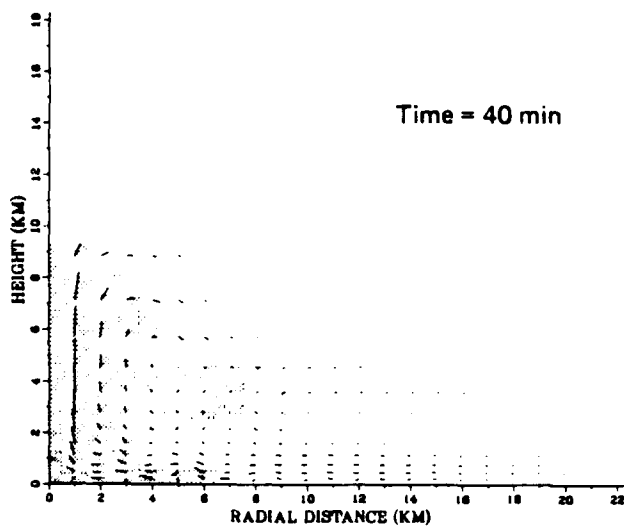
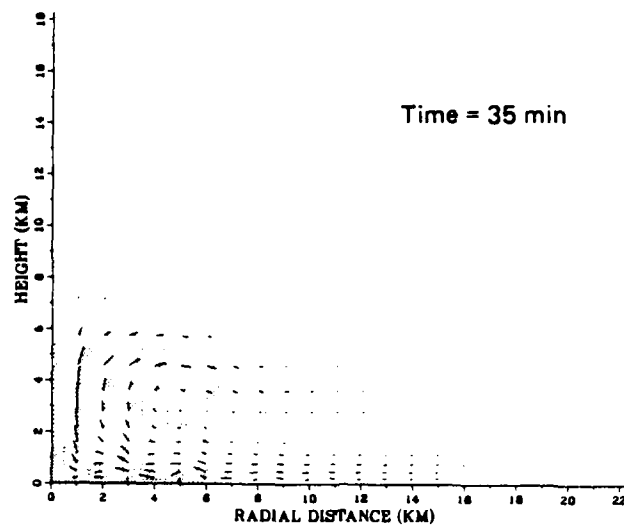


Figure 24. Smoke cloud and velocity vectors for case 9--low-resolution grid (Concluded).

is positive (warm) near the cloud core, negative within a region capping and surrounding the warm central core, and then positive again in the region capping and surrounding the aforementioned cold region. Apparently, the warm air rising along the centerline (the first warm region) overshoots its equilibrium level because of its momentum. This air continues to rise, but due to moist adiabatic expansion it becomes colder than its surroundings (the first cold region). It then falls downward, but once again overshoots equilibrium and warms due to adiabatic compression (the second warm region). This process may be repeated at successively larger radii and corresponds to gravity waves propagating radially outward. The base of the cloud initially consists entirely of liquid water but later becomes a mixture of super-cooled water and ice. The cloud base first occurs near the 0°C level (2.3 km) but later rises to as high as 5 km due to low-level heating. At later times (50 to 55 min) an observed feature of large smoke clouds is reproduced--the folding into the smoke column of pockets of clear air near the base of the mushroom cap. This process apparently enhances the mixing of clear surrounding air with the smoke by bringing clear air into the vicinity of greatest turbulence and smoke concentration.

Case 3: Low Heating Rate (0.25 kW/m^3), Large Radius (10 km).

This case has the lowest heat release, buoyancy production, and thus, the smallest pressure gradients. The fire edge vortex is accordingly sustained longer than in the two previous cases, and the water and moisture clouds never reach significant height (9 km maximum). For this "weak" heating the flow develops slowly and the mass flux to the centerline is limited. The plume and cloud also develop slowly.

Case 4: High Heating Rate (1.00 kW/m^3), Medium Radius (7 km).

Strong updrafts associated with the concentrated heat source near the surface carry air and smoke above the level of neutral buoyancy within 10 min. The warm-core, cloud-free vault is visible at all times, not just in the later stages of cloud development. Pockets of

clear air are constantly being advected into the cloud. The top of the smoke cloud reaches 22 km--the lower stratosphere. The inflow boundary layer is unusually thick. The large radial flux of air into the fire region is consistent with the lofting of air to high altitude.

Case 5: Medium Heating Rate (0.50 kW/m^3), Medium Radius (7 km).

This is the baseline case previously discussed. The complete time sequence is given in Figs. 11 and 20.

Case 6: Low Heating Rate (0.25 kW/m^3), Medium Radius (7 km).

The radial extent of the fire is too great to sustain a large organized circulation to the centerline. Soon after the flow reaches the centerline, the vortex at the fire perimeter reforms, reducing flow to the inner radii. The cloud top seems to be stationary at 12 km by 55 min, and the only change thereafter is the radial spread of smoke at lower altitudes. Much of the inflow between 1 and 3 km appears to be driven by viscous entrainment (which "drags" the air inward over the fire region) rather than by pressure. This inflow is at such a high altitude that it is not heated by the fire. Thus, it never has much buoyancy and does not develop sufficient momentum to be lofted to higher altitudes. It quickly returns to its equilibrium level. This is clearly evident in the streamline patterns at late times.

Case 7: Medium Heating Rate (0.50 kW/m^3), Small Radius (5 km).

The characteristic pattern of a warm core cloud surrounded by alternating regions of cold and warm air occurs within 40 min. The inflow velocity achieves a maximum of 15 m/s (54 km/h). Between 55 and 60 min, a cold bubble of air separates from the cloud at about the level of the cloud base. At the same time, a pocket of clear air is being folded into the core region of the cloud. The cold bubble is probably a result of the evaporation of condensate as the air detrains from the cloud, since the flow is nearly horizontal and does not appear to undergo adiabatic expansion. This process is reminiscent of

smoke detraining from the base of moisture clouds formed by large wildland fires: The downward rolling motion near the cloud base causes the moisture component to evaporate leaving cold, stable, smoky air, which then separates from the cloud. Since it is well above the region of inflow, it does not immediately reenter the smoke column.

Case 8: Dry Atmosphere.

The complete time sequence for the dry atmosphere case is shown in Figs. 14 and 23.

Case 9: Low Grid Resolution.

The complete time sequence for the low grid resolution case is shown in Figs. 15 and 24.

SECTION 4

DISCUSSION

The motions generated by large area fires are, in general, three-dimensional; the burning region is likely to be asymmetric, and wind shears can obviously influence the plume rise and downwind diffusion of smoke. Nevertheless, plume motions--even in strong winds--are often virtually axisymmetric over most of the rise in the atmosphere. The approximation is best near the fire or region of strong buoyancy and least appropriate at the plume top. Although there is some loss in generality, the higher resolution of an axisymmetric simulation more realistically models (within the burning region and plume volume) the entrainment of low-level moisture, the water-phase transitions, and the smoke transport than does a three-dimensional simulation of lower resolution.

We use a volume heat source rather than a surface heat flux to model the fire energy release. The volume source is an approximation of the concentrated effects of actual fire complexes, but it does provide a more realistic distribution of buoyancy than does a surface condition. As a consequence, more accurate representations of the pressure field, fire winds, and low-level moisture convergence into the plume are obtained. Our simulations show that for a range of fire sizes and intensities, plume development is primarily determined by fire intensity and is little affected by fire area (for radii greater than 5 km).

We have shown that atmospheric moisture contributes significantly to plume evolution, and that early scavenging of smoke particles by precipitation is likely to reduce the amount injected into the upper atmosphere. Moreover, the confinement of the plume to a local area suggests greater smoke deposition locally. Except for the largest fires, the tropopause is an effective barrier against the injection of smoke into the stratosphere; since the height of the tropopause varies with season and latitude, these features must be taken into account when determining plume injection heights.

Rain can influence the plume dynamics. Rain either can be evaporated and thus cool the air or fall to the ground. Cooling the air above the fire reduces its buoyancy and inhibits the plume rise. However, latent heat is stored during the evaporation process and its later release within the rising plume may actually enhance the plume rise. The fire-generated cloud extends radially beyond the fire region. Precipitation from such clouds is more likely to evaporate before reaching the ground above the fire than outside the fire region. Moisture entrainment by the fire winds to the burning region could thus be increased. This influences the energy-momentum exchanges (perhaps only slightly). In some cases, fire spread is possible beyond the initial fire start area; rain could prevent or at least moderate such spread. Smoke scavenging and deposition of radioactive material beyond the principal weapon effects region by fire-induced (or augmented) rain may be significant. The inter-relationship between thermodynamics, combustion, and dynamics is subtle and not yet completely defined for large area fires; further modeling and simulations are in progress.

SECTION 5
LIST OF REFERENCES

- Bacon, D. P., R. A. Sarma, and F. H. Proctor, Smoke Injection Into the Atmosphere from Large Area Fires, Science Applications International Corporation, McLean, Virginia, Report No. 86/1922, 1986.
- Bond, H. (ed.), Fire and the Air War, National Fire Protection Association, Boston, Massachusetts, 1946.
- Committee for the Compilation of Materials on Damage Caused by the Atomic Bombs in Hiroshima and Nagasaki, Hiroshima and Nagasaki, E. Ishikawa and D. L. Swain (trans.), Basic Books, Inc., New York City, 1981.
- Cotton, W. R., "Atmospheric Convection and Nuclear Winter," Amer. Scientist, Vol. 73, 1985, pp. 275-280.
- Hassig, P. J., and M. Rosenblatt, "Firestorm Formation and Environment Characteristics after a Large-Yield Nuclear Burst, Proceedings of the 17th Asilomar Conference on Fire and Blast Effects of Nuclear Weapons, Pacific Grove, California, 1983, pp. 54-59.
- Hirt, C. W., A. A. Amsden, and J. L. Cook, "An Arbitrary Lagrangian-Eulerian Computing Method for All Flow Speeds," J. Comp. Phys., Vol. 14, pp. 227-253.
- Larson, D. A., and R. D. Small, Analysis of the Large Urban Fire Environment, Part I: Theory. Pacific-Sierra Research Corporation, Los Angeles, California, Report 1210, 1982.
- Manabe, S., and R. T. Wetherald, "Thermal Equilibrium of the Atmosphere with a Given Distribution of Relative Humidity," J. Atmos. Sci., Vol. 24, 1967, pp. 241-259.
- Manins, P. C., "Cloud Heights and Stratospheric Injections Resulting from a Thermonuclear War," Atmos. Environ., Vol. 19, 1985, pp. 1245-1255.
- Ogura, Y., and N. W. Phillips, "Scale Analysis of Deep and Shallow Convection in the Atmosphere," J. Atmos. Sci., Vol. 19, 1962, pp. 173-179.
- Penner, J. E., L. C. Haselman, and L. L. Edwards, "Smoke-Plume Distributions above Large-Scale Fires: Implications for Simulations of 'Nuclear Winter,'" J. Clim. App. Met., Vol. 25, No. 10, October 1986, pp. 1434-1444.

Pittock, A. B., et al., SCOPE 28: Environmental Consequences of Nuclear War, Vol. 1, "Physical and Atmospheric Effects," Scientific Committee on Problems of the Environment, Chichester, Great Britain, pp. 67-68.

Small, R. D., and D. A. Larson, "Velocity Fields Generated by Large Fires," Israel J. Technol., Vol. 22, 1984/5, pp. 173-186.

Small, R. D., D. A. Larson, and H. L. Brode, "Asymptotically Large Area Fires," J. Heat Trans., Vol. 106, 1984, pp. 318-324.

Small, R. D., D. Remetch, and H. L. Brode, The Physics of Large Fires, presented at DNA Conference on Large-Scale Fire Phenomenology, Gaithersburg, Maryland, 1984.

-----, Atmospheric Motions from Large Fires, presented at AIAA 23d Aerospace Sciences Meeting, Reno, Nevada, Paper No. AIAA 85-0458, 1985.

Tripoli, G. J., and S. W. Kang, A Numerical Simulation of the Smoke Plume Generated by a Hypothetical Urban Fire near San Jose, California, presented at Scientific Committee on Problems of the Environment, Bangkok, Thailand, 1987.

U.S. Standard Atmosphere, U.S. Government Printing Office, Washington, D.C., 1962.

APPENDIX A SMOKE PRODUCTION

The smoke production rate per unit area \dot{S}_A for a 3 percent smoke emission (assuming a $2 \text{ g/cm}^2/\text{h}$ burn rate) is

$$\begin{aligned}\dot{S}_A &= \text{burn rate} \times \frac{\text{smoke mass}}{\text{fuel mass}} \\ &= \frac{2 \text{ g fuel}}{\text{cm}^2 \text{ h}} \times \frac{0.03 \text{ g smoke}}{1.00 \text{ g fuel}} \\ &= 0.166 \frac{\text{g smoke}}{\text{m}^2 \text{ s}}\end{aligned}\quad (8)$$

Now let the smoke produced at the surface immediately fill a 100-m high volume. Then the smoke release rate per unit volume \dot{S}_V is

$$\dot{S}_V = \dot{S}_A / 100 \text{ m} = 1.66 \times 10^{-3} \frac{\text{g smoke}}{\text{m}^3 \text{ s}}\quad (9)$$

Assuming that a burn rate of $2 \text{ g/cm}^2/\text{h}$ corresponds to a 1 kW/m^3 volume heating rate in a 100-m high volume and that burn rate is directly proportional to a heating rate \dot{q}_f , the volume smoke production is given by

$$\dot{S}_V = \dot{S} = 1.66 \times 10^{-3} \frac{\text{g smoke}}{\text{m}^3 \text{ s}} \frac{\dot{q}_f}{\text{kW/m}^3},\quad (10)$$

or

$$\dot{S} = 1.66 \times 10^{-6} \frac{\text{kg smoke}}{\text{m}^3 \text{ s}} \frac{\dot{q}_f}{\text{kW/m}^3}.\quad (11)$$

APPENDIX B WATER PROCESSES

The type of water phase transition that takes place is determined by the temperature, availability of condensate, condensate phase, and vapor density relative to the temperature-dependent saturation value. The incremental latent heat release Δq , during a single time step Δt , is

$$\Delta q = -L_{1v} \Delta \rho_v - L_{1i} \Delta \rho_i = c_p \Delta p / \rho, \quad (12)$$

where L_{1v} is latent heat of vaporization [$0.4604 \times 10^6 - 2.369 \times 10^3 (T - T_f)$ J/kg], L_{1i} is latent heat of fusion (0.3336×10^6 J/kg), ρ_v is vapor density, ρ_i is ice density, c_p is specific heat at constant density, T_f is freezing point temperature (-15°C), and T is temperature. This is a constant pressure process and, therefore, $\Delta p = 0$. The change in water vapor density occurring during Δt is

$$\Delta \rho_v = \min (\rho_{vs} - \rho_v, \rho_l + \rho_i), \quad (13)$$

where R_v is the gas constant for water vapor (0.4604×10^3 J/kg/K), p_{vs} is saturation vapor pressure or $610.78 \exp [6.8355 \times 10^3 (1/T_f - 1/T) + 5.1455 \ln T_f/T]$, ρ_{vs} is saturation vapor density ($\rho_{vs} = p_{vs}/R_v/T$), and ρ_l is liquid density. Thus, if supersaturated conditions exist, there is a decrease in vapor density equal to $|\rho_{vs} - \rho_v|$. If subsaturated conditions exist, the water vapor deficit $|\rho_{vs} - \rho_v|$ is compensated for by a conversion of condensate to vapor until saturation is reached, as long as $\rho_l + \rho_i$ exceeds $|\rho_{vs} - \rho_v|$. If $|\rho_{vs} - \rho_v|$ exceeds $\rho_l + \rho_i$, the increase in water vapor density is $\rho_l + \rho_i$.

The parameters defining the amount of precipitation are set so that one-third the liquid water and one-half the ice formed during Δt are removed by precipitation:

$$\alpha_1 = \frac{2}{3} ,$$

$$\alpha_i = \frac{1}{2} . \quad (14)$$

If the air is subsaturated ($\Delta\rho_v \geq 0$) at the beginning of the time step then there is no precipitation, so:

$$\alpha_i = 1 . \quad (15)$$

The water vapor density is updated and the preliminary heat release is set:

$$\begin{aligned} \rho_v &\leftarrow \rho_v + \Delta\rho_v \\ q &\leftarrow -L_{lv} \Delta\rho_v . \end{aligned} \quad (16)$$

where q is heat release in joules per cubic meter. The decision-making process built into the code takes account of the temperature. If the temperature exceeds the melting point $T_m (= 0^\circ\text{C})$, then cooling takes place due to the fact that all ice melts:

$$q \leftarrow q - L_{li} \rho_i . \quad (17)$$

The amount of liquid water increases by the amount of melted ice. It decreases by evaporation if the air is subsaturated ($\Delta\rho_v \geq 0$, $\alpha_1 = 1$) or increases by the amount of condensation not lost to precipitation if the air is supersaturated ($\Delta\rho_v < 0$, $\alpha_1 = 2/3$):

$$\rho_l \leftarrow \rho_l + \rho_i - \alpha_1 \Delta\rho_v , \quad (18)$$

and finally

$$\rho_i \leftarrow 0 . \quad (19)$$

Due to the scarcity of suitable freezing nuclei in the atmosphere, the freezing point T_f is taken to be -15°C rather than 0°C . Supercooled water and ice coexist within the temperature range $T_m \geq T \geq T_f$. A high concentration of smoke particles may alter this phenomenon but barring definitive observations to the contrary, we adhere to the stated parameterization.

If $\Delta\rho_v \geq \rho_l \geq 0$ (subsaturated) and $\rho_i \geq 0$, cooling occurs due to sublimation of ice and evaporation of water:

$$q \leftarrow q - L_{li}(\Delta\rho_v - \rho_l) . \quad (20)$$

The term $L_{li}(\Delta\rho_v - \rho_l)$ arises from the water vapor deficit being first made up by evaporation of liquid, then by supercooled water, and finally by sublimation of ice. This is commensurate with the vapor pressure over water being less than that over ice at the same temperature. The change in the liquid and ice components is, respectively,

$$\rho_i \leftarrow \rho_i + \rho_l - \Delta\rho_v , \quad (21)$$

and

$$\rho_l \leftarrow 0 . \quad (22)$$

If $\Delta\rho_v \leq \rho_l$, the change in the liquid water component is

$$\rho_l \leftarrow \rho_l - \alpha_l \Delta\rho_v . \quad (23)$$

Since $\alpha_i = \alpha_l = 1$ for $\Delta\rho_v \geq 0$, the process used for the supercooled water temperature range also holds for $T \leq T_f$.

APPENDIX C WATER CONTENT DUE TO COMBUSTION

The amount of water normally present in the atmosphere far exceeds that produced by combustion. Consider the combustion of F, a typical fuel load F ($F = 10 \text{ kg/m}^2$). The hydrogen content of urban fuels is approximately 5 percent by mass, slightly higher (~ 6.5 percent) for cellulose. The molecular weight of hydrogen is 1 and that of oxygen is 16. A 5 percent hydrogen content, when combined with atmospheric oxygen, results in water due combustion of $0.45 F$. Assume that the water produced at the surface is lofted relatively slowly at vertical velocity v ($v = 3 \text{ m/s}$), so as to maximize water vapor density, and that it fills a volume directly above the surface where it was produced. If the fuel is completely consumed in time $t = 1 \text{ h}$, then the water vapor density ρ_v in the column above the site of combustion is

$$\rho_{v \text{ combustion}} = 0.45 F/v/t = 4.2 \times 10^{-4} \frac{\text{kg}}{\text{m}^3} \text{ H}_2\text{O} . \quad (24)$$

Now consider the atmospheric water vapor density for a low relative humidity (20 percent), so as to minimize the atmospheric water vapor density. The relative humidity is the ratio of ambient mixing ratio w to the saturation mixing ratio w_s :

$$\text{mixing ratio} = \frac{w}{w_s} = \frac{e}{e_s} = 0.2 , \quad (25)$$

where e and e_s are the ambient and saturation vapor pressures, respectively.

At 20°C,

$$e_s(20^\circ\text{C}) = 23.373 \times 10^2 \text{ N/m}^2, \quad (26)$$

and

$$\begin{aligned} \rho_{v \text{ ambient}} &= \frac{e}{R_v T} = \frac{4.68 \times 10^2 \text{ N/m}^2}{(460 \text{ J/kg/K}) (293 \text{ K})}, \\ &= 3.5 \times 10^{-3} \text{ kg/m}^3. \end{aligned} \quad (27)$$

Thus, even under extreme conditions, the atmospheric water vapor density exceeds that produced by combustion by an order of magnitude.

DISTRIBUTION LIST

DEPARTMENT OF DEFENSE

ARMED FORCES RADIOBIOLOGY RSCH INST
ATTN: V BOGO

ASSISTANT TO THE SECRETARY OF DEFENSE
ATOMIC ENERGY
ATTN: LTCOL L MILLS

DEFENSE INTELLIGENCE AGENCY
ATTN: DB-6E2 C WIEHLE
ATTN: N BARON
ATTN: RTS-2B
ATTN: RTS-2B
ATTN: WDB-4CR

DEFENSE NUCLEAR AGENCY
ATTN: DFRA
ATTN: DFSP G ULLRICH
ATTN: OPNS
ATTN: RAAE
ATTN: RAAE K SCHWARTZ
ATTN: RAAE L WITTWER
ATTN: RAAE G BAKER
ATTN: RAAE R WEBB
ATTN: RARP D AUTON
ATTN: SPAS M FRANKEL
ATTN: TDTD/C CORSETTI
2 CYS ATTN: TDTR
4 CYS ATTN: TITL

DEFENSE TECHNICAL INFORMATION CENTER
12CYS ATTN: DD

DIRECTOR
ATTN: LTCOL G BETOURNE
ATTN: R RUFFIN

FIELD COMMAND DEFENSE NUCLEAR AGENCY
ATTN: FCTXE
ATTN: FTTD W SUMMA

JOINT STRAT TGT PLANNING STAFF
ATTN: JKCS

NATIONAL DEFENSE UNIVERSITY
ATTN: COL S GARDINER
ATTN: G FOSTER MOB CONCEPTS DEV CTR
ATTN: H ALMOND

OFFICE OF THE SECRETARY OF DEFENSE
ATTN: COL A RAMSAY

DEPARTMENT OF THE ARMY

U S ARMY ATMOSPHERIC SCIENCES LAB
ATTN: R SUTHERLAND
ATTN: SLCAS-AR-M MR RUBIO

U S ARMY CORPS OF ENGINEERS
ATTN: DAEN-RDM R GOMEZ
ATTN: DR CHOROMOKOS DAEN-RDM

U S ARMY CORPS OF ENGINEERS
ATTN: L ZIEGLER
ATTN: R BECKER

U S ARMY ENGR WATERWAYS EXPER STATION
ATTN: L LINK

U S ARMY MISSILE INTELLIGENCE AGENCY
ATTN: J GAMBLE

U S ARMY NATICK RSCH DEV & ENGRG CENTER
ATTN: H M EL-BISI

U S ARMY STRATEGIC DEFENSE COMMAND
ATTN: DR J LILLY
ATTN: G EDLIN
ATTN: J VEENEMAN
ATTN: M CAPPS
ATTN: R BRADSHAW

DEPARTMENT OF THE NAVY

CNO EXECUTIVE PANEL
ATTN: CAP L BROOKS

NAVAL RESEARCH LABORATORY
ATTN: R JEK

NAVAL SURFACE WEAPONS CENTER
ATTN: K-44 S MASTERS

DEPARTMENT OF THE AIR FORCE

AF/INYXC
ATTN: LTCOL N BARRY

AIR FORCE GEOPHYSICS LABORATORY
ATTN: D CHISHOLM
ATTN: LS/R MURPHY
ATTN: LSI/ H GARDINER
ATTN: LYC/R BANTA
ATTN: LYP H S MUENCH

AIR FORCE INSTITUTE OF TECHNOLOGY/EN
ATTN: AFIT/ENP MAJ S R BERGGREN

DNA-TR-87-176 (DL CONTINUED)

AIR FORCE OFFICE OF SCIENTIFIC RSCH
ATTN: D BALL

AIR FORCE SPACE DIVISION
ATTN: YNC CAPT K O'BRYAN

AIR FORCE TECHNICAL APPLICATIONS CTR
ATTN: J MARSHALL

AIR FORCE WEAPONS LABORATORY
ATTN: CAPT LEONG
ATTN: J JANNI
ATTN: J W AUBREY, NTEd

BALLISTIC MISSILE OFFICE
ATTN: LT ROTHCHILD
ATTN: MYSP/CAP TOMASZEWSKI

DEPUTY CHIEF OF STAFF/XOX
ATTN: AFXOX

STRATEGIC AIR COMMAND/XPXF
ATTN: T BAZZOLI

DEPARTMENT OF ENERGY

ARGONNE NATIONAL LABORATORY
ATTN: H DRUCKER
ATTN: M WESLEY

BROOKHAVEN NATIONAL LABORATORY
ATTN: B MANOWITZ
ATTN: E WEINSTOCK

DEPARTMENT OF ENERGY
ATTN: I NEDDOW
ATTN: T HARRIS

DESERT RESEARCH INSTITUTE
ATTN: J HALLETT
ATTN: J HUDSON

LAWRENCE BERKELEY NATIONAL LAB
ATTN: H ROSEN

LAWRENCE LIVERMORE NATIONAL LAB
ATTN: C R MOLENKAMP
ATTN: C SHAPIRO
ATTN: F LUTHER
ATTN: G BING
ATTN: G SIMONSON
ATTN: J PENNER
ATTN: J POTTER
ATTN: L-10 A GROSSMAN
ATTN: L-262 A BROYLES
ATTN: L-262 J KNOX
ATTN: L-442, J BACKOVSKY
ATTN: L-453 L ANSPAUGH
ATTN: M MACCRACKEN
ATTN: N ALVAREZ
ATTN: R MALONE

ATTN: R PERRET
ATTN: R PERRETT
ATTN: S GHAN

LOS ALAMOS NATIONAL LABORATORY
ATTN: D SAPPENFIELD
ATTN: DR. D CAGLIOSTRO
ATTN: E J CHAPYAK
ATTN: E JONES
ATTN: E SYMBALISTY
ATTN: G GLATZMAIER/ESS
ATTN: G M SMITH
ATTN: L H AUER
ATTN: L CLOUTMAN
ATTN: P HUGES
ATTN: R MALONE
ATTN: T YAMATTA

OAK RIDGE NATIONAL LABORATORY
ATTN: D FIELDS

SANDIA NATIONAL LABORATORIES
ATTN: A L JOHNSON
ATTN: B ZAK
ATTN: D DAHLGREN 6440
ATTN: D FORDHAM
ATTN: D WILLIAMS
ATTN: DIV G-449 K D BERGERON
ATTN: L TROST
ATTN: M D BENNETT
ATTN: ORG 332 R C BACKSTROM

OTHER GOVERNMENT

CENTRAL INTELLIGENCE AGENCY
ATTN: A WARSHAWSKY
ATTN: 7E47 R NELSON

DEPARTMENT OF AGRICULTURE
ATTN: D HAINES

DEPARTMENT OF COMMERCE
ATTN: H BAUM
ATTN: R LEVINE

DEPARTMENT OF TRANSPORTATION
ATTN: COL M ROESCH

DIRECTOR, FFASR
ATTN: C CHANDLER

ENVIRONMENTAL PROTECTION AGENCY
ATTN: R COTHERN
ATTN: W E FALLON

FEDERAL EMERGENCY MANAGEMENT AGENCY
ATTN: B W BLANCHARD
ATTN: D BENSON NP-CP-MR
ATTN: D KYBAL
ATTN: H TOVEY

DNA-TR-87-176 (DL CONTINUED)

ATTN: J POWERS ATTN: J RUMBARGER ATTN: OFC OF RSCH/NP H TOVEY ATTN: S ALTMAN	OFFICE OF SCIENCE AND TECH POLICY ATTN: B HEALY ATTN: COL S WYMAN
GENERAL ACCOUNTING OFFICE ATTN: A PIERCE ATTN: P J BOLLEA ATTN: V BIELECKI	OFFICE OF TECHNOLOGY ASSESSMENT ATTN: R WILLIAMSON
NASA ATTN: N CRAYBILL ATTN: W R COFER	U S ARMS CONTROL & DISARMAMENT AGCY ATTN: B DOENGES NWC-DPA ATTN: G PITMAN ATTN: H SCHAEFFER ATTN: R GODESKY ATTN: R O'CONNELL NWC-DPA
NASA ATTN: R HABERLE ATTN: O TOON ATTN: R YOUNG ATTN: T ACKERMAN	U S DEPARTMENT OF STATE ATTN: A CORTE ATTN: C CLEMENT,(OES.STS) ATTN: S CLEARY ATTN: T VREBALOVICH OES.STS
NATIONAL BUREAU OF STANDARDS ATTN: G MULHOLLAND ATTN: R LEVINE ATTN: R REHM ATTN: R SCHRACK	U S GEOLOGICAL SURVEY ATTN: R DECKER
NATIONAL BUREAU OF STANDARDS ATTN: H BAUM	U S GEOLOGICAL SURVEY ATTN: E SHOEMAKER
NATIONAL CENTER ATMOSPHERIC RESEARCH ATTN: J KIEHL ATTN: S SCHNEIDER ATTN: S THOMPSON ATTN: V RAMASWAMY	U S HOUSE OF REPRESENTATIVES ATTN: C BAYER ATTN: COMMITTEE ON SCI & TECH J DUGAN
NATIONAL CLIMATE PROGRAM OFFICE ATTN: A HECHT ATTN: M YERG	U S HOUSE OF REPRESENTATIVES ATTN: J FREIWALD ATTN: M HERBST
NATIONAL OCEANIC & ATMOSPHERIC ADMIN ATTN: F FEHSENFELD ATTN: J DELUISI ATTN: R PUESCHEL ATTN: V DERR	US DEPARTMENT AGRICULTURE ATTN: D WARD
NATIONAL OCEANIC & ATMOSPHERIC ADMIN. ATTN: B HICKS	DEPARTMENT OF DEFENSE CONTRACTORS
NATIONAL RESEARCH COUNCIL ATTN: K BEHR ATTN: R DEFRIES	AERO-CHEM RESEARCH LABS, INC ATTN: D B OLSON
NATIONAL SCIENCE FOUNDATION ATTN: E BIERLY ATTN: H VIRJI ATTN: L HAMATY ATTN: R SINCLAIR ATTN: R TAYLOR	AERODYNE RESEARCH, INC ATTN: C KOLB ATTN: J LURIE
NUCLEAR REGULATORY COMMISSION ATTN: R ALEXANDER	AEROJET ELECTRO-SYSTEMS CO ATTN: A FYMAT ATTN: S HAMILTON ATTN: R PAN
	AEROSPACE CORP ATTN: C RICE ATTN: L R MARTIN
	AEROSPACE CORPORATION ATTN: G LIGHT
	ALLEN RESEARCH CORP ATTN: R ALLEN

DNA-TR-87-176 (DL CONTINUED)

AMERICAN ASSN ADVANCEMENT OF SCIENCE
ATTN: D M BURNS

ANALYTIC SERVICES, INC (ANSER)
ATTN: R BROFFT

APPLIED RESEARCH CORP
ATTN: A ENDAL

AT&T DEFENSIVE SYSTEMS STUDIES
ATTN: R JANOW

ATMOSPHERIC AND ENVIRONMENTAL RES
ATTN: N SZE

AUDIO INTELLIGENCE DEVICES INC
ATTN: H BAUM

AVCO CORPORATION
ATTN: G GRANT, DEPT MGR

BALL AEROSPACE SYSTEMS DIVISION
ATTN: B CUMMINGS
ATTN: C BRADFORD

BDM CORP
ATTN: J LEECH

BERKELEY RSCH ASSOCIATES, INC
ATTN: S BRECHT

BOEING AEROSPACE COMPANY
ATTN: N GERONTAKIS

BOEING TECHNICAL & MANAGEMENT SVCS, INC
ATTN: G HALL

C. L. CONSULTING SERVICES
ATTN: F FEER

CALIF RESEARCH & TECHNOLOGY, INC
ATTN: M ROSENBLATT
ATTN: R GAJ
ATTN: S KRUEGER

CALSPAN CORP
ATTN: R MAMBRETTI
ATTN: R MISSERT

CARNEGIE CORPORATION OF NEW YORK
ATTN: D ARSENIAN

CARPENTER RESEARCH CORP
ATTN: H J CARPENTER

CASSIDY AND ASSOCIATES
ATTN: J JACOBSON

CHARLES SCAWTHORN
ATTN: C SCAWTHORN

CHARLES STARK DRAPER LAB, INC
ATTN: A TETEWSKI

COLORADO STATE UNIVERSITY
ATTN: D KRUEGER
ATTN: W COTTON

COMPUTER SCIENCES CORP
ATTN: G CABLE

DARTSIDE CONSULTING
ATTN: A FORESTER

DEFENSE ELECTRONICS GROUP
ATTN: H BURNSWORTH
ATTN: J BELING

DELTA RESEARCH, INC
ATTN: L WEINER
ATTN: M RADKE

DYNAMICS TECHNOLOGY, INC
ATTN: D HOVE

ENW INTERNATIONAL, LTD
ATTN: J CANE

EOS TECHNOLOGIES, INC
ATTN: B GABBARD
ATTN: N JENSEN
ATTN: W LELEVIER

FACTORY MUTUAL RESEARCH CORP
ATTN: M A DELICHATSIOS
ATTN: R FRIEDMAN

FEDERATION OF AMERICAN SCIENTISTS
ATTN: J STONE

GENERAL ELECTRIC CO
ATTN: R E SCHMIDT

GENERAL RESEARCH CORP
ATTN: B BENNETT
ATTN: J BALTES

HAROLD ROSENBAUM ASSOCIATES, INC
ATTN: G WEBER

HORIZONS TECHNOLOGY INC
ATTN: A EDWARDS
ATTN: J AMBROSE

HORIZONS TECHNOLOGY, INC
ATTN: R W LOWEN
ATTN: W T KREISS

HUGHES AIRCRAFT CO
ATTN: E DIVITA

IIT RESEARCH INSTITUTE
ATTN: H NAPADENSKY

DNA-TR-87-176 (DL CONTINUED)

INFORMATION SCIENCE, INC
ATTN: W DUDZIAK

INSTITUTE FOR DEFENSE ANALYSES
ATTN: C CHANDLER
ATTN: E BAUER
ATTN: F ALBINI
ATTN: L SCHMIDT

JOHNS HOPKINS UNIVERSITY
ATTN: M LENEVSKY
ATTN: R FRISTROM
ATTN: W BERL

KAMAN SCIENCES CORP
ATTN: J RUSH
ATTN: J SCRUGGS

KAMAN SCIENCES CORP
ATTN: P GRIFFIN
ATTN: P TRACY

KAMAN SCIENCES CORP
ATTN: E CONRAD

KAMAN SCIENCES CORPORATION
ATTN: D ANDERSON
ATTN: DASAC

KAMAN TEMPO
ATTN: B GAMBILL
ATTN: D FOXWELL
ATTN: DASAC
ATTN: E MARTIN
ATTN: R RUTHERFORD
ATTN: R YOUNG
ATTN: S FIFER
ATTN: W KNAPP

LOCKHEED MISSILES & SPACE CO, INC
ATTN: J HENLEY
ATTN: J PEREZ

LOCKHEED MISSILES & SPACE CO, INC
ATTN: P DOLAN
ATTN: W MORAN

M I T LINCOLN LAB
ATTN: S WEINER

MARTIN MARIETTA DENVER AEROSPACE
ATTN: D HAMPTON

MAXIM TECHNOLOGIES, INC
ATTN: J MARSHALL

MCDONNELL DOUGLAS CORP
ATTN: T CRANOR
ATTN: T TRANER

MCDONNELL DOUGLAS CORP
ATTN: A MONA
ATTN: F SAGE
ATTN: G BATUREVICH
ATTN: J GROSSMAN
ATTN: R HALPRIN
ATTN: S JAEGER
ATTN: W YUCKER

MERIDIAN CORP
ATTN: E DANIELS
ATTN: F BAITMAN

MIDWEST RESEARCH INSTITUTE
ATTN: J S KINSEY

MISSION RESEARCH CORP
ATTN: R ARMSTRONG

MISSION RESEARCH CORP
ATTN: C LONGMIRE
ATTN: D ARCHER
ATTN: D KNEPP
ATTN: D SOWLE
ATTN: F FAJEN
ATTN: J BALL
ATTN: K R COSNER
ATTN: R BIGONI
ATTN: R GOLDFLAM
ATTN: R HENDRICK
ATTN: T OLD
ATTN: W WHITE

MITRE CORPORATION
ATTN: J SAWYER

MODELING SYSTEM, INC
ATTN: G BERLIN

MRJ INC
ATTN: D FREIWALD

NATIONAL ADVISORY COMMITTEE
ATTN: J ALMAZAN
ATTN: J BISHOP

NATIONAL INST. FOR PUBLIC POLICY
ATTN: K PAYNE

NICHOLS RESEARCH CORP, INC
ATTN: H SMITH
ATTN: J SMITH
ATTN: M FRASER
ATTN: R BYRN

NORTHROP SERVICES INC
ATTN: T OVERTON

NOTRE DAME DU LAC, UNIV OF
ATTN: T J MASON

DNA-TR-87-176 (DL CONTINUED)

ORLANDO TECHNOLOGY INC
ATTN: R SZCZEPANSKI

PACIFIC-SIERRA RESEARCH CORP
ATTN: G ANNO
ATTN: H BRODE, CHAIRMAN SAGE
2 CYS ATTN: K HEIKES
2 CYS ATTN: L RANSOHOFF
ATTN: M DORE
2 CYS ATTN: R SMALL

PHOTOMETRICS, INC
ATTN: I L KOFSKY

PHOTON RESEARCH ASSOCIATES
ATTN: J MYER

PHYSICAL RESEARCH CORP
ATTN: A CECERE

PHYSICAL RESEARCH INC
ATTN: H FITZ

PHYSICAL RESEARCH INC
ATTN: D MATUSKA

PHYSICAL RESEARCH INC
ATTN: J WANG
ATTN: W SHIH

PHYSICAL RESEARCH, INC
ATTN: D WESTPHAL
ATTN: D WHITENER
ATTN: H WHEELER
ATTN: R BUFF
ATTN: R DELIBERIS
ATTN: T STEPHENS
ATTN: W C BLACKWELL

PHYSICAL RESEARCH, INC
ATTN: G HARNEY
ATTN: J DEVORE
ATTN: J THOMPSON
ATTN: R STOECKLY
ATTN: W SCHLUETER

PHYSICAL RESEARCH, INC
ATTN: H SUGIUCHI

POLYTECHNIC OF NEW YORK
ATTN: B J BULKIN
ATTN: G TESORO

PRINCETON UNIVERSITY
ATTN: J MAHLMAN

QUADRI CORP
ATTN: H BURNSWORTH

R & D ASSOCIATES
ATTN: A KUHL
ATTN: D HOLLIDAY
ATTN: F GILMORE
ATTN: G JONES
ATTN: J SANBORN
ATTN: R TURCO

R & D ASSOCIATES
ATTN: B YOON

R J EDWARDS INC
ATTN: R SEITZ

RADIATION RESEARCH ASSOCIATES, INC
ATTN: B CAMPBELL
ATTN: M WELLS

RAND CORP
ATTN: G L DONOHUE
ATTN: P DAVIS
ATTN: P ROMERO

RAND CORP
ATTN: B BENNETT
ATTN: J GERTLER

ROCKWELL INTERNATIONAL CORP
ATTN: J KELLEY

S-CUBED
ATTN: B FREEMAN
ATTN: K D PYATT, JR
ATTN: R LAFRENZ

S-CUBED
ATTN: C NEEDHAM
ATTN: S HIKIDA
ATTN: T CARNEY

SCIENCE APPLICATIONS INC
ATTN: R EDELMAN

SCIENCE APPLICATIONS INTL CORP
ATTN: C HILL

SCIENCE APPLICATIONS INTL CORP
ATTN: B MORTON
ATTN: B SCOTT
ATTN: D SACHS
ATTN: G T PHILLIPS
ATTN: J BENGSTOM
ATTN: M DRAKE
ATTN: M MCKAY
ATTN: D HAMLIN

SCIENCE APPLICATIONS INTL CORP
ATTN: D BACON
ATTN: DR L GOURE
ATTN: F GIESSLER
ATTN: J COCKAYNE

DNA-TR-87-176 (DL CONTINUED)

ATTN: J SHANNON	TELEDYNE BROWN ENGINEERING
ATTN: J STUART	ATTN: D GUICE
ATTN: M SHARFF	TEXAS ENGR EXPERIMENT STATION
ATTN: W LAYSON	ATTN: W H MARLOW
SCIENCE APPLICATIONS INTL CORP	TOYON RESEARCH CORP
ATTN: J SONTOWSKI	ATTN: C TRUAX
SCIENCE APPLICATIONS INTL CORP	ATTN: J GARBARINO
ATTN: T HARRIS	ATTN: J ISE
SCIENTIFIC RESEARCH ASSOC, INC	TRW ELECTRONICS & DEFENSE SECTOR
ATTN: B WEINBERG	ATTN: M HAAS
SCIENTIFIC SERVICES, INC	TRW INC
ATTN: C WILTON	ATTN: F FENDELL
SRI INTERNATIONAL	ATTN: G KIRCHNER
ATTN: C WITHAM	ATTN: H CROWDER
ATTN: D GOLDEN	ATTN: J FEDELE
ATTN: D MACDONALD	ATTN: M BRONSTEIN
ATTN: D ROBERTS	ATTN: R BACHARACH
ATTN: E UTHE	ATTN: S FINK
ATTN: G ABRAHAMSON	ATTN: T NGUYEN
ATTN: J BACKOVSKY	VISIDYNE, INC
ATTN: W CHESNUT	ATTN: H SMITH
SRI INTERNATIONAL	ATTN: J CARPENTER
ATTN: R BRAMHALL	WASHINGTON, UNIVERSITY OF
ATTN: R WOOLFOLK	ATTN: J I KATZ
ATTN: W VAIL	FOREIGN
STAN MARTIN ASSOCIATES	AERE ENVIRONMENTAL AND MEDICAL SC
ATTN: S B MARTIN	ATTN: S PENKETT
ATTN: S MARTIN	ATOMIC WEAPONS RESEARCH ESTABLISHMENT
STANTON CONSULTING	ATTN: P F A RICHARDS
ATTN: M STANTON	ATOMIC WEAPONS RESEARCH ESTABLISHMENT
SWE'L, INC	ATTN: D L JONES
ATTN: T PALMER	ATTN: D M MOODY
ATTN: T Y PALMER	AUSTRALIA EMBASSY
SYSTEM PLANNING CORP	ATTN: DR LOUGH
ATTN: B GARRETT	ATTN: MAJ GEN H J COATES
ATTN: C FELDBAUM	ATTN: P PROSSER
ATTN: J SCOURAS	BRITISH DEFENCE STAFF
ATTN: M BIENVENU	ATTN: C FENWICK
ATTN: R SCHEERBAUM	ATTN: J CRANIDGE
SYSTEMS AND APPLIED SCIENCES CORP	ATTN: J EDMONDS
ATTN: M KAPLAN	ATTN: M NORTON
TECHNOLOGY INTERNATIONAL CORP	ATTN: P WEST
ATTN: W BOQUIST	CANADIAN FORESTRY SERVICE
TELEDYNE BROWN ENGINEERING	ATTN: B STOCKS
ATTN: A ORTELL	ATTN: T LYNHAM
ATTN: F LEOPARD	CSIRO
ATTN: J FORD	ATTN: I GALBALLY

DNA-TR-87-176 (DL CONTINUED)

CSIRO: ATMOSPHERIC RESEARCH
ATTN: A PITTOCK

EMBASSY OF BELGIUM
ATTN: L ARNOULD

ISRAEL EMBASSY
ATTN: N BELKIND

MAX-PLANCK INSTITUTE FOR CHEMISTRY
ATTN: P J CRUTZEN

MINISTRY OF DEFENCE
ATTN: R RIDLEY

NATIONAL DEFENCE HEADQUARTERS
ATTN: H A ROBITALLE

TRINITY COLLEGE
ATTN: F HARE

DIRECTORY OF OTHER

ATMOS. SCIENCES
ATTN: G SISCOE

BROWN UNIVERSITY
ATTN: R K MATTHEWS

BUCKNELL UNIVERSITY
ATTN: O ANDERSON

CALIFORNIA, UNIVERSITY
ATTN: R WILLIAMSON

CALIFORNIA, UNIVERSITY OF
ATTN: L BADASH/DEPT OF HIST

COLORADO, UNIVERSITY LIBRARIES
ATTN: J BIRKS
ATTN: R SCHNELL

DREXEL UNUNIVERSITY
ATTN: J FRIEND

DUKE UNIVERSITY
ATTN: F DELUCIA

GEORGE MASON UNIVERSITY
ATTN: PROF S SINGER
ATTN: R EHRLICH

GEORGE WASHINGTON UNIVERSITY
ATTN: R GOULARD

GEORGIA INST OF TECH
ATTN: E PATTERSON

HARVARD COLLEGE LIBRARY
ATTN: W PRESS

HARVARD UNIVERSITY
ATTN: G CARRIER

HARVARD UNIVERSITY
ATTN: D EARDLEY

IOWA, UNIVERSITY OF
ATTN: HISTORY DEPT/S PYNE

MARYLAND UNIVERSITY OF
ATTN: A ROBOCK DEPT METEOROLOGY
ATTN: A VOGELMANN DEPT METEOROLOGY
ATTN: R ELLINGSON DEPT METEOROLOGY

MIAMI LIBRARY UNIVERSITY OF
ATTN: C CONVEY

MIAMI UNIV LIBRARY
ATTN: J PROSPERO ATMOS SC

NEW YORK STATE UNIVERSITY OF
ATTN: R CESS

OAK RIDGE ASSOCIATED UNIVERSITIES
ATTN: C WHITTLE

PENNSYLVANIA STATE UNIVERSITY
ATTN: D WESTPHAL

SOUTH DAKOTA SCH OF MINES & TECH LIB
ATTN: H ORVILLE

TENNESSEE, UNIVERSITY OF
ATTN: K FOX

UNIVERSITY OF SOUTH FLORIDA
ATTN: S YING

UNIVERSITY OF WASHINGTON
ATTN: C LEOVY
ATTN: L RAOKE
ATTN: P HOBBS

VIRGINIA POLYTECHNIC INST LIB
ATTN: M NADLER

WASHINGTON STATE UNIVERSITY
ATTN: DR A CLARK

WISCONSIN UNIVERSITY OF
ATTN: P WANG

END

DATE

FILMED

5-88
DTIC